# Combining iPSC-derived fibroblasts and FRET biosensors to unravel GPCR-mediated cardiac fibrosis activation in dilated cardiomyopathy.

Grace R. Mazarura

Department of Pharmacology and Therapeutics

McGill University, Montreal, Quebec, Canada

August 2023

A thesis submitted to McGill University

in partial fulfillment of the requirements of the degree of Master of Science

# ABSTRACT

Dilated cardiomyopathy (DCM) is a condition marked by ventricular dilation, leading to impaired heart function and heart failure—a significant cause of death globally. Activated cardiac fibroblasts (CFs) contribute to adverse cardiac remodeling in DCM, yet current therapies mainly focus on cardiomyocytes with no therapies approved for targeting cardiac fibrosis yet available on the market. Angiotensin II type-1-receptors (AT1R) and endothelin-1 receptors (ETR) have been shown to activate the extracellular signal-regulated kinase 1/2 (ERK1/2) signaling pathway - a pathway significantly upregulated in the failing hearts of DCM patients that modulates the activation state of fibroblasts and the development of fibrosis. While G protein-coupled receptor (GPCR) signaling in cardiomyocytes and vascular smooth muscle cells has been extensively studied, its role in fibroblasts remains less well-characterized. Our objective was to develop tools for understanding GPCR-mediated fibrosis signaling. Using human induced pluripotent stem cell-derived cardiac fibroblasts (hiPSC-CFs), we explored the signaling mechanisms driving fibrotic responses. We validated a differentiation protocol for generating CFs from hiPSCs confirming their identity through qPCR and immunofluorescence to ensure hiPSC-CFs expressed key cell-specific signatures. Subsequently, fluorescence resonance energy transfer (FRET)-based biosensors, localized to the cytoplasm and nucleus were utilized to monitor ERK1/2 signaling downstream of AT1R and ETR stimulation in hiPSC-CFs. We characterized AT1R and ETR signaling through bulk and single-cell analysis, revealing intricacies often overlooked in bulk analysis. Our investigation identified distinct cell clusters based on ligand response and concentration. Endothelin-1 (ET-1) induced ERK signaling in both cytoplasmic and nuclear compartments of hiPSC-CFs, while Angiotensin II triggered nuclear ERK signaling only. This

study uncovered subcellular compartmentalization of ERK signaling and unveils novel single-cell response dynamics. This research contributes to a broader initiative establishing a comprehensive pipeline from bedside to bench to bedside. This initiative aims to characterize cardiac cell types in DCM, enabling patient stratification based on clinical data, drug response, and phenotype. Ultimately, our work aims to drive more effective treatment strategies for DCM.

# RÉSUMÉ

La cardiomyopathie dilatée (CMP) est une maladie cardiaque caractérisée par la dilatation ventriculaire, ce qui mène à une diminution de fonction cardiaque. Souvent, cette maladie entraîne l'insuffisance cardiaque, ce qui est associé à un taux de mortalité élevé à l'échelle mondiale. Les fibroblastes cardiaques activés (FC) contribuent au remodelage cardiaque indésirable dans la CMP, mais les thérapies actuelles se concentrent principalement sur les cardiomyocytes et aucune thérapie n'est encore approuvée pour cibler la fibrose. Il a été démontré que les récepteurs de l'angiotensine II de type 1 ($AT_1R$) et les récepteurs de l'endothéline-1 (ETR) activent la voie de signalisation de la kinase 1/2 régulée par le signal extracellulaire ($ERK_{1/2}$). Cette voie de signalisation est régulée positivement dans les cœurs défaillants des patients diagnostiqués avec la CMP et module l'état d'activation des fibroblastes et le développement de la fibrose. Bien que la signalisation des récepteurs couplé aux protéines G (RCPG) dans les cardiomyocytes et les cellules musculaires lisses vasculaires ait été largement étudiée, son rôle dans les fibroblastes reste moins bien caractérisée. Notre objectif était de développer des outils pour comprendre la signalisation de la fibrose médiée par les RCPG. À l'aide de fibroblastes cardiaques (FC) dérivés de cellules

souches pluripotentes induites (CSPi-FC), nous avons exploré les mécanismes de signalisation à l'origine des réponses fibrotiques. Nous avons validé un protocole de différenciation pour générer des FC à partir de CSPi, en confirmant leur identité par l'expression des gènes et l'immunofluorescence. Par la suite, des biosenseurs basés sur le transfert d'énergie par résonance de fluorescence (FRET), localisés dans le cytoplasme et le noyau, ont été utilisés pour mesurer la signalisation $ERK_{1/2}$ en aval de la stimulation $AT_1R$ et ETR dans les CSPi-CF. Nous avons caractérisé la signalisation $AT_1R$ et ETR en 'mode population' et en 'mode unicellulaire', révélant des subtilités souvent négligées dans l'analyse globale. Notre enquête a identifié des groupes de cellules distincts en fonction de leur réponse et de la concentration du ligand. L'endothéline-1 a induit la signalisation ERK dans les compartiments cytoplasmiques et nucléaires des CSPi-CF, tandis que l'Ang II a seulement déclenché la signalisation nucléaire ERK. Cette étude a révélé la compartimentation subcellulaire de la signalisation ERK et dévoile une nouvelle dynamique de réponse unicellulaire. Cette recherche contribue à une initiative plus large établissant un programme itératif du chevet au laboratoire et de nouveau au chevet. Cette initiative vise à caractériser les types de cellules cardiaques dans la CMP, permettant une stratification des patients basée sur les données cliniques, la réponse aux médicaments et leur phénotype. En fin de compte, notre travail vise à élaborer des stratégies de traitement plus efficaces pour la CMP.

# TABLE OF CONTENTS

# i. LIST OF TABLES AND FIGURES

**Supplementary Figures**

**List of tables**

# ii. ACKNOWLEDGEMENTS

Over the last two years, I have learned two key things, firstly that research is less about the end goal but the joy (and pain) of dancing in the scientific question and exploring it with awe and wonder. Awe and wonder create light for seeing more than banging your head on a problem – at least for me it did. Secondly, enjoy each moment, experiment, presentation and, all the people - taking joy in each encounter. To my supervisor, Dr. Terry Hébert, thank you for taking a chance on me and fostering a place where science and wonder/curiosity went hand-in-hand. I am grateful for your guidance throughout my project and support through the challenges and for celebrating the victories with me. Thank you for all the opportunities you provided for me to grow as a scientist and for nudging me to grow. Thank you for the pleasure of your company through this journey for and reminding me to take everything one step at a time.

To my advisor, Dr. Daniel Bernard I appreciate your time, insight, and encouragement – I am truly grateful to have had you as an advisor. To the members of my thesis advisory committee Dr. Bruce Allen and Dr. Jason Tanny, I value your guidance and input in my project, and preparing me for my first-year presentation and helping me to see where I needed to learn more about the topic I had decided to study. I appreciate you.

To Dr. Jace Jones-Tabah, thank you for taking me under your wing in my undergraduate final year project and believing in me. I appreciate your mentorship and how you inspired me.

To Hanan Mohammad, thank you for always encouraging me as a scientist even when imposter syndrome kicked in.

To the “Heart-In-a-Dish” (HID) project team; Dr. Kyla Bourque, Alyson Jiang, and Dr. Karima Alim, I am grateful for all the support ranging from weekend medium changes, troubleshooting, and karaoke sessions in 1307 while culturing cells, not to mention the great company. You were an indispensable part of what made this project. A special thank you to Dr. Kyla Bourque for providing essential support especially in the early stages of this project, and for teaching me the skills I needed to complete my project. Dr. Karima Alim, thank you for helping me in the coding portion of my project and encouraging me as I mastered that part of my project. Alyson, I thank you for always being keen to help and the great moments shared in 1307.

To Phan Trieu, Darlaine Pétrin, Dr. Dominic Devost, thank you for all the support and helping me whenever I needed help, be it troubleshooting an experiment, or getting tools I needed to complete my work. Thank you for being patient and available to field all my questions and keeping the lab running smoothly.

To the members of the Hébert lab (Dr. Étienne Billard, Kim Martins-Cannavino, Jacob Blaney, Emma Paulus, Deanna Sosnowski, Robert Rizk, and Dr. Juliana Dallagnol), thank you for your help I could not have asked for a better group of people to have worked with during the last 3 years. Thank you for your valuable insight at lab meetings and whenever I came to you for help. To the past members of the Hébert lab, thank you for being the shoulders I stood on and for establishing protocols that were instrumental in my project before I even joined the lab.

To Dr. Paul Clarke I appreciated the opportunity to work in your lab before and the doors you opened for me. I also appreciated the great conversations.

Thank you to Xavier Ng who helped me achieve my project goals.

I would also like to thank our HID project team collaborators Dr. Nadia Gianetti, Dr. Renzo Cecere, Natalie Gendron, and their teams, as this project would not have been possible without them.

I would like to thank Dr. Nicolas Audet from IMBP and the McGill University Advanced BioImaging Facility (ABIF) team for helping with teaching me microscopy. Thank you for being available to field all my questions.

A special thank you to my parents and siblings for their continued support. The phone calls helped especially on the days I wanted to give up. A special thanks to Ann-Kathrin Johow for the emotional support throughout my master's.

To all my friends in the department. Thank you for your support.

Thank you to everyone who helped me along the way, even if I did not have the space to mention you by name. I appreciate you.

# iii. AUTHOR CONTRIBUTIONS

Generation of hiPSC lines for the HID project was done by by Ida Derish, Jeremy Zwaig, Kashif Khan, David Derish, Janice To, and Patrick Young. Dr. Jace Jones-Tabah and Dr. Karima Alim provided original computer code for analysis of single-cell FRET data. Xavier assisted with running the RT-qPCR experiments in section 3.2. Dr. Kyla Bourque contributed to the conception of the project and helped with the translation of the abstract into French. Terry Hébert contributed to the conception of the project, experimental design, interpretation of results, provided supervisory support and edited the manuscript.

Unless stated above, all work in this thesis was completed by Grace Mazarura. Grace Mazarura conducted and designed experiments, validated methodologies, analyzed data, assembled figures, and wrote the original manuscript.

# iv. ABBREVIATIONS

| Abbreviation | Definition |
|---|---|
| AC | Adenylyl cyclase |
| ACE | Angiotensin converting enzyme |
| ACM | Arrhythmogenic cardiomyopathy |
| AcOH | Acetic acid |
| AKT | Protein kinase B |
| Ang II | Angiotensin II |
| ARB | Angiotensin II receptor blockers |
| AT1R | Angiotensin II type I receptor |
| AT2R | Angiotensin II type II receptor |
| ATR | Angiotensin II receptor |
| cAMP | Cyclic adenosine 3,5-monophosphate |
| CFP | Cyan fluorescent protein |
| CF | Cardiac Fibroblast |
| *CHIR99021* | Chemical compound that inhibits GSK3 |
| CM | Cardiomyocyte |
| c-myc | MYC Proto-Oncogene, BHLH Transcription Factor |
| CTGF | Connective tissue growth factor |
| DAG | Diacylglycerol |
| DCM | Dilated cardiomyopathy |
| DSP | Desmoplakin |
| ECM | Extracellular matrix |
| EGF | Epidermal growth factor |
| EGFR | Epidermal growth factor receptor |
| EHT | Engineered heart tissue |
| ERK1/2 | Extracellular signal regulated kinases 1/2 |
| ET-1 | Endothelin-1 |
| $ET_AR$ | $ET_A$ receptor |
| $ET_BR$ | $ET_B$ receptor |
| ETR | Endothelin receptor |
| fDCM | Familial dilated cardiomyopathy |
| FGF | Fibroblast growth factor |
| FRET | Fluorescent resonance energy transfer |
| GDP | Guanosine diphosphate |
| GFP | Green fluorescent protein |

| | |
|---|---|
| GPCR | G protein-coupled receptor |
| GTP | Guanosine-5’-triphosphate |
| GSK3 | Glycogen synthase kinase 3 |
| HEK 293 | Human embryonic kidney 293 cell line |
| HF | Heart failure |
| $IP_3$ | Inositol trisphosphate |
| $IP_3R$ | Inositol trisphosphate receptor |
| hiPSC | Human induced pluripotent stem cell |
| hiPSC-CF | Human induced pluripotent stem cell derived cardiac fibroblast |
| hiPSC-CM | Human induced pluripotent stem cell derived cardiomyocyte |
| Iso | isoproterenol a non-selective β-adrenergic receptor agonist |
| *IWP2* | Inhibitor of Wnt porcupine 2 |
| Klf4 | Krüppel-like factor 4 |
| LMNA | Lamin A/C |
| LV | Left ventricle |
| MAPK | Mitogen-activated protein kinase |
| MF | Myofibroblast |
| MMPs | Matrix metalloproteinases |
| MOI | Multiplicity of infection |
| NES | Nuclear export sequence |
| NE | Norepinephrine |
| NLS | Nuclear localization sequence |
| Oct-04 | Octamer-binding transcription factor 4 |
| PBMCs | Peripheral blood mononuclear cell |
| PDGFR | Platelet-derived growth factor receptor |
| PI3K | Phosphoinositide 3-kinase |
| PIP2 | Phosphatidylinositol 4,5-bisphosphate |
| PKA | Protein kinase A |
| PKC | Protein kinase C |
| PMA | Phorbol myristyl acetate |
| p38 | p38 mitogen activated protein kinases (p38MAPK) |
| RAAS | Renin-angiotensin aldosterone system |
| RNC | Rat neonatal cardiac fibroblasts |
| SB431542 | Potent inhibitor of the TGF-β pathway |
| SCN5A | Sodium Voltage-Gated Channel Alpha Subunit 5 |
| sc-RNA-seq | single-cell RNA-sequencing |
| sn-RNA-seq | single-nucleus RNA-sequencing |
| Sox2 | SRY-Box Transcription Factor 2 |
| TCF21 | Gene encoding Transcription factor 21 |
| TIMPs | Tissue inhibitors of metalloproteinases |
| TGFβ1 | Transforming growth factor-beta 1 |

| | |
|---|---|
| TNFα | Tumor necrosis factor alpha |
| VEGF | Vascular endothelial growth factor |
| Wnt | Wingless-related integration site |
| YFP | Yellow fluorescent protein |
| β-AR | β-adrenergic receptor |
| $\beta_1$AR | $\beta_1$-adrenergic receptor |
| $\beta_2$AR | $\beta_2$-adrenergic receptor |
| $\beta_3$AR | $\beta_3$-adrenergic receptor |

# 1 BACKGROUND

## 1.1 INTRODUCTION

Dilated cardiomyopathy (DCM) is a disease of the heart muscle marked by left ventricular wall thinning resulting from both cardiomyocyte death and fibrosis. This thinning of the heart wall compromises the heart's ability to pump blood to the rest of the body and ultimately leads to heart failure. Genetic mutations that affect cardiomyocyte electrical-contractile coupling in cardiomyocytes are key drivers of dilated cardiomyopathy and the leading cause of heart transplantation (1). The adverse/pathological cardiac remodeling in heart failure and DCM is partially attributed to proliferation and activation of cardiac fibroblasts (CFs) in the heart. Angiotensin II type-1-receptors (AT1R) and endothelin-1 receptors (ETR) have been shown to activate the extracellular signal-regulated kinase 1/2 (ERK1/2) signaling pathway - a pathway significantly upregulated in the failing hearts of DCM patients that modulates the activation state of fibroblasts and the development of fibrosis. However, signaling mediated by these G protein-coupled receptors (GPCRs) remains understudied in fibroblasts as compared to cardiomyocytes.

Research efforts to understand DCM pathology have primarily focused on the cardiomyocyte, while neglecting other cell types in the heart such as endothelial cells and fibroblasts. Cardiac fibroblasts are of particular interest in light of their role in driving changes in heart structure and function during the development of DCM. Given the heart's limited capacity to regenerate post-injury, insults (genetic, chemical, or viral) that cause cardiomyocyte death are repaired via two process that work together to compensate for the loss of cardiomyocytes, namely 1) cardiomyocyte remodeling, whereby the remaining cardiomyocytes adapt and increase in size

(hypertrophy) and 2) fibrosis, whereby lost cardiomyocytes are replaced by fibrotic tissue. The latter occurs primarily when an insult overwhelms the myocardium's limited regenerative potential as more cardiomyocytes die. Paradoxically, fibrosis ultimately affects cardiac compliance and can result in more cardiomyocyte death, resulting in more fibrotic scarring, generating in a vicious cycle that ultimately worsens disease progression. In this thesis, we aim to investigate the mechanisms associated with the fibrosis context of dilated cardiomyopathy.

## 1.2 DILATED CARDIOMYOPATHY

Cardiomyopathies can broadly be categorized into five categories based on functional and morphological criteria. These categories are dilated, hypertrophic, arrhythmogenic, restrictive, dilated, and unclassified cardiomyopathies. Dilated cardiomyopathy (DCM) accounts for 60% of all cases of cardiomyopathy. The prevalence of DCM was estimated to be between 1:2500 to 1:250 individuals (2), with DCM accounting for just over half of all heart transplants (3, 4). DCM is defined by left or biventricular dilation/thinning and reduced ejection fraction (below 40%) in the absence of coronary heart disease, congenital heart disease or conditions that lead to abnormal loading (e.g. valvular disease, hypertension) (5, 6) .

The atypical enlargement of the ventricle seen in DCM causes changes in the heart shape whereby the ventricle(s) becomes larger and changes the geometry from the normal elliptical shape of the heart to a spherical shape (7). These changes in myocardial architecture consequently lead to compromised cardiac function. To compensate for this decreased cardiac output, cardiomyocytes (CMs) can respond to increased release of components of neurohormonal stimulation and the renin-angiotensin-aldosterone system (RAAS). However, over time chronic stimulation by neurohormones can be detrimental to myocardial health leading to CM death and

promoting fibrosis through activation of fibroblasts (reviewed here (8-10). Activate fibroblasts adopt a secretory phenotype responsible for scarring with paracrine effects on CMs as well. DCM is a progressive disease, which can ultimately lead to heart failure. Although fibrosis is indeed a reparative process aimed at preserving structural integrity of the myocardium resulting from wear and tear over the course of a lifetime, pathological fibrosis in the heart can lead to changes compliance of the heart (11). However, mediators released by activated fibroblasts may have deleterious effects on the cardiomyocytes and lead to more cardiomyocyte cell death and more replacement of lost cardiomyocytes with additional fibrotic scarring. Consequently, this creates a feedforward loop that leads to chronic pathological remodeling of the heart (12).

As heart function declines over time, the lack of oxygenated blood reaching the body causes other key organ systems (e.g., kidney, liver) to fail as well - at this point, advanced heart failure becomes a life-threatening condition, resulting in symptoms seen in DCM patients such as dyspnea (shortness of breath) due to pulmonary oedema (fluid retention in the lungs), peripheral oedema/fluid retention due to blood backing up into the veins, and fatigue or weakness due to a lack of oxygenated blood in the body (13). Unfortunately, many individuals remain asymptomatic until the disease has advanced into its severe stages, making it impossible to intervene sooner to delay or stop progression (14).

Typically, diagnosis involves methods such as echocardiography to visualize dilation of the ventricles and measure ventricular systolic ejection fraction. This can be complemented by cardiac magnetic resonance tomography, assessment of family history, and genetic testing. Nonetheless, 20- 50% of cases are termed as idiopathic, whereby the cause remains unknown, although the causes could possibly be resolved if more genetic testing was done. However, such testing is costly and in Quebec it is only covered by health insurance in the case of suspected

familial DCM (fDCM). DCM is classified as familial when at least two first- or second-degree relatives meet diagnostic criteria for DCM, or when a first-degree relative of a DCM patient dies unexpectedly and inexplicably before age 35 (15). Genetic/familial DCM accounts for 30-50% of DCM cases (15). Aside from genetic mutations, causes of DCM include viral infections, autoimmune diseases, exposure to certain chemotherapeutic drugs (such as anthracyclines), excessive exposure to certain drugs (e.g., alcohol or cocaine) as well as exposure to poisons such as arsenic. However, late diagnosis of DCM is associated with more serious disease progression, and the disease usually progresses slowly from initial insult to onset of symptoms and emergence of a diagnosis. This makes it particularly difficult to intervene early enough in the disease process to prevent irreversible damage.

Pharmacological interventions for DCM include angiotensin II receptor blockers (ARBs), angiotensin converting enzyme (ACE) inhibitors, β-blockers, mineralocorticoid receptor antagonists, sodium/glucose cotransporter-2 (SGLT2) inhibitors, aldosterone receptor antagonists as well as a combination therapy with ARBs and neprilysin inhibitors (7). Recently, myosin modulators, a novel class of drugs that augment cardiomyocyte contractility was added to the possible options for intervening in DCM(16). Despite these interventions, 50% of patients, have a prognosis of death within 5 years following diagnosis with DCM (8-10). Furthermore, existing DCM therapy options are only partially effective, with no approved therapies on the market to target cardiac fibrosis, even though fibrosis aggravates cardiac structural remodeling and is a measure of disease severity (11).

The value of genetic testing of family members of those with DCM is that it may allow us to catch the disease early in family at risk members. Equally as important as earlier diagnosis is creating interventions that slow or stop disease progression and perhaps stop disease penetrance in

fDCM. More knowledge of disease initiation and progression is needed to understand disease pathology before overt failure develops. By understanding the mechanisms that underpin DCM progression we could treat disease earlier and prevent or slow disease progression, reducing the burden of disease on both individuals and the healthcare system. We can further develop better treatment strategies by developing molecular profiles and taking clinical data into account to link these profiles to disease outcome, we could cluster patients into groups with similar phenotypes, based on molecular profiles and outcomes. These clusters could be used to improve treatment by offering an avenue for more personalized medicine and more effective therapeutic strategies (17).

In the next section we will discuss genes that have been linked to DCM, with a focus on how they affect cardiac fibroblasts.

## 1.3 GENETIC CAUSES OF DCM

Several key genes that affect cardiomyocyte contractility have been linked to DCM. The list of genes includes genes involved in the sarcomere, dystrophin, cytoskeleton, nuclear envelope (e.g. *LMNA*, lamin A/ C), ion channels (e.g. *SCN5A*, sodium voltage-gated channel alpha subunit 5), mitochondria as well genes implicated in calcium homeostasis and cell-cell adhesion (e.g. DSP, desmoplakin) and transcription factors (e.g. *RBM20*, RNA binding motif protein 20) (5). While most of these mutations do not affect clinical management of disease, mutations in *LMNA* and *SCN5A* pose a higher risk of arrhythmia and call for different clinical management of disease (18).

*LMNA* is a gene encoding laminin A and C. These are intermediate filament proteins that form part of the nuclear envelope and are essential for nuclear integrity and processes such as regulation of gene expression and signal transduction. Although mutations in *LMNA* have been mostly studied in cardiomyocytes, linking these mutations to disease phenotype has proven difficult. To attempt to underpin molecular mechanisms underlying DCM in families *LMNA* mutation, Widyastuti et al. used RNA-seq on primary skin fibroblasts from a family bearing a mutation in *LMNA* to evaluate the gene profile that caused DCM. They were able to show that genes involved in ERK signaling were dysregulated in DCM patients, as opposed to cells from the control group, thus making ERK a candidate pathway that may be perturbed and lead to cardiomyopathy (19). Another study that complemented this finding showed ERK upregulation in induced-pluripotent stem cell-derived cardiac fibroblasts (hiPSC-CFs) of DCM patients harboring a mutation in the *LMNA* gene. Out of the 7 samples examined, 6 of the hiPSC-CFs from DCM-patients harboring specific *LMNA* mutations (M1I, R216C/R399H, R541C, R377H, R399H, R216C) showed an increase in ERK phosphorylation (a surrogate for ERK activation), while one mutation (*LMNA*- R335Q) did not show a significant difference relative to controls (20). Thus, perturbations in ERK signaling may be involved in the molecular mechanisms underlying disease progression, and these perturbations may be distinct depending on the specific mutation in *LMNA*.

Moving into an *in vivo* model, Rouhi and colleagues used a Cre-knock out mouse model to selectively knock out *LMNA* in cardiac fibroblasts. They were able to show that *LMNA*-associated DCM could be recapitulated by ablation of *LMNA* in cardiac fibroblasts, implying that both CMs and non-CMs synergistically cause the DCM phenotype (21). Knocking out *LMNA* in CFs of these mice led to arrhythmias, myocardial fibrosis, conduction defects and cardiac

hypertrophy(21). These studies all underscore the significance of both cardiomyocytes and other non-cardiomyocyte cells within the heart as crucial contributors to the development of DCM.

One of the reasons mutations in CFs may affect CM function can be illustrated by several studies that have highlighted the need to understand CF in disease, given that crosstalk between CMs and cardiac fibroblasts evolves with disease progression. In terms of paracrine crosstalk, one study showed that media conditioned cardiomyocytes derived from induced pluripotent stem cells (hiPSC-CM) of DCM patients contained exosomes that increased cardiac fibrosis both *in vivo* and *in vitro*. These exosomes contained the microRNA, miR-218-5p, which activated TGFβ signaling by suppressing TNFAIP3, (gene encoding TNFα-induced protein 3, an inhibitor/negative regulator of inflammation and immune response) (22).

Conversely, CFs from DCM patients have also been shown to influence cardiomyocyte function through paracrine signaling via secretion of mediators or through direct cell-cell contact between the two cell types. Ventricular hiPSC-CMs cultured with DCM cardiac fibroblasts, led to altered calcium cycling within CMs (23). Furthermore, using 3D engineered heart tissue (EHT), it has been shown that DCM cardiac fibroblasts or DCM cardiac myocytes grown together or individually were stiffer than control EHT, thus CFs were contributors to contractile pathophysiology in DCM (24).

Fibrosis has conventionally been thought of as a consequence or reaction to injury, however recent study has brought to light that changes in the myocardium ECM that are mediated by CFs occur even before the onset of fibrosis. Cardiac fibroblasts appear to work in tandem with cardiomyocytes to drive disease pathology. Mutations that are specific to genes expressed by cardiomyocytes can impact fibroblasts, where fibroblasts “sense” the consequences of the mutations (e.g., reduced contractility) and then attempt to compensate or adapt accordingly. For

example, cardiac troponin C (cTnC) is a component of cardiac muscle involved in connecting calcium influx in cardiomyocytes to contraction. Mutations in cTnC are drivers of DCM. In particular, the I61Q point mutation in cTnC desensitizes myofilaments to calcium influx, thereby impairing cardiomyocyte force generation during contraction and leads to a dilated phenotype in mice harboring this mutation. In transgenic mice harboring the I61Q mutant, there are changes in the cardiomyocyte stiffness and extracellular matrix before any fibrotic remodeling of the heart tissue takes place. At 2 months, the myocardium in transgenic mice had stiffened without much increase in the ECM. This stiffening was attributed to changes in the organization of collagen fibers. Furthermore fibroblasts were said to have mediated these changes through proliferation rather than activation – and this stiffening could be ameliorated by targeting MAPK p38α in cardiac fibroblasts specifically (25). Finally, this study called into question the assumption that enlarged structural remodeling of cardiomyocytes is secondary to ECM remodeling. This also highlights the role of fibroblasts as "mechanical rheostats" that play a role in shaping the myocardium during disease progression. Furthermore, it highlights that success in treating DCM may be better achieved by targeting the behaviors of cells in the heart as a whole as opposed to targeting cardiomyocyte function alone (25).

Given the key role that fibroblasts play in the pathology of cardiomyopathy, it is essential to also study these non-myocyte cell contributions to the disease. In the next section I provide an overview of cardiac fibroblasts and their role in the heart under normal and pathophysiological conditions.

## 1.4 THE CARDIAC FIBROBLAST IN HEALTH AND DISEASE

Cardiac fibroblasts are plastic cells that can change phenotype in response to environmental cues. In terms of developmental origin, CFs develop from the mesoderm layer during heart development. While cardiomyocytes make up 70% of the cardiac volume, in terms of cell number they are estimated to make up only 25-35% of the cells in the heart. By combining single-cell RNA-seq (sc-RNA-seq) and single-nucleus RNA-seq (sn-RNA-seq) data, ventricular cell composition was shown to be 25.7% cardiomyocytes, 18.3% fibroblasts, 16.6% endothelial cells, 15% mural cells, the remainder consisting of immune cells, endocardial cells, adipocytes and neural cells (26). The composition also varies slightly between atria and ventricles (27).

While cardiomyocytes are responsible for the contraction-relaxation cycle within the heart, fibroblasts are part of the stroma and provide trophic support to cardiomyocytes and other cell types within the heart, as well as maintaining the structural framework of the heart. Along with mesenchymal stem cells, fibroblasts and immune cells, stroma also contains blood vessels and extracellular matrix. The ECM is a complex network which plays pleiotropic roles in the heart. It provides structure and trophic support. It comprises fibrous proteins such as collagen and elastin which are necessary for the structure and plasticity of the myocardium; matricellular proteins like periostin and thrombospondins necessary for modulating cellular responses and adhesion – they also tend to be upregulated during inflammation (28). It is also comprised of glycoproteins like fibronectin, and laminin that mediate anchoring of cells to ECM as well as for and mechano-signaling in the heart as well as growth factors and metalloproteases (29). All these work towards the common function of maintaining tissue homeostasis. The composition of the ECM is not static; it changes to keep up with the needs of the cells it supports in the myocardium. The ECM does not

play a passive role in the function of the myocardium; indeed, it regulates the abundance of receptors, growth factors available to cells and various cell modalities like proliferation and cell survival and higher-level modalities like tissue plasticity and architecture. For more in-depth review of the ECM the reader is referred to (28, 30).

Apart from structural support and providing nutrients, the stroma can modulate tissue stiffness, tensile strength and it aids in force transmission in cardiac tissue. Signaling cues provided by stroma-parenchymal interactions regulate myocardium function and development. Regarding how stroma regulates parenchymal cells (such as cardiomyocytes), the interactions that facilitate CM and stroma interactions include bidirectional communication via paracrine signaling (for example, growth factors such as VEGF and PDGF (31, 32), cytokines (33, 34), and chemokines and micro-RNAs (35)), biochemical and biophysical signals from the extracellular matrix (ECM) and direct cell-cell interactions between stroma and CMs that provide biomechanical and electrical signaling. For more comprehensive descriptions of stroma-parenchymal interactions, readers may consult these reviews (35-38).

The cell types responsible for regulating the ECM appear to be the stromal cells (cardiac fibroblasts, mesenchymal stromal cells, endothelial cells, and immune cells). However, the major cell types involved in the synthesis of ECM are fibroblasts (21). One of the key determinants of DCM severity is the pathological expansion of the extracellular matrix, known as fibrosis, that results in the stiffening of the myocardium (39). In DCM patients, the ECM has been shown to lose complexity and there is reduced elasticity as measured by Young's modulus in decellularized human ventricular tissue(12). As the CF is an important regulator of the ECM it becomes important to discuss how it modulates ECM in health and disease.

The cardiac fibroblast is a cell type of mesenchymal origin that develops from various sources in the heart including the endocardium (via endothelial to mesenchymal transition), epicardium (via epicardial epithelial-mesenchymal transition) and the neural crest. The vast majority of ventricular cells are believed to be of epicardial origin (TCF21-positive), while atrial fibroblasts are believed to originate from second heart field progenitor cells. In a study that employed sc-RNA-seq and sn-RNA-seq, up to 9 distinct fibroblast populations were identified within the heart (26). This diversity may be attributed to the various cell niches supported by cardiac fibroblasts and the different developmental origins of cardiac fibroblasts (40, 41).

In the uninjured heart, CFs mediate homeostatic ECM turnover through secretion of ECM proteins (e.g., collagen, elastin, periostin), growth factors, and critical enzymes such as tissue inhibitors of metalloproteinases (TIMPs) and matrix metalloproteinases (MMPs) that are responsible for breakdown and buildup of the ECM (42). It is important to distinguish between the regular wear and tear of the heart that requires homeostatic ECM turnover and the pathological ECM accumulation that ensues after significant injuries that causes extensive cardiomyocyte death. Following myocardial cell injury such as that caused by sustained hypertension, myocardial infarction, infection, and toxic insult there can be a large loss of CMs can occur, leading to the release of damage-associated molecular patterns (DAMPs) by necrotic cardiomyocytes (43). These activate the initial inflammatory response whereby resident macrophages and neutrophils release pro-inflammatory chemokines such as ineterleukin-6 (IL-6), ineterleukin-16 (IL-16), and tumor necrosis factor alpha (TNFα) (40, 44). Fibroblasts respond to these stimuli by becoming activated and adopting a pro-inflammatory phenotype that contributes to secretion of inflammatory cytokines that include TNFα (45) and IL-6 (46) at the site of injury. Following this, fibroblasts transition to a proliferative phenotype in the subsequent phase of wound healing. During this

phase, their gene expression shows a decrease in apoptotic genes, such as *CASP3* (the gene encoding caspase 3), along with an increase in angiogenic (e.g., VEGF), proliferative, pro-fibrotic genes, and anti-inflammatory mediators like TGFβ1 (40, 47, 48). In the final stage of wound healing, termed maturation, CFs adopt a contractile phenotype which secretes large amount of ECM proteins to facilitate scar formation (40). Fibroblasts isolated from region near a myocardial infarction exhibit an increase in collagen synthesis of up to 196% (49). This fibroblast phenotype characterized by the expression of stress fibers containing α-smooth muscle actin and the secretion of the matricellular protein, periostin, is referred to as a myofibroblast (MF) and is associated with pathological fibrosis. In the long-term, after the maturation phase, fibroblasts adjust to a new homeostatic state within the myocardium, where the niche of CFs within the myocardium includes a larger number of MFs for the maintenance of scar tissue (50).

CMs are terminally differentiated cells that do not reenter the cell cycle, instead their response to most cues is to increase contraction, enlarge via hypertrophy or undergo apoptosis(51). Owing to the lack of regeneration of the myocardium, the heart may compensate for reduced cardiac function through chronic neurohormonal stimulation (11, 52). This increase in neurohormonal stimulation ultimately has deleterious effects on CMs and causes fibroblasts to become activated and adopt a MF phenotype thereby leading to pathological expansion of the ECM, termed fibrosis. This dysregulation in ECM increases myocardial stiffness, affects electrical coupling in the heart and leads to remodeling of the heart tissue that is associated with disease progression and, ultimately, heart failure. Additionally, CFs are also mechano-sensitive cells that can respond to mechanical stimuli and are likely affected by changes in the stiffness of the myocardium. For instance, the angiotensin II type-1-receptor (AT1R) is a receptor implicated in cardiac fibroblast activation and is triggered by mechanical strain and substrate stiffness (53, 54).

The sources of MFs within the heart are still highly controversial and different injuries (e.g., ischemic, hypertensive, diabetic cardiomyopathy, dilated cardiomyopathy) appear to recruit different populations of fibroblasts (33). Sources may include resident cardiac fibroblasts, bone marrow derived cells (55), hematopoietic cells (56), immune cells, pericytes and endothelial cells via (endo-EMT). Lineage tracing showed that endocardium-derived fibroblasts are associated with a pressure overload model of heart injury, whereas in ischemic injury, epicardial-origin fibroblasts were a more abundant driver of fibrosis (57).

Previously, fibroblasts have been mostly seen as reactive modulators or passive responders, primarily reacting to the demands of the heart muscle. Alterations in the extracellular matrix (ECM) were thought to be secondary to changes in the structure of the heart muscle in DCM. However, this notion has been challenged by research that demonstrated that stiffening of the myocardium preceded any visible indicators of fibrosis in mice with a cardiac troponin mutation. Furthermore, CF number, rather than conversion to myofibroblasts, appeared to be the driver of fibrosis (25). This finding goes hand in hand with a study showing that the number of CFs was essential in modulating the stiffness of engineered heart tissue. In a study that used hiPSC-CMs and human CFs to construct 3D engineered tissues, it was shown that adding 5% CFs was important to improve the electrochemical responses and contractile function of the engineered cardiac tissues. Conversely, adding 15% CFs (similar to proliferation of CFs in a disease context) resulted in tissues with higher spontaneous beating rates (58). Furthermore,in another study, Chaffin et al. used single-cell RNA-seq to show that the number of CFs in the hearts of DCM patients was indeed increased (59), thus implying CF number may play a role in disease progression.

In this same study, they found that pathways including MAPK and ECM synthesis were upregulated in DCM hearts. They identified eight different populations of CFs in the heart and showed that these populations were shifted in abundance in diseased hearts. More, specifically the showed that fibroblast populations which expressed *POSTN* (encoding periostin) increased in DCM. Furthermore the population of fibroblasts in DCM showed an increase in genes indicative of increased activation (e.g. *COL1A1, CTGF, FAP*) (26). This is in parallel with another study that found that a population of activated cardiac fibroblasts was found in DCM hearts but not healthy donor hearts.(59)

All these changes in activation state are coordinated by several mediators including neurohormones (angiotensin II, endothelin-1, norepinephrine, and epinephrine), interleukins (IL)-IL-6, IL-10, IL-4 etc.), growth factors such as TGFβ, fibroblast growth factor and platelet-derived growth factor, as well as chemokines of the cysteine-cysteine (CC) or cysteine-any amino acid-cysteine (CXC) family. However how each of these is involved remains unresolved, this is further complicated by the mix of different cues e.g., mechano-sensing and the variety of different chemokines that CFs respond to in the myocardium and how all these responses are integrated. One common downstream integrator of these cues is angiotensin II signaling has been suggested to be atop the hierarchy of events that activate fibroblasts (41). Through stimulation of AT1R, Ang II mediates secretion of TGF-β (a potent activator of fibroblasts) and collagen as well as other mediators like endothelin-1 (60-62). CFs express a large number of GPCRs that modulate cardiac fibroblast behavior and activation state. In the next section, I will provide an overview of GPCR signaling and key GPCRs downstream of neurohormones (angiotensin II, endothelin-1, norepinephrine, and epinephrine) involved in CF activation (see Figure 1).

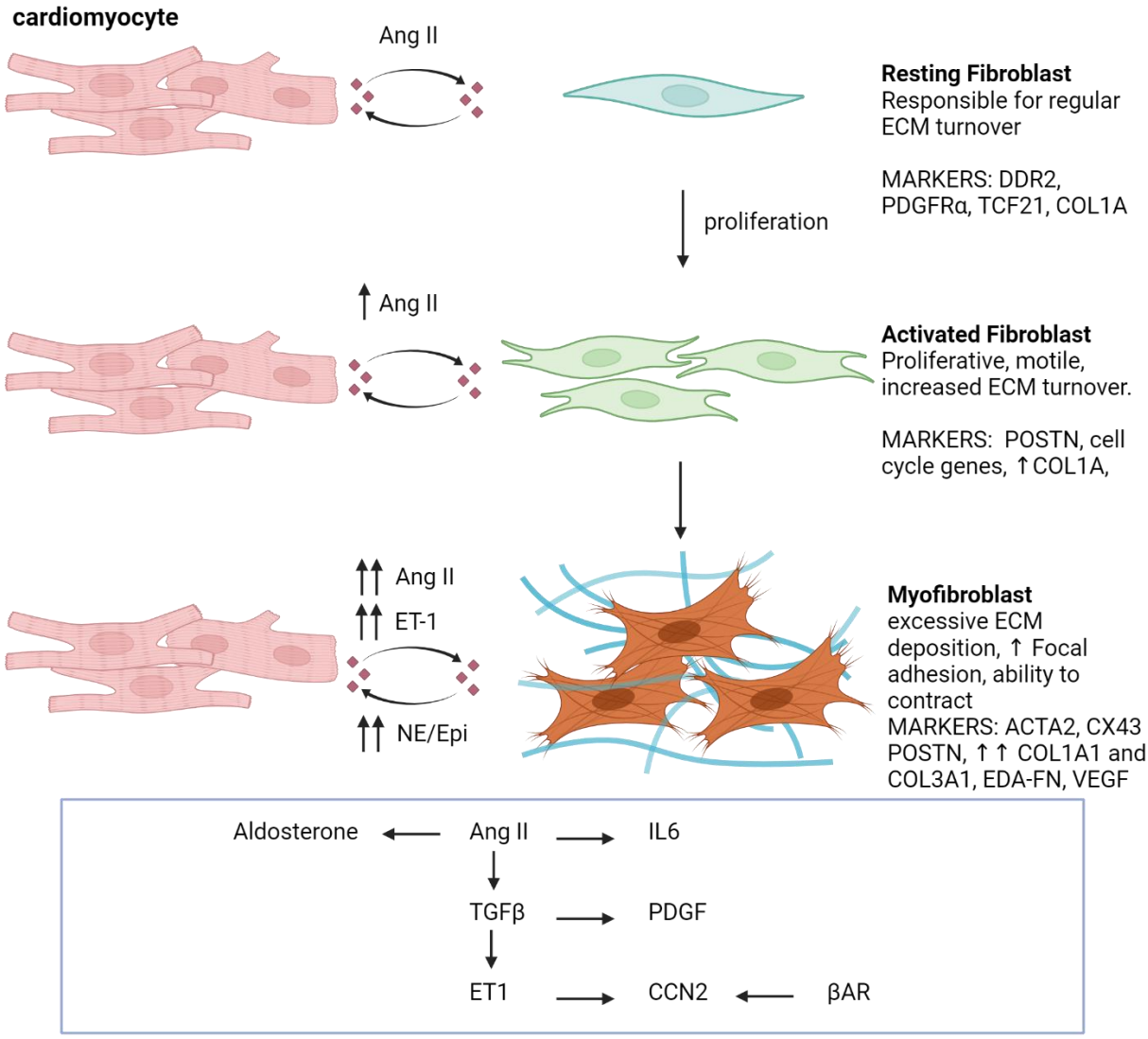


***Figure 1: Activation of quiescent fibroblasts to activated myofibroblasts.***

Cross-talk between cardiac fibroblasts and cardiomyocytes is essential to cardiac functions and these interactions evolve as fibroblasts become activated. In their homeostatic state fibroblasts are responsible for normal turnover of the ECM and providing trophic support for cells in the myocardium. Following injury, an increase in Ang II and other mediators leads to activation of cardiac fibroblasts. Activated fibroblasts are proliferative, motile and secrete an increased amount of ECM to mediate healing and scarring for preservation of heart function. Ang II is believed to be atop the hierarchy of events that leads to an increase in other mediators that further drive activation of fibroblasts. Sustained innervation of fibroblasts by these mediators leads to conversion of fibroblasts into the myofibroblast phenotype. Ang II, angiotensin II; IL-6, interleukin-6; CCN2, connective tissue growth factor; PDGF, Platelet-derived growth factor; ECM, extracellular matrix; ET-1, endothelin-1; NE, norepinephrine; Epi, Epinephrine; TGF-β, transforming growth factor-β. [Created with BioRender.com.] Image reused under licence from (41).

## 1.5 AN OVERVIEW OF GPCR SIGNALING

GPCRs constitute the largest druggable receptor family, with approximately 36 % of the drugs prescribed on the market targeting GPCRs (63). GPCRs are 7 helix transmembrane-proteins with an extracellular N-terminus and an intracellular C-terminus. They mediate transduction of extracellular stimuli into intracellular responses. The receptors can be divided into five receptor families based on sequence homology and phylogenetic analyses. These classes are the rhodopsin, secretin, glutamate, adhesion and Class F frizzled family of receptors (64). The signal transduction by GPCRs mediates human physiological functions including smell, sight, taste, blood pressure and pain sensitivity. They may act as mediators of physiological responses such as cellular differentiation, proliferation, motility, and survival at a cellular level.

GPCRs have both ligand-independent constitutive activity and different activation states. They may or may not have constitutive activity based on the equilibrium between inactive and active states (65). As the name suggests, GPCRs transduce their signaling though heterotrimeric G proteins. The ability of G proteins to bind to GTP and GDP is what gives them their name. They exist in heterotrimeric complexes consisting of $\alpha$, $\beta$ and $\gamma$ subunits. Furthermore, G proteins exists in an "OFF" state when the G$\alpha$ subunit is bound to GDP and an "ON" state when bound to GTP (66). Diverse stimuli such as small molecules, peptides, ions, osmotic pressure, and mechanical strain lead to conformational changes in the receptor which then leads to subsequent conformational changes in the G protein heterotrimer. The G$\alpha$ subunit exchanges its bound GDP molecule for GTP (67). This exchange causes the GTP-bound G$\alpha$ subunit and its cognate G$\beta\gamma$ subunit to dissociate and signal via their own distinct downstream pathways. Signal transduction

is terminated upon hydrolysis of GTP by the α subunit and then the reassociation of the Gα subunit with Gβγ subunits. There are 21 known Gα subunits which can be classed into 4 groups: Gq, $G\alpha_{stimulatory}$ (Gs), $G\alpha_{inhibitory/olfactory}$ (Gi/o), and Gα12/13(68). The Gq family signals via phospholipase C (PLCβ) which cleaves membrane-bound phosphatidylinositol 4,5–bisphosphate (PIP2) to inositol 1,4,5–triphosphate (IP3) and diacylglycerol (DAG). IP3 leads to release of intracellular calcium through its action on its receptor, IP3R. Both $Ca^{2+}$ and DAG can lead to activation of plasma membrane-bound protein kinase C (PKC) which phosphorylates downstream effector molecules (69-71). Gs signaling leads to activation of the enzyme adenylyl cyclase (AC), which then produces the second messenger cyclic AMP (cAMP). cAMP then activates PKA which subsequently phosphorylates different substrates downstream of it to dictate cellular behaviours (72). Conversely, Gi signaling inhibits adenylyl cyclase thus reducing the cellular pool of cAMP, thus dampening Gs signaling. G12/13 signals via Rho GTPase (71).

Gβγ subunits can act as a guanine nucleotide dissociation inhibitor to stop spontaneous release of GDP under basal conditions (73, 74) Gβγ subunits can interact with diverse signaling effectors, including ion channels (e.g., Kir 3 $K^+$ channels), protein kinases and transcription factors (75, 76). Notably, there are five Gβ subtypes, and 12 Gγ subunits which form obligate Gβγ dimers, thus making a plethora of different signaling modalities possible (66). For an overview of GPCR signaling pathways, please consult Figure 2.

Activation of receptors can lead to both G protein- and β-arrestin-dependent signalling. β-arrestin signalling is often mediated by G protein-coupled receptor kinases (GRKs). Upon agonist stimulation, GRKs are recruited to the plasma membrane where they phosphorylate the C-terminus tail of the receptor, thus creating a scaffold for β-arrestin to bind and activate β-arrestin dependent signalling via ERK or other protein kinases, receptor internalization or desensitization and

internalization of the receptor. This is reviewed in detail here (77, 78). Through a phenomenon known as biased signaling, different ligands may preferentially stimulate or inhibit a subset of signaling pathways mediated by a given GPCR. This opens an avenue to the development of therapeutic compounds that preferentially promote signaling pathways that are cardioprotective while inhibiting those detrimental to myocardium function. One such example of an approved therapeutic that shows bias is carvedilol which is a β-adrenergic receptor (βAR) antagonist that is used in treatment of heart failure patients, but has a unique profile compared to other β-blockers. In HEK 293 cells, it antagonized Gs-mediated signaling by the βAR while stimulating β-arrestin-mediated signaling (79).

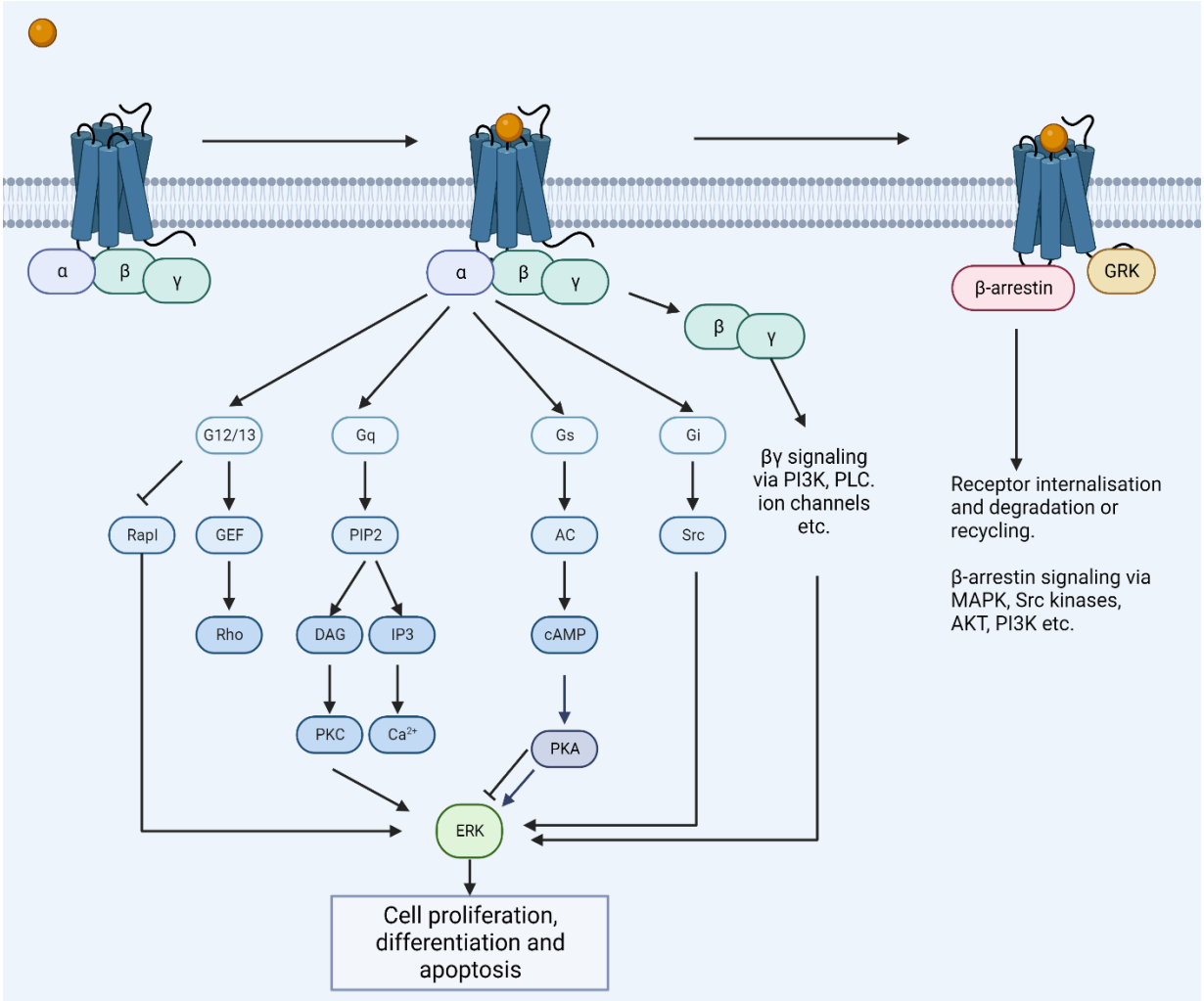


***Figure 2: GPCR signaling pathways modulate ERK signaling.***

Binding of a ligand to the receptor leads to dissociation of the heterodimer, whereby the Gα subunit can signal via their respective effector molecules and modulate ERK signaling. Gβ signaling can also activate ERK through some of it signaling partners e.g., Src kinase and PLCβ. Eventually GRKs will phosphorylate the C-terminal tail of the receptor forming a scaffold for β-arrestin to bind and initiate β-arrestin signaling pathways and/or receptor desensitization, recycling, or degradation. Image adapted from (80). [Image made using BioRender].

GPCRs reside in different subcellular domains in addition to the cell surface- endosomal, nuclear, and mitochondrial, as well as nanodomains within these subcellular components. The localization of receptors and where these signals are delivered is essential to study. For example, endosomal cAMP was shown to differentially impact gene transcription and phosphorylated proteins in comparison to plasma membrane cAMP. Notably, similar amounts of cAMP production at the endosomal compartment had more pronounced effect than plasma membrane changes in cAMP (81). This location bias also reflected in activation of protein kinases such as Raf1 (upstream of ERK) whose activation was differentially regulated based on cAMP localization. One impact of localization of intracellular nanodomains is seen in cardiomyocytes using FRET biosensors targeted to different microdomains. In healthy adult rat cardiomyocytes, $\beta_2$ARs were confined to the transverse tubule (surface invaginations), whereas in a rat model of chronic heart failure, $\beta_2$AR-mediated cAMP was redistributed more broadly to other domains and more diffusely located (82). Heart failure may thus be accompanied by changes in cAMP nanodomains, whether these are causative of disease progression remains unclear.

GPCRs activate several downstream effector proteins. Of interest, ERK is activated by both G protein- and β-arrestin signaling. The compartmentalization of the signals depends on which pathway elicited it, with β-arrestin stimulating cytoplasmic ERK signaling, and G protein signaling being linked to nuclear ERK signaling. G protein-dependent pathways have been connected to early, transient ERK1/2 activation, whereas β-arrestin has been linked to later, persistent ERK1/2 phosphorylation (83, 84). See Figure 2 for a summary of the diverse ways GPCR signaling modulates ERK signaling.

Crosstalk between GPCRs and other receptors and receptor pathways also adds another layer of complexity to signaling outcomes. For example, $\beta_2$AR transactivation of the EGFR was

shown to mediate ERK signaling and is possibly one of the main pathways which mediates adrenergic-mediated mitogenesis and DNA synthesis in cardiac fibroblasts (85). The Ang II type I receptors have also been shown to dimerize with EGFR. In neonatal rat cardiac fibroblasts, inhibiting EGFR using a small molecule inhibitor (AG1478) or introducing a dominant-negative EGFR mutant abrogated Ang II-mediated ERK signaling (86). This increase in ERK was mediated by a pathway that was independent of PKC, but dependent on $Ca^{2+}$/calmodulin-signaling.

Tissue and cell-type specific differences are important to factor in when studying GPCRs, as it is critical to study a GPCR in the relevant cell type of interest. For example, coupling partners can differ depending on the cell type. This is possibly due to differential expression of G proteins in distinct cell types or tissues. An example is the Ang II stimulation of ERK signaling downstream of Gi signaling by AT1R activation. However, in cardiomyocytes this increase is likely mediated by PKC signaling downstream of Gq signaling. Conversely in vascular smooth muscle cells, Src/Ras signaling mediates ERK signaling downstream of Ang II stimulation. This highlights that the same ligand may have different outputs depending on the cell type (87). For this reason, we have chosen to examine receptor signaling fibroblasts, rather than HEK 293 cells. We have chosen to examine three GPCRs involved in homeostasis of the heart and cardiac fibroblast function, namely the angiotensin 1 receptor, the endothelin receptor, and the β-adrenergic receptor. How each receptor contributes to fibrosis is discussed in more detail next.

## 1.6 ANG II SIGNALING IN CARDIAC FIBROBLASTS

Ang II is an octapeptide hormone that plays a role in blood pressure homeostasis. It is a component of the renin-angiotensin-aldosterone system (RAAS). It is derived from its precursor,

angiotensinogen which is produced by the liver, then subsequently cleaved in the kidney by the enzyme renin, forming the decapeptide angiotensin I. Ang I is subsequently converted to Ang II via cleavage of two residues by angiotensin-converting enzyme (ACE) in the lung and kidney or chymase from mast cells. Ang II has its effect on maintaining blood pressure via its actions on the adrenal gland, blood vessels as well as the brain. Furthermore, it can be further cleaved to form other active peptides such as Ang III, Ang IV, and Ang (1-7). Although initially thought to signal in an endocrine fashion alone, it has now been shown that tissues can have their own local RAAS, essential in supporting tissue function. This has been evidenced by expression of the essential components of the RAAS at both the level of mRNA (88) and functional peptides (89) in human cardiac tissue as well as other animals.

Within the cardiac system, Ang II has been shown to induce production of TGFβ1 and endothelin-1 by cardiac fibroblasts. These mediators have been shown to signal in a paracrine manner to induce hypertrophy in CMs (61). TGFβ1 itself, is also a potent activator of cardiac fibroblasts and could act in an autocrine manner to drive conversion of CFs to MFs (90, 91). Additionally, Ang II induces cardiac fibroblast proliferation and production ECM components such as collagen in rat cardiac fibroblasts both *in vitro* and *in vivo* (92-94). In human cardiac fibroblasts (ventricular and atrial), it has been shown that CFs express both ACE and the angiotensin type 1 receptor (AT1R) (95). Different aspects of Ang II signaling have been shown to be affected in DCM. For example, *ACE2* was shown to be downregulated in fibroblasts of hearts of DCM patients (26). *ACE2* is the gene encoding angiotensin converting enzyme 2, an enzyme involved in RAAS regulation by cleaving Ang II to Ang (1-7), an Ang II derivative that alter CF functions by counteracting Ang II-induced collagen synthesis (96, 97).

In the late 1980s, it became apparent that Ang II signals through two receptors, the Ang II type 1 receptor (AT1R) and the Ang II type 2 receptor (AT2R). The two receptor types share only 34 % sequence homology. In comparison to AT1R, the AT2R is less well characterised. Whether AT2R is a GPCR is debated owing to evidence AT2R does not appear to bind G proteins or β-arrestins as prototypical GPCRs (98, 99). Broadly speaking, AT1R and AT2R are believed to antagonize each other. The AT1R mediates vasoconstriction, and increases fibrosis, cell proliferation and cell growth and blood pressure while AT2R mediates vasodilation, reduces fibrosis, cell proliferation and growth and blood pressure. In terms of affinity to Ang II the affinity of both receptors is similar (3 to 4 nM) (100, 101). Unlike AT1R, AT2R has constitutive activity in its unbound state. Furthermore in HEK 293 cells it was shown to not undergo receptor internalization or desensitization in the presence of ligand (101).

In terms of receptor expression, it has been shown that the ratio of AT1R:AT2R in biopsies from non-failing hearts was 59:41. Moreover the level of AT2R increased a little over 3-fold at the level of protein and mRNA, and AT1R expression was decreased in the ventricles of failing hearts of DCM patients (102). AT2R was upregulated in failing hearts, thus changing the ratio of AT1R to AT2R in the failing heart, however total ATR expression levels remained unchanged according to these studies. Furthermore, this AT2R expression was seen in cardiac fibroblasts in close proximity to fibrotic regions. Ang II-mediated ERK signaling was greatly reduced in fibroblasts from failing hearts, however antagonizing AT2R led to an increase in Ang II-induced ERK activity (102).

The majority of established cardiovascular functions are governed by AT1R, which will be the main focus hereon in. AT1R has the capacity to interact with various G protein subtypes, including Gαq/11, Gαs, Gαi/o, and Gα12/13.- although it is suggested that it couples primarily to

Gq (103). Beyond its response to its primary ligand, angiotensin II, AT1R can also be triggered by mechanical stretching. There is substantial evidence demonstrating that rigid substrates can trigger the conversion of cardiac fibroblasts (CF) to myofibroblasts (MF), partially through AT1R involvement (54, 104). Cardiomyocyte-specific overexpression of the AT1R in a mouse model of myocardial infarction has been shown to induce cardiomyocyte hypertrophy and increase collagen deposition and interstitial fibrosis, suggesting that AT1R plays an important role in heart physiology (105). AT1Rs have been a promising target in the development of drugs for cardiovascular diseases, given their key role in cardiac physiology. AT1R activation by Ang II leads to secretion of collagen, TGFβ, IL-6 and other growth factors that promote cardiac fibroblast activation and proliferation. TGFβ1 is one of the most potent drivers of cardiac fibroblast to myofibroblast conversion that is released downstream of Ang II-mediated AT1R stimulation and can further increase synthesis of Ang II. Blockade of TGFβ1 and inhibition of ERK1/2 have been shown to abrogate Ang II-mediated fibrogenic effects (106).

Using human cardiac fibroblasts, it has been shown that sustained activation of AT1R receptor signaling via Gq led to an upregulation in production of growth factors like VEGF and TGF-β1 as well as ERK1/2 signaling. TGFβ receptor signaling is also known to activate ERK1/2-dependent pathways, inhibiting TGFβ signaling reduced ERK activation by Ang II suggesting that TGFβ in this case also plays a part in Ang II-mediated ERK signaling. furthermore, the increase in ERK was Gαq-mediated. However, activation of PKC was not involved in upregulation of VEGF, CTGF and TGFβ1 (107). Therefore, Ang II and TGFβ1 function as part of the same signaling network. AT1R can also signal via β-arrestin. Treatment of human cardiac fibroblasts with TRV120055 (an AT1R ligand that is Gαq-biased ligand) led to an increase in CF proliferation and production collagen and α-SMA. In contrast, treatment of CFs with TRV120027 (an AT1R

ligand that is β-arrestin biased) did not affect the levels of α-SMA or collagen as seen by western blot. Thus, the pro-fibrotic effects of Ang II appear to be Gαq mediated, and β-arrestin-independent (106).

Angiotensin receptor blockers (ARBs), employed in the treatment of heart failure patients, effectively impede both G protein and β-arrestin mediated pathways of AT1R. Delving into the realm of biased signaling offers a compelling avenue for advancing drug development. The allure of exploiting biased agonism continues to capture the attention of researchers, driven by compelling evidence that AT1R-mediated Gq signaling detrimentally impacts myocardial function, while β-arrestin signaling is cardioprotective through reduced cardiomyocyte death and heightened cardiac contractility during acute cardiac injury (108). However, the outcomes of the BLAST-AHF human trial, which evaluated TRV027 in cases of acute heart failure, did not reveal substantial benefits compared to a placebo (109, 110). Intriguingly, revisiting the assessment of this drug through a prolonged, chronic heart failure trial, mirroring methodologies employed in animal models, holds the potential to yield valuable insights (111).

Ang II regulates blood pressure cardiac function such as blood pressure changes and the baroreflex. The discerning factor between regular Ang II signaling and its pathological counterpart likely lies in its acuteness and extent of signaling in the myocardium. Ang II production and signaling is normally transient. However, the repercussions of prolonged and heightened levels of Ang II, prevalent in heart failure patients, result in unfavorable outcomes. Hence, it would make sense for there to be feedback loops that help distinguish the normal acute Ang II fluxes the heart experiences, from chronic Ang II that requires activation of fibroblasts as seen during a myocardial infarction. Consequently, the tight regulation of AT1R signaling necessitates built-in safeguards to restrain cardiac fibroblasts activation in typical signaling scenarios. Recent work from our lab

showed that the Gβγ subunit may act as a transient brake on AT1R signaling. It was shown that in rat neonatal cardiac fibroblasts, Gβγ subunits interact with RNA polymerase II (RNAPII) and negatively regulates gene transcription. RNAPII is a multiprotein complex that synthesizes RNA (mRNA, microRNA, and small nuclear RNA) from DNA. Knocking out Gβγ led to an upregulation of pro-fibrotic genes (e.g., the genes transcribing collagen I, serpine1, CTGF) at the level of mRNA and protein as revealed by both qPCR and mass spectrometry respectively (112). In HEK 293 cells, Gβγ signaling has been shown to mediate ERK signaling when coupled to Gαi and promote β-arrestin biased signaling, thus revealing further complexity for signaling pathways elicited by AT1R (113). This change in coupling to G protein coupling of the AT1R can be modulated by stretch/mechano-transduction, whereby stretch can stabilize receptor conformation that favour β-arrestin-biased conformation in AT1R conformation which can independently signal via β-arrestin (114). The increase in ERK signaling via Gβγ was also seen in neonatal rat cardiac fibroblasts, which are more physiologically relevant to study cardiac fibrosis compared to HEK 293 cells. In rat neonatal CFs, AT1R was shown to activate the ERK signaling and enhanced DNA synthesis via Gβγ-mediated signaling.

The complex nature of GPCR signaling is further exemplified by the crosstalk that occurs between distinct receptors, showcasing how these receptors can mutually influence each other by forming heterodimers. A compelling instance of this phenomenon can be observed in NIH3T3 fibroblasts, where the AT1R has demonstrated the ability to transactivate the epidermal growth factor receptor (EGFR), subsequently facilitating the activation of ERK1/2 through the action of EGF—the ligand for the EGFR. This EGF- induced ERK1/2 activation was abrogated by inhibiting AT1R with losartan. Conversely, in cells expressing the AT2R, the activation of ERK1/2 induced by EGF was notably diminished (115). Another level of complexity in ATR signaling

arises from the presence of both nuclear and extracellular pools of ATRs in cardiac fibroblasts. A study by Tadevosyan and colleagues showed that canine atrial fibroblasts expressed both AT1R and AT2R on the nucleus. Furthermore, the machinery needed for GPCR signaling was present in these nuclei, and the intracellular receptors were able to signal via calcium and nitric oxide (NO) dependent pathways. By using a model of chronic heart failure (CHF), the group showed that the concentration of intracellular Ang II as well as expression of nuclear AT1R increased in atrial cardiac fibroblasts of a canine CHF model in comparison to controls. To further study the implications of nuclear receptor pools, the group used a novel photo-releasable caged-Ang-II derivative, [Tyr(DMNB)$_4$]Ang-II. These are ligands that are caged/ inactive, however these ligands are cell permeable and can be 'uncaged' inside the cell using UV light - leading to the release of an active peptide inside the cells. Interestingly, their data also suggested that the plasma pool of receptors mediated proliferation of fibroblasts, while intracellular Ang II increased both collagen secretion and proliferation in fibroblasts (116). More recently, further work reported by Dallagnol and colleagues, used caged Ang II in as well as caged biased Ang II analogues to interrogate intracellular ATR signaling in rat cardiac myofibroblasts. Their findings revealed that that intracellular Ang II or with G protein-biased Ang II analogues led to collagen secretion, while caged β-arrestin ligand did not elicit collagen release. Taken together, thus suggests that intracellular and cell surface receptors may be distinct therapeutic targets. The presence of other GPCRs including ETR (117) and adrenergic receptors (118, 119) has been reported in cardiomyocytes, thus showing that different receptors are expressed. Figure 3 shows how we imagine these receptors may play a role in disease progression.

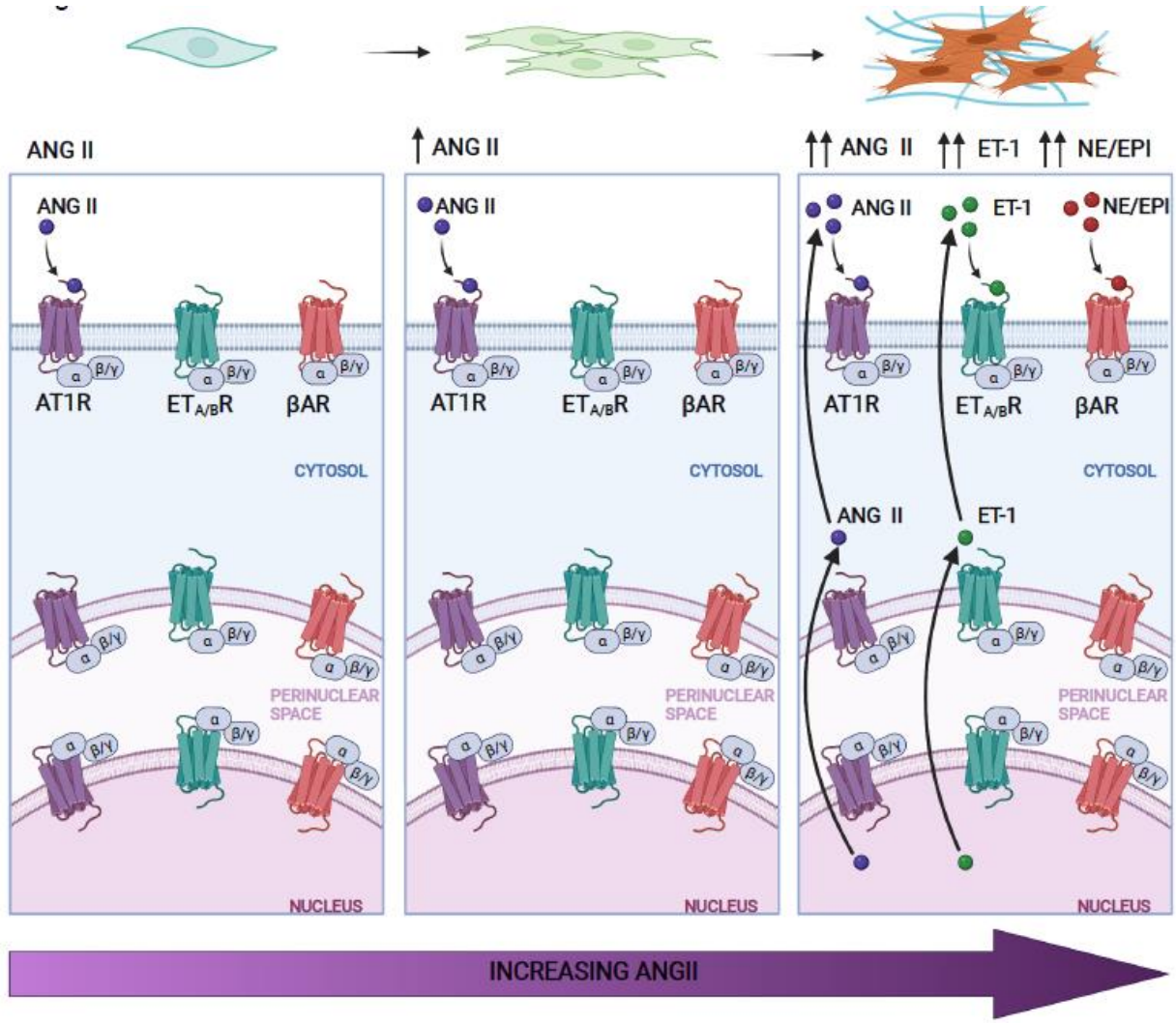


***Figure 3: Distinct pools of intracellular and extracellular receptors in cardiac fibrosis may mediate different cellular outcomes.***

As cardiac fibroblasts become activated the expression of different ligands that modulate cardiac fibroblast function in the myocardium changes. Endothelin-1 (ET-1), Angiotensin II (Ang II), Norepinephrine (NE) and Epinephrine (Epi) secretion within the myocardium increase as activation increases. These ligands are synthesised by cardiac fibroblasts and can be secreted by cardiac fibroblasts or possibly activate an internal pool of receptors eliciting different signaling pathways and outcomes depending on the pool of receptors. [Created with BioRender.com.] [Republished with permission from (41)]

## 1.7 ENDOTHELIN-1 SIGNALING IN CARDIAC FIBROSIS

Endothelin-1 is a peptide that is primarily produced by the endothelial cells but also by cardiomyocytes and cardiac fibroblasts. Its effects include vasoconstriction, cell adhesion, and fibrosis across various tissues (120). In both human and rat cardiac fibroblasts, ET-1 has pro-fibrotic effects by inducing proliferation, collagen production and α-SMA expression indicating heightened fibroblast activation (60). Notably, cardiac fibroblasts can produce ET-1, influencing cardiomyocyte hypertrophy in a paracrine manner or affecting fibroblast function in an autocrine manner (121). It has also been suggested that CFs can produce endothelin that stimulates the intracellular pool of receptors (see Figure 3), with its expression being induced by ET-1 via a ROS/ERK/AP-1-dependent pathway in human atrial MFs (122). While the presence of a nuclear pool of endothelin receptors have been shown in in cardiomyocytes, the presence of nuclear ETRs in fibroblasts has yet to be confirmed(123).

ET-1 signals through two receptors: endothelin receptor type-A (ETAR) and type-B (ETBR), with ETBR being predominant in rat and adult cardiac fibroblasts (124, 125). When ET-1 binds to its receptor, it prompts the separation of Gq and Gβγ subunits. This event triggers Gq signaling, which in turn activates PLC, leading to the cleavage of membrane-bound PIP2 into IP3 and DAG. IP3 can cause an elevation in intracellular calcium through its receptor on the endoplasmic reticulum, while DAG can activate protein kinase C (PKC), culminating in the activation of the ERK signaling cascade (126). Inhibition of ET-1 induced ERK1/2 signaling led to a reduction in fibroblast activation, myofibroblast conversion and cell proliferation. In human CFs, ET-1 has its proliferative and collagen-production inducing effects effect via the $ET_AR$/Gq/ERK signaling pathway (60).

Circulatory and myocardial ET-1 levels are elevated in heart failure patients and heart failure animal models (127, 128). In the explants of patients with idiopathic DCM, the concentration of the ET-1 peptide and the density of $ET_AR$ were markedly increased (129). After myocardial infarction, both Ang II and TGFβ1 are markedly increased in heart (130, 131), and studies have shown that both of these peptides can upregulate ET-1 synthesis at the level of mRNA in neonatal rat cardiac fibroblasts (61). Moreover, in a mouse model of hypertension, it was demonstrated that Ang II-induced cardiac fibrosis and hypertrophy relied on endothelial cell-derived ET-1—being the primary ET-1 producers. Specifically, in mice with vascular endothelial cell-specific ET-1 deficiency (VEETKO), Ang II-induced expression of TGFβ, collagen I and III, and CTGF was diminished, highlighting their dependence on ET-1. Additionally, VEETKO mice exhibited lower ERK1/2 activation, leading to reduced CTGF expression. Notably, CTGF induction by TGFβ necessitates ERK signaling in fibroblasts. These findings underscore the interconnectedness of signaling pathways, suggesting ET-1's potential modulation of the TGFβ/ERK1/2/CTGF pathway and its role as a crucial factor in Ang II-induced fibrosis. (132).

Blocking ET-1 signaling has been investigated and shown to provide benefits in animal models of heart disease. In a rat model of deoxycorticosterone acetate (DOCA)-salt hypertension, antagonizing ET-1 signaling via the ETAR increased fibronectin deposition. Fibronectin is a component of ECM that can form bridges between collagen and cells and plays a role in cell-ECM connections in the remodeling heart. ET-1 also mediated upregulation in metalloproteases and collagen deposition in these rat hearts (133). Administering bosentan (an antagonist of both ETRs) improved hemodynamics and reduced cardiac output in patients with severe heart failure. Despite this, there was no improvement in remodeling and one consequence of antagonizing ETR was a

reflexive increase in circulating ET-1 and RAAS system activation. Furthermore, a major cause of concern was fluid retention observed in patients treated with bosentan (134). Although these clinical results were underwhelming, perhaps understanding the effects of ET-1 on different cell types and perhaps cellular organelles could lead to better targeting of therapeutic agents targeting the receptor, as opposed to imposing whole organism effects which could affect perfusion of different organs and adversely affect other organ systems.

There is evidence that ET-1 mediated proliferation is dependent on ET-1 acting as a co-factor for $\beta_2$AR signaling. Turner and colleagues showed that ET-1 treatment of human CFs did not stimulate proliferation, however ETAR inhibition, antagonized $\beta_2$AR-induced proliferation (135). Adrenergic receptor signaling is discussed in the next section.

## 1.8 BETA-ADRENERGIC SIGNALING IN CARDIAC FIBROSIS

Chronic adrenergic receptor signaling is a prominent feature in failing hearts. It is initially a compensatory mechanism; whereby sympathetic tone is increased in the myocardium in an effort to increase cardiac output. However, prolonged activation has deleterious effects on cardiac function which have been studied extensively in CMs and to some degree in CFs.

Although $\beta_1$AR is the predominant receptor type on CMs, the $\beta_2$AR seems to be the subtype that is predominantly expressed in rat and human cardiac fibroblasts (136, 137). In rat neonatal and adult cardiac fibroblasts, $\beta_2$AR was expressed at high levels, while levels of $\beta_1$AR were negligible (137). Activation of $\beta_2$AR signaling using isoproterenol ($\beta$AR agonist) increased secretion of IL-6 and proliferation but had no effect on the migration or $\alpha$-SMA expression in rat

cardiac fibroblasts. These isoproterenol-mediated responses were eliminated by the inhibition of ERK1/2 and Gαs in rat CFs. IL-6 has been shown to cause CF conversion to the MF phenotype as well as proliferation, and its release aids in bringing about isoproterenol induced proliferation in CFs (137). In primary cultured adult rat cardiac fibroblasts grown on plastic, $\beta_2$AR has also been shown to increase cardiac fibroblast autophagy. Given that chronic β-adrenergic signaling inhibits CM autophagy, whist increasing CF autophagy, the authors suggest that autophagy may serve a protective against chronic adrenergic stimulation (138).

In studies involving rat CFs grown on gelatin, βAR has been found to mostly signal through the Gαs pathway. Stimulation of $\beta_2$AR leads to an increase in cAMP followed by PKA activation. Stimulation of CFs with isoproterenol, led to activated ERK1/2 signaling via both G protein-dependent and independent pathways, with ERK signaling peaking between 2-5min. Additionally, chronic (but not acute) adrenergic signaling in human CFs results in $\beta_2$AR desensitization (136). In a study that compared CFs from non-failing and failing human ventricular fibroblasts, this desensitization was shown to be mediated by Gβγ-GRK. Rescuing this desensitization by using gallein to inhibit Gβγ-GRK, led to a restoration of isoproterenol-induced cAMP production (139). Elevated cAMP levels have been shown to reduce collagen secretion and potentially inhibit activation of TGFβ-stimulated fibroblasts (140, 141). Furthermore, Ang II has been shown to potentiate βAR increase of cAMP, through crosstalk of the Gq (AT1R) and Gs (βAR) signaling pathways. Treatment of CFs with both agonists, potentiated isoproterenol-induced reduction of collagen synthesis (142). It's important to note that cAMP can either increase or decrease ERK signaling depending on cellular context and this may lead to proliferation (reviewed here (143)) .

Finally, *in vitro* studies have demonstrated that ET-1 secreted by human cardiac acts as a co-factor for $\beta_2$AR-induced cardiac proliferation in myofibroblasts, although $\beta_2$AR stimulation did

not alter ET-1-mediated events. These effects are thought to be mediated through PKC signaling downstream of the ET-1 receptor (136). Additionally, βAR was also shown to increase expression gap junction protein (Cx43) in cardiac fibroblasts in response to isoproterenol, thus leading to a remodeling of the cell-cell interactions in the myocardium connection between CFs and CMs (144).

More recently, it became evident that the previously unexplored contributions of biological sex, is important when investigating $\beta_2$AR signaling in cardiac fibroblasts. Stimulation of βAR differentially affected male and female rates treated with isoproterenol. Isoproterenol caused an increase in PKA activation, collagen expression and βAR expression in cardiac fibroblasts, as well as an increased mortality for male rats. In contrast, female rats showed a decrease in receptor expression with no PKA activation in response to isoproterenol (145). This emphasizes the need to study fibrosis and consider biological sex in studies, as well as to consider the treatment for cardiomyopathies in light of the sex differences. Usually, the treatment strategy for heart disease follows the order in which the drug was discovered without regard to sex or any way to determine the best therapy suitable for a patient. We hope to address this issue by using hiPSC-CFs and hiPSC-CMs to help group patients into groups that can better direct the order of intervention based on different factors that include sex, phenotype, and age. The use of hiPSCs is discussed below.

## 1.9 MODELING FIBROSIS IN HIPSCS

Disease models have evolved over the years. Immortalized cell lines such as Chinese hamster ovary cells (CHO) and human embryonic kidney 293 (HEK 293) cells have been useful for the study of different signaling pathways. The drawback, however, is that these cells might

harbor a wide range of mutations and karyotypic anomalies, additionally the same cell lines can differ significantly between labs at different passages. Additionally, receptor signaling is cell-type specific. Taken together, investigating a heart condition in a kidney cell may lead to translational difficulty between tissue or cell types. A study looked at a mutation in a cardiac sodium channel (A735V-$Na_V1.5$) in hiPSC-derived CMs as well as in HEK 293T cells and *Xenopus* oocytes. In the study, they noted that hiPSC-derived cardiomyocytes revealed a leftward shift of sodium channel inactivation which was not seen in either *Xenopus* oocytes or HEK 293 cells. They postulated that this was due to a subunit in CMs that was lacking in HEK 293T cells. However, the heterologous system was useful in showing differences that were not cell-type specific, making them a useful tool (146).

No model is perfect for studying disease, it all comes down to selecting the best model for the purpose of the study. While animal models are valuable for examining pharmacokinetics, toxicity, and whole organism effects, variability exists in druggable GPCRs among species, as evidenced in histamine and adenosine receptors (147, 148). This variation has implications for their applicability to humans. Species-specific differences influence receptor pharmacology, exemplified by variations in A3 adenosine receptor sensitivity to antagonists and receptor cycling across rats, mice, and humans. This highlights the need to be cautious about directly applying findings from animal studies to humans (147). Consequently, there's a strong emphasis on studying GPCRs using relevant human cell models, with hiPSCs offering a promising avenue for such research.

Given the limited availability of heart tissue from patients, human pluripotent stem cells provide a scalable and patient-relevant technique for drug development and studying aspects of heart disease. The discovery that specific transcription factors such as the Yamanaka factors (Oct4,

Sox2, Klf4, and c-myc) induced stemness in adult somatic cells, transforming them into pluripotent stem cells with diverse differentiation potential, marked a significant breakthrough in heart disease research (149, 150). This innovation circumvented the previous bottleneck in studying heart disease, which relied on limited *in vitro* cultures of human cardiac cells sourced from biopsies, post-mortem tissue, or non-transplantable hearts. The Yamanaka factors possess the remarkable ability to reprogram adult somatic cells into pluripotent stem cells capable of differentiating into the three germ layers: endoderm, mesoderm, and ectoderm (149). The advantage of harnessing hiPSC technology is its capacity to leverage the uniqueness of each donor. By obtaining blood samples or skin biopsies from patients with the disease of interest, then inducing these terminally differentiated cells into pluripotent stem cells, it becomes possible to generate diverse cell types from various tissues. Induced pluripotency is achieved by inducing expression of pluripotent genes (e.g., Oct3/4, Sox2, Klf4, c-myc) using episomal or viral delivery methods. The use of hiPSC technology allows us to obtain different cell types pertinent to the disease of interest. While the process that induces stemness may erase epigenetic markers (151), it is essential to note that genomic mutations are preserved and recapitulated in the hiPSC-derived stem cell of interest. Consequently, hiPSCs have been employed to simulate cardiomyopathy associated with specific mutations such as *LMNA*(20), *RBM20* (152, 153), and *TNNT2* (gene enoding cardiac troponin T) (154), to name a few (For a more comprehensive review of DCM mutations that have been studied using hiPSCs, refer to sources (155, 156)).

As the availability of human cardiac tissue from patients is extremely limited, fibroblasts derived from human pluripotent stem cells serve as an evolving technology to study physiological and pathophysiological functions of fibrosis in human heart diseases and help us model fibrosis in a dish. Given the relatively simple and non-invasive method for sample collection, hiPSCs offer

us the opportunity of building a large bank of donors to study disease in a larger population. Furthermore, hiPSCs can be an avenue to personalized medicine where we can cluster patients into pheno-groups which can be used to advise the best treatment method. As part of a larger project, the “Heart-in-a-dish” project, we have collaborated with the McGill University Research Centre.

## 1.10 ERK AS AN INTEGRATOR OF SIGNALS THAT MODULATE CF CELL STATE

The extracellular signal-reduced kinases (ERK) pathway is activated by a wide range of stimuli ranging from GPCRs (e.g., Gβγ and PKC activated via Gq signaling), growth factor and cytokine receptors (e.g., EGFR, FGFR), viruses and oncogenes. ERK1 and ERK2 (collectively called ERK1/2) integrate signals from several pathways and transduce these signals to modulate gene transcription and important cell functions like proliferation and differentiation. Key molecules in the ERK/MAPK signaling pathway include the small G proteins Ras which activates Raf kinase through swapping GDP with GTP, Raf, which then activates MEK1/2, and ERK1/2 which is activated by MEK1/2. In their inactive state, ERKs are anchored in the cytoplasm by MEK. Activated ERK can translocate to the nucleus where it can phosphorylate transcription factors and other mediators (157). Inhibiting this pathway has been used in treatment of certain cancers and has been proposed for hypertension. Tissue explants from failing hearts have shown that ERK activity is increased in the failing myocardium. Whether elevated ERK is a protective mechanism or cause of remodeling is not yet understood. However, ERK activation is proposed to be beneficial for cardiomyocyte survival, for example ERK is beneficial to cardiomyocytes in

pressure overload induced hypertrophy (158). The effects of ERK signaling on cardiac fibroblasts varies and the findings are explored below.

Several studies have suggested that inhibiting ERK may be beneficial for limiting fibrosis. *In vivo*, cardiac fibroblast specific knock out of GSK-3α in mice led to less CF to MF activation coupled with reduced ECM gene expression. GSK-3α appeared to have its effects by lowering ERK activation, suggesting ERK inhibition as a possible target for treating fibrosis (159). Sustained AT1R stimulation led to an increase in pro-fibrotic genes in via Gαq/TGF-β/ERK signaling, again pointing to ERK inhibition leading to favourable outcomes in cardiac fibrosis.

In contrast to these findings, Rubino et al. (160), showed that treating cells with SW033291 (an inhibitor of 15-PGDH, an enzyme that degrades eicosanoids) led to an increase in hydroxy eicosatetraenoic acid (12-HETE). 12-HETE, acting through its receptor, GPR1, effectively mitigated fibrosis through a mechanism involving an increasing ERK signaling. Both SW033291 and 12(S)-HETE prevented TGF-β–induced activation of adult rat ventricular fibroblasts as well as normal human CFs. Additionally, these treatments were able to reverse persistent activation of CFs taken from human failing hearts. This effect was also observed *in vivo*, where the authors used an Ang II infusion fibrosis model and demonstrated that intervention with SW033291 led to a reduction in fibrosis in these mice through an ERK-dependent pathway.

Interestingly, in the same study that identified SW03329 as a potential anti-fibrotic target, during the initial screening for compounds that could block TGFβ1-induced expression of α-SMA in adult rat ventricular fibroblasts, some of the hits were compounds that had differential effects on ERK signaling. Whereas SW033291 appeared to lead to an increase in ERK signaling, the other

hits included PLX7904, a Raf inhibitor, and sotrastaurin, a potent and selective pan-PKC inhibitor that, both of which reduce ERK signaling.

Sotrastaurin, being a pan-PKC inhibitor, was identified as a promising candidate to inhibit activation of CFs in response to TGFβ1 signaling. PKC is known to act downstream of growth factor receptor signaling and Gq signaling. However, the literature on the effects of blocking PKC has yielded conflicting results regarding its role in cardiac fibroblast (CF) remodeling. One study with contrasting findings involved the treatment of primary adult cardiac fibroblasts with phorbol 12-myristate 13-acetate (PMA), a compound that potently activates PKC. Remarkably, this treatment resulted in a 50% reduction in α-SMA expression, alongside decreased mRNA levels of periostin, type I collagen, and type II collagen. These findings collectively suggested a beneficial role for PKC activation in mitigating fibrosis. This contrast in results may have been sex-specific, given that this second study used female rats. Alternatively, it could underscore the need for a deeper understanding of how PKC and ERK collectively impact fibroblast activation states.

Protein Kinase C (PKC) isoforms can be categorized into classical PKCs (α, βI, βII, and γ), which require both diacylglycerol (DAG) and calcium for activation, and novel PKCs (isoforms: δ, ε, η, and θ), for which only DAG is required for activation. Notably, inhibiting classical PKCs inhibited the ability of phorbol 12-myristate 13-acetate (PMA) to reduce the expression of αSMA in cardiac fibroblasts, suggesting that classical PKCs play a role in regulating cardiac fibroblast trans-differentiation and periostin expression. On the other hand, novel PKCs appeared to regulate cardiac fibroblast proliferation and collagen synthesis. In adult fibroblasts, novel PKCs reduced collagen secretion and proliferation through PMA-induced activation of ERK1/2, indicating that different PKCs mediate distinct aspects of fibrosis (161). However, it is important to note that this increase in ERK was seen 30 min after treatment with PMA, whereas

αSMA and proliferation were assessed at 48 hours. Thus, it would be essential to examine ERK dynamics at different timepoints along the 48 hours to understand its implication in the observed phenotype.

Several studies have proposed ERK as a target for fibrosis. However, the evidence is conflicting as to whether inhibition or potentiation of ERK is beneficial as demonstrated in the examples above. Although ERK signaling is seen to be upregulated in the hearts of HF patients, whether this upregulation is a driver of disease or rather a reflection of the heart's attempt to mitigate the effects of the deteriorating myocardium is unclear. What further complicates interpretation is that ERK signaling is not a matter of simple upregulation or downregulation of ERK. ERK can encode signaling outcomes in features such as signaling amplitude, frequency, onset, and duration (162). Different factors such as the receptor and signaling pathway that it elicits the response will modulate these features. Furthermore, what level of the signaling pathway you inhibit could lead to different outcomes. For example EGFR can lead to ERK activation via the Raf/MEK/ERK pathway, in a study by Albeck and colleagues (163), they reported that inhibiting MEK led to a reduction in ERK amplitude while targeted inhibition of EGFR decreased the frequency of ERK activity transients.

Other determinants of ERK signaling may include microdomains where ERK signaling takes place. For example, substrate stiffness has been shown to modulate ERK signaling with softer substrate stiffness dampening ERK activation by lowering the amplitude and frequency of ERK (164). This effect was shown to be related to substrate stiffness affecting receptor expression as well as spatial distribution of EGFR. Given that the myocardial stiffness changes during disease progression, the landscape of receptors likely changes as disease progresses. ERK signaling likely differs between quiescent fibroblasts and myofibroblasts owing to changes in the microdomains

signaling takes place in. Utilizing FRET-based biosensors with a signaling localised to different subcellular compartment in both quiescent and activated fibroblasts is a possible avenue to decipher the seemingly conflicting findings regarding whether ERK signaling is advantageous or disadvantageous to cardiac fibroblast activation.

In lung myofibroblasts, it has been shown that FGF2 led to a dedifferentiation of myofibroblasts through a MEK/ERK pathway. This study suggested that perhaps ERK signaling induced by the fibroblast growth factor receptor by increasing proliferation which in part causes these cells to lose their α-SMA stress fibre network and revert to a morphology that resembled quiescent fibroblasts (165). Taken together all these studies suggests that ERK's ability to modulate fibroblast activation state can drive fibroblast either way along their activation spectrum.

Although no therapies as yet target fibrosis in the myocardium, there are therapies for pulmonary fibrosis which have not been shown to ameliorate cardiac fibrosis. Currently the only FDA-approved therapies for fibrosis are pirfenidone and nintedanib. The latter is a tyrosine kinase inhibitor that inhibits ERK signaling. Given recent finding that ERK signaling may cause reversion of myofibroblasts to a less activated state, it calls into question whether therapies like nintedanib can inadvertently lead to persistence of MFs in the myocardium owing to their inhibition of the ERK pathway (160).

Cardiac fibroblast specific inhibition of ERK may be better suited to earlier in the disease when upregulation of ERK could help disease progression by promoting proliferation, whereas ERK promotion may be essential in later phases of fibrosis where MFs are already in the myocardium. Myofibroblast are resistant to apoptosis, and it has been suggesting that ERK increase will revert them back to a less differentiated state in lung and cardiac fibroblasts (160, 165). All of this remains unknown. Understanding the effects of ERK signaling along the entire

activation spectrum of CFs becomes essential, as well as modelling ERK signaling dynamics over longer periods of time to look at spatio-temporal dynamics. To this end we propose the use of FRET-based biosensors as a tool that will allow spatial-temporal resolution of ERK dynamics to better understand mechanisms leading to fibroblast activation. Coupling FRET technology together with hiPSCs allows us to use a model of ERK signaling in health controls and patient cell lines. Unlike rat neonatal cardiac fibroblasts which tend activate quickly after removal from their organs, hiPSCs also allows us to work with a mostly quiescent cardiac fibroblast population and activate these cells to model fibrosis along the whole activation pathway of the cardiac fibroblast.

## 1.11 BIOSENSORS TO TRACK CELLULAR SIGNALING EVENTS

In contrast to traditional biochemical assays, which provide a static view of cellular signal events, genetically-encoded biosensors (GEB) report on the dynamics of cellular signaling pathways and allow us to resolve these signaling cascades spatially and temporally in live cells. GEBs can be based on either an intensiometric or a resonance energy transfer (RET) readout. Both sensors report on conformational changes as a result of changes in a sensing domain, which varies depending on the event of interest. Intensiometric sensors measure variations in the brightness of a single fluorophore, whereas RET sensors measure relative changes in the intensity of two moieties based on their proximity. RET sensors can be categorized based on their energy source, and among those widely used in research are bioluminescence-based sensors (BRET: which often employs Renilla luciferase as the donor) and fluorescence-based sensors (FRET: e.g., which us fluorophores such as cyan fluorescent protein as the donor). For our study, we opted for FRET biosensors due to their ability to enable the tracking of individual cells. The reader is referred to reference (166) for a more comprehensive review of biosensors.

FRET is a transfer of non-radiative energy from an excited donor fluorophore (e.g., CFP) to the acceptor fluorophore (e.g., YFP). The efficiency of this energy transfer depends on the distance between the fluorophores. It is inversely proportional to the sixth power of the distance between the donor-acceptor pair. FRET biosensors are composed of two fluorescent proteins fused to a sensing domain. Conformational changes in the sensing domain bring the sensors closer or further apart thus affecting the efficiency of resonance energy transfer.

These biosensor reporters can detect changes in calcium concentration, enzyme activity (e.g., kinases and GTPases), concentration of second messengers, and voltage. ERK1/2, PKA, PKC, DAG, IP3, CAMKII, cAMP are all examples of GPCR-signaling events can be detected with FRET biosensors (see (167)). By coupling FRET-biosensors and hiPSC-CFs we hope to be able to underpin the molecular pathways that are dysregulated in DCM pathology. Given that ERK signaling is altered in DCM and how the kinase plays a key role in integrating several signaling pathways downstream of GPCRs implicated in fibrosis, we decided to interrogate ERK to better understand disease pathology. The use of single-cell analysis helps us to garner information that would other wise be obscured by bulk analysis. For example, Jones-Tabah and colleagues showed that in primary striatal neurons, two ligands that activated PKA signaling and appeared to elicit the same response, had different populations of responding cells. Single-cell analysis revealed that one ligand produced a large number of weakly responding cells, whereas the other had a small population of cells that elicited a strong response in response to receptor stimulation may result (168). Furthermore, in this study we see that bulk-analysis can hide signaling modalities such as fluctuations when cells fluctuate asynchronously.

Lastly, as previously mentioned, looking at nanodomain signaling is an important aspect of studying disease pathology as localisation of cAMP and kinases has been shown to differ in

disease and health in a rat and mouse model of heart failure (82). FRET-based biosensors also can be tagged with different targeting sequences to target them to various organelles such as mitochondria, ER and nucleus, thus giving better spatiotemporal resolution of signaling.

To this end we have incorporated the FRET-based biosensor which can localise to the nucleus or cytoplasm for better comprehension of signaling dynamics. This compartmentalisation could help us tease apart the receptor pool that is essential in therapy, given that GPCR signaling may be compartment specific. Ultimately understanding compartmental consequences of signaling could open an avenue for old drugs to be repurposed and targeted to the pool of receptors that is apropos to disease pathology.

## 1.12 RATIONALE AND OBJECTIVES

Given the dearth of therapies that specifically target fibroblasts in dilated cardiomyopathy (DCM) and the pivotal role of CFs in modeling the myocardium before and after the onset of the disease, it becomes evident that understanding signaling events triggering fibroblast activation is critical. Evaluating perturbations in signaling in control or DCM patients could yield a deeper insight into the mechanisms driving fibrosis in DCM. Human induced pluripotent stem cells (hiPSCs) provide a distinct advantage, enabling us to explore gender disparities due to our diverse pool of donors encompassing both males and females. Moreover, hiPSCs offer a pertinent cell type for disease modeling, carrying the mutations found in DCM patients. Our focus lies in harnessing the potential of hiPSC technology to enhance our understanding of fibrosis within the context of DCM. Our eventual goal is to categorize patients into pheno-groups, which could inform treatment strategies for patients. Moreover, this categorization has the potential to unveil unique molecular pathways that play a causal or significant role in the development of pathological fibrosis.

Subsequently, these insights could serve as a compass for drug development, allowing us to capitalize on the knowledge gained from patient clusters. As we delve deeper into patient clustering, the prospect of honing our search for effective therapies becomes increasingly precise and focused.

The overarching aim was to create tools to investigate disease etiology with the eventual goal of clustering patients into groups that can potentially impact drug development and therapy. To this end, in the current thesis, I undertook the three main aims. The first aim involved the validation of a previously established protocol for differentiating hiPSCs into quiescent fibroblasts and introducing it into our laboratory. To confirm successful differentiation of hiPSCs into cardiac fibroblasts, validation of hiPSC-CFs identity was carried out through qPCR and immunofluorescence to ensure the cells expressed key tissue-specific signatures. Importantly, the protocol's effectiveness was verified across various cell lines. Following this my second aim was to optimize the conditions for transducing biosensor expression in hiPSC-CFs. As proof-of-concept experiment, FRET-based biosensors were expressed in hiPSC-CF to report GPCR signaling events downstream of Ang II, ET-1, NE, and Epi treatment. Lastly, we used FRET-based biosensors to track ERK1/2 signaling downstream of AT1R and ETR stimulation in hiPSC-CFs derived from a healthy subject. We sought to characterize the concentration-dependent dynamics of these ligands in hiPSC-CFs, exploring how cells respond both at the individual cell level and globally to varying concentrations of Ang II and ET-1.

# 2 MATERIALS AND METHODS

## 2.1 REAGENTS

Unless stated otherwise, common lab reagents were purchased from Sigma-Aldrich. Cells were treated with phorbol-12-myristate-13-acetate (PMA-, Cedarlane 10008014-1) reconstituted in DMSO was used as a direct protein kinase C (PKC) activator; angiotensin II (Sigma, A9525) prepared in water, endothelin-1 (Bachem, H6995.0001) prepared in acetic acid (Fisherbrand, 351270-212); isoproterenol (Sigma Aldrich, I6504) and norepinephrine (Sigma Aldrich, A9512) prepared in water.

Reagents used for differentiation and hiPSC maintenance and differentiation are specified below:

| **Reagent** | **company** | **Catalogue number** |
|---|---|---|
| Accutase | Sigma-Aldrich | # A6964 |
| Advanced DMEM/F12 medium | Life Technologies | # 12634-028 |
| B27 Supplement Minus Insulin | Life Technologies | # A1895601 |
| mTeSRPlus media | STEMCELL | # 100-1130 |
| mTeSRPlus5 x supplement | STEMCELL | # 100-0276 |
| Fetal Bovine Serum | Gibco | # 26140079 |
| Fibroblast Growth Medium | Cell Applications | # 116-500 |
| GlutaMAX | Gibco | # 35050-061 |
| GSK3 inhibitor CHIR99021 | Cayman Chemical | # 13122 |
| Matrigel Matrix | Corning | # 354277 |

| | | |
|---|---|---|
| Recombinant Human FGF2 Protein | peprotech | # 100-18B |
| Retinoid acid | Sigma | # R2625 |
| ROCK inhibitor (Y27632 2 HCl) | Selleckchem | # S1049 |
| RPMI 1640 medium | Gibco | # 11875-119 |
| TGFβ inhibitor (SB431542) | STEMCELL | # 72234 |
| Wnt inhibitor, IWR-1-endo | Tocris Bioscience | # 1614 |
| Wnt inhibitor, IWP2, | Selleckchem, | #S7085 |
| CryoStor® CS10 | STEMCELL | #07930 |

## 2.2 CELL LINES

The use of hiPSCs in this thesis was approved by the McGill University Health Centre Research Ethics Board. hiPSC lines were generated from blood samples collected from both male and female subjects who were recruited at the McGill University Health Centre cardiology clinic as part of the "Heart-in-a-Dish" project (REB approval HID-B/2020-6362). Family members of patients or volunteers who were in good health and had no known cardio-pulmonary disease served as the control subjects. The generation of hiPSC lines were done by the Cecere Lab (MUHC-RI). Briefly, peripheral blood mononuclear cells (PMBCs) were grown in StemSpan SFEMII supplemented media (STEMCELL Technologies, CA), then were reprogrammed into iPSCS using the Epi5™ Episomal hiPSC Reprogramming Kit (Thermofisher, USA) along with the Neon Transfection System (Invitrogen) to introduce Oct4, Sox2, Lin28, Klf4, and L-myc. The electroporation parameters used were 3 pulses, 10 ms, 1650 V. HiPSCs were validated by 1) colony morphology; 2) alkaline phosphatase; 3) immunofluorescent staining and RT-qPCR for pluripotency markers (e.g., Nanog, SSEA4, SOX2, Klf4, Tra 1-60) and 4) trilineage differentiation

assay to validate the ability of hiPSCs to differentiate into the three germ layers (i.e ectoderm, mesoderm and endoderm (Ida Derish, data not shown)) (169). RT-qPCR and karyotyping were also used to validate the chromosomal integrity of the cell lines (Dr. Kyla Bourque, data not shown). Cells-lined with the prefix HID were provided through the "Heart-in-a-Dish" initiative described above.

The AIW002-2 hiPSC line was provided to us by the Montreal Neurological Institute through the Open Biorepository, C-BIGR. This hiPSC line has previously been validated by examining expression of pluripotency gene/protein, tri-lineage differentiation as described in (170).

The cell lines used in this thesis are outlined below:

| Cell line | Abbreviation | DCM | Sex | Age range | Race |
|---|---|---|---|---|---|
| HID04004 | HID-04C | No | Female | 40-45 | Caucasian |
| HID040019 | HID-19D | Yes | Female | 40-45 | Caucasian |
| AIW002-2 | AIW | No | Male | 37 | Caucasian |

***Table 1: Cell lines used in study.***

## 2.3 CELL MAINTENANCE

HiPSCs were plated on 100mm dishes (VWR, 10062-880) coated with Matrigel and maintained in mTeSR Plus media with media changes every second day and double fed on weekends. Spontaneously differentiated cells were scraped off at every media change to ensure that the cells were of good quality. When the cells reached 80% confluency they were passaged or plated for differentiation.

*Passaging*: For maintenance of hiPSCs, 100mm dishes were coated with a 1:100 dilution of Matrigel matrix in cold DMEM/F12 then left to polymerize at 37˚C for at least one hour. Cells were washed once with DMEM /F12 that had been previously warmed to 37 ˚C then incubated

with 5mL of Gentle Cell Dissociation Reagent (GCDR) at room temperature for 5-8 minutes. The Gentle Cell Dissociation Reagent was aspirated from the dish, and the cells were rinsed once with 5mL of DMEMF12 and left in 10 mL DMEMF12. The cells were gently scraped and collected into a 15 mL tube (1mL of cell suspension was placed into a 15mL tube for a 1:10 split ratio). A glass pipette was used for pipetting iPScs to avoid spontaneous differentiation of cells. The cell suspension was then centrifuged for 3 minutes at 1,200 rpm. The DMEM/F12 was aspirated from the test tube and the pellet was resuspended by gently pipetting up and down 2-3 times in 2mL mTeSR Plus media and the cell suspension was transferred to a Matrigel-coated plate with a final volume of 8mL mTeSR Plus. All cells were kept in a humidified cell culture incubator set to 37˚C and 5% $CO_2$. hiPSCs and their derivatives were routinely screened for mycoplasma contamination. hiPSCs used in this study were mycoplasma free.

## 2.4 DIFFERENTIATION OF HIPSCS INTO HIPSC-CFS

*Coating of plates:* All work in this thesis using hiPSCs and their derivatives was done on plates coated with Matrigel. Dishes were coated with a 1:100 dilution of Matrigel matrix in cold DMEM/F12 then left to polymerize at 37˚C for at least one hour before cells were used. For 100mm dishes, 5mL of media was used to coat the plate, for 12-well plates 500µL of media was used, and for 6 well plates, 1mL of media was added per well to coat the bottom. Coated dishes were wrapped in parafilm to avoid evaporation and kept at 4 ˚C for up to a week before use.

*Differentiation*: To ensure the quality of cells used, only hiPSCs between passages 2 to 8 post-thawing, were differentiated into cardiac fibroblasts following a protocol previously described by Zhang et al. (171, 172). Briefly, only good quality hiPSCs that had minimal spontaneous differentiation were used (no more than 5%). HiPSCs were scraped to remove

spontaneously differentiated cells and were rinsed twice with DMEM/F12 before being dissociated using Accutase. The cells were seeded at a density of 40 000-500 000 cells (depending on the cell line) onto Matrigel-coated 12-well dishes in 2mL mTeSR Plus media supplemented with Y-27632-HCl (Rho kinase inhibitor). The cells were allowed to attach overnight, and then media was exchanged for fresh mTeSR Plus media. On Day 0 of the protocols, the cells were 80-90% confluent. Media was exchanged for 2mL RPMI 1640 media supplemented with B27 minus insulin and 6μM CHIR99021 (an activator of Wnt signaling). The time of the media change was recorded, and all media changes were done at the same time. On Day 2 media was exchanged for RPMI 1640 media supplemented with B27 minus insulin. On Day 3, the cells were treated with 2 mL RPMI 1640 media supplemented with B27 minus insulin and 5μM IWP2 or IWR-1 (Wnt inhibitor). On Day 5 the cells were treated with RPMI 1640 media supplemented with B27 minus insulin. On day 6, the cells were replated into a 6-well plate (Thermo Scientific, 140675) at a 1:12 split ratio (~ 20,000 cells per $cm^2$) in 2mL Advanced DMEM/GlutaMAX medium containing 5 μM of CHIR99021, 2 μM of retinoid acid, 5 μM of Y27632 (ROCK inhibitor), and 1% FBS. Cells were incubated at 37˚C in 5% $CO_2$ overnight to allow cells to attach. On Day 7, media was exchanged for 2 ml of Advanced DMEM/GlutaMAX medium containing 5 μM of CHIR99021 and 2 μM of retinoid acid per well. At Day 9, the media was changed to 2 ml of Advanced DMEM/GlutaMAX medium per well. At Day 11 cells were epicardial cells and replated on a 6 well plate in Advanced DMEM/GlutaMAX medium containing 2 μM SB431542 (a TGFβ inhibitor) and 1%FBS + 5 μM rock inhibitor. The cells were seeded onto a Matrigel-coated cell culture dish at a split ratio of 1:3 to 1:6. The plate was incubated at 37˚C at 5% $CO_2$ overnight to allow cell attachment. The following day (Day 12), the medium was exchanged for 2mL Advanced DMEM/GlutaMAX containing 2 μM of SB431542. At Day 14 cells were confluent and replated

to drive them down the fibroblast differentiation line. Cells were seeded at 2 wells of 6-well plates per dish, in 100 mm dishes coated with Matrigel. The media used was fibroblast growth medium with 20 ng/ml of FGF2 and 10 μM of SB431542. Thereafter, the media was changed every 2 days for 2 ml freshly prepared fibroblast growth medium with 20 ng/ml of FGF2 and 10 μM of SB431542. At Day 20, and each other day thereafter, the media was changed to 2 ml per well of fibroblast growth medium with 10 μM of SB431542. At this staged we had quiescent CFs which could be passaged (a 1:3 ratio was used for passaging), frozen down for long-term storage, or collected for characterization. Zhang et al. (171) report that cells can preserve a quiescent state (~5% αSMA+ cells) until passage 5, therefore all signaling experiments used cells at passage 4 at the most when they were imaged. >89% of the cells were hiPSC-CFs (VIM+) as assessed by immunofluorescent staining.

*Freezing cells:* The cells were frozen at ($15cm^2$ per vial) and cryopreserved in CryoStor CS10 medium (1ml/vial). The hiPSC-CFs were frozen at passage 1 in CryoStor® CS10 (STEMCELL #07930) (1ml per vial). In brief, hiPSC-CFs in 100 mm dish were detached using 4ml Accutase for 5-10 minutes at 37. Following this, 4 mL Fibroblast Growth Media was added to the dish and the cell suspension was collected into a 15 mL tube. The cell suspension was then centrifuged for 3 minutes at 1,200 rpm at room temperature. The supernatant was aspirated from the test tube and the pellet without disturbing the cell pellet. Cells were resuspended by gently flicking the tube. 4mL of CryoStor® CS10 was added to the tube and 1 mL of cell suspension was transferred to each cryovial. Cells were frozen using a standard slow rate-controlled cooling protocol ( -1°C/minute in a -80°C freezer) to maintain cell viability. Cells were moved to liquid nitrogen for long term storage within 48-96 hours after freezing.

*Thawing cells:* Cells were quickly thawed by shaking the vial gently in a 37°C water bath. The vial was removed when a small pellet of frozen cells was available. 1mL warmed media was added to the tube and the cell suspension was collected into a 15mL test tube containing 8mL warmed Fibroblast Growth media. The cell suspension was then centrifuged for 10 minutes at 1,200 rpm at room temperature. Supernatant was aspirated from the test tube, taking care not to touch the pellet. The cells were then resuspended by flicking the tube. 2 mL of fibroblast growth medium with 10 μM of SB431542 was added to the test tube. Cells were then plated in Matrigel coated 100 mm dish with 8mL media, for a final volume of 10mL fibroblast growth medium with 10 μM of SB431542. The cells were allowed to attach overnight, and media was changed every second day thereafter. The maintenance media for fibroblasts hereon consisted of fibroblast growth medium supplemented with 10 μM of SB431542.

## 2.5 CELL FIXATION, IMMUNOFLUORESCENT STAINING AND HIGH-CONTENT IMAGING

hiPSC-CFs at passage 1 or 2 were seeded at a density of 20 000 cells/well into 96-well black optical bottom imaging plates (Thermo Scientific, 165305) coated with Matrigel. The cells were allowed to attach overnight, and then they were fixed in warmed 2% paraformaldehyde prepared in PBS for 10 minutes. Cells were then washed twice with PBS and permeabilized with 0.3% Triton X-100 in PBS for 10 minutes and then blocked using 5% bovine serum albumin (BSA, Bioshop, 9048-46-8) solution in PBS for an hour at room temperature. Cells were then incubated with primary antibody in 5% BSA in PBS solution overnight at 4°C mRNA extraction and RT-qPCR. The following day, the cells were washed twice with PBS and incubated with the secondary antibody in PBS containing 5% BSA for 1-2 hours at room temperature. The cells were then

washed twice with PBS and on the third wash cells were incubated with 1 μg/mL (1:10 000 dilution) of Hoechst (Thermo Scientific, H3570) in PBS for 10-20 minutes at room temperature. The cells were subsequently imaged using the Operetta high content confocal microscope (Perkin Elmer, now Revvity) at 20X magnification. The following primary antibodies and dilutions were used. The following primary antibodies were used, and dilutions: anti-actin, a-Smooth muscle, mouse, (1:1000, Sigma #A2547), Anti-vimentin (D21H3) antibody, rabbit, (1:500, Cell signaling #5741S), Anti-endothelin-1 receptor, mouse (1:500, BD Bioscience # 611252)

The Secondary antibodies were Alexa 488 anti-mouse (1:1000; Invitrogen A11029) and Alexa 647 anti-rabbit (1:1000; Invitrogen A21245).

## 2.6 RNA EXTRACTION AND RT-QPCR

hiPSC-CFs were collected between Days 22 to 24 for RT-qPCR experiments. For RT-qPCR experiments, RNA was isolated from samples lysed in 1 mL TRI reagent® RNA Isolation Reagent (Sigma, T9424) and RNA was extracted as per the manufacturer's protocol. Isolated RNA was quantified using a NanoDrop microvolume spectrophotometer and treated with DNAse to digest any contaminant genomic DNA which could interfere with reverse transcription or lead to false positives. Reverse transcription was performed on 2 μg of RNA with random hexamer primers using MMLV-RT enzyme (Promega) according to the manufacturer's protocol.

Gene expression was quantified by RT-qPCR using BrightGreen 2X qPCR Mastermix – No Dye kit (Applied Biological Materials, MasterMix-S-XL) on a ViiA 7 Real Time PCR System (Applied Biosystems). Primers (supplied by IDT) were designed in-house using NCBI Primer

Blast and validated for specificity and efficiency before use. Ct values were normalized to the housekeeping gene, GAPDH, and fold-changes were relative to the housekeeping gene and quantified using the 2-ΔCt method. See table below for primer sequences:

| **Primer name** | **Sequence (5'→ 3')** |
|---|---|
| GAPDH | F: GGCAAATTCCATGGCACCGTCA |
| | R: ATCGCCCCACTTGATTTTGGAGG |
| VIM | F: AGCTACGTGACTACGTCCACCC |
| | R: AGAGGAGCGCGTGGCATACA |
| ACTA2 | F: AACAGGAATACGATGAAGCCGGG |
| | R: GAAGCATTTGCGGTGGACAATGGA |
| DDR2 | F: TCATGGCATCGAGTTTGCCCC |
| | R: ATTTCCATCCAGCACCTGTTTCCC |
| POSTN | F: AATCCAAGTTGTCCCAAGCC |
| | R: GCACTCTGGGCATCGTGGGA |
| TCF21 | F: GTCAACCTGACGTGGCCCTTT |
| | R: CGCGGTCACCACTTCTTTCAGG |
| COL1A1 | F: GCTTCACCTACAGCGTCACTGTCG |
| | R: AGAGGAGTTTACAGGAAGCAGACAG |

| | |
|---|---|
| AGTR1 | F: GATTGCTTCAGCCAGCGTCAG |
| | R: TTGGCTACAAGCATTGTGCGT |
| AGTR2 | F: CTGACCTTCCTGGATGCTCTG |
| | R: ACACACTGCGGAGCTTCTGTTG |
| ADRB1 | F: GGCAATGTGCTGGTGATCGTG |
| | R: CTCGCAGAAGAAGGAGCCGTAC |
| ADRB2 | F: GATGGTGTGGATTGTGTCAGGC |
| | R: AATGGCATAGGCTTGGTTCGTG |
| ADRB3 | F: TGGCCTCACGAGAACAGCTCTC |
| | R: ACGATGACCAGCAGGTTGCCTC |

***Table 2: Primer sequences used for RT-qPCR***

## 2.7 AAV TRANSDUCTION AND HIGH-CONTENT FRET MICROSCOPY

The FRET-based ERK1/2 protein kinase biosensors EKAR-EV were generously provided by Dr. Michiyuki Matsuda (173) and expressed with either nuclear localization (NLS) or nuclear export (NES) peptide sequence. These biosensors were introduced into an AAV compatible backbone, pENN-AAV-CAG-tdTomato (Addgene catalog #105554) as described in (155). All experiments used biosensors packaged in the AAV serotype DJ produced by the Neurophotonics Platform Viral Vector Core at Laval University, Quebec. AAVs were aliquoted into low-retention

Eppendorf tubes to minimize freeze-thaw cycles and were stored long-term at -80°C. Once thawed AAVs were not used after they were more than three freeze-thaw cycles.

The serotype selection kit offered by the Neurophotonics Platform was used to determine the optimal serotype for transducing hiPSC-CFs with. The AAV serotypes tested were 1, 2, 5, 6, 8, 9, DJ, DJ8. Based on these results, we chose to transduce hiPSC-CFs AAV serotype DJ.

*Transduction:* hiPSC-CFs at passage 1 or 2 were plated at a density of 500 000-100 000 cells per dish the day before transduction. On the day of transduction, the media was exchanged for 5mL Advanced DMEM/GlutaMAX which contained no serum to increase transduction efficiency. AAV was added to culture media using a multiplicity of infection of 20 000 viral genomes/cell and left overnight. The media was exchanged for 5 mL fibroblast growth medium the next day. The cells were imaged 3 to 5 days after transduction. Transduced cells were replated the day before imaging to ensure the cell density was similar for all measurements. Briefly, cells were seeded at a density of 20 000 cells/well into 96-well black optical bottom imaging plates (Thermo Scientific, 165305) coated with Matrigel that was diluted at a 1:100 ratio in PBS. The cells were allowed to attach overnight in fibroblast growth medium. On the day of imaging the cells were viewed under a microscope to assess morphology and if they were deemed healthy, they were washed 3 times with warmed PBS, and media was exchanged for 90µL HBSS without phenol red, with calcium, magnesium, and sodium bicarbonate (Wisent #311-513-CL). The cells were then allowed to re-equilibrate to the new media and to reduce the basal kinase activities of ERK for 2 hours prior to imaging in a humidified atmosphere of 37°C with 5% $CO_2$. Ligands used in FRET signaling assays were diluted in HBSS at a 10X concentration so 10µL would be added per a well for the final desired concentration.

[*Exception*: For the pilot experiment in section 3.5.6, the assay was performed in OptiMEM (Gibco, #31985-047) instead of HBSS as the media for imaging and drug dilution. All other assays

were done in HBSS to allow us to be able to compare between other assays performed on hiPSC-cardiac myocytes in the lab as part of the larger "Heart-in-a-Dish" project]

*Imaging*: Live-cell imaging of hiPSC-CFs was performed at 37°C and 5% $CO_2$ using an Opera Phenix high-content confocal microscopy system (Perkin Elmer, now Revitty). The cells were allowed to re-calibrate to the change in temperature for 20 mins prior to starting imaging. Image acquisition was done using a 20X water-immersion objective using a 425 nm laser for excitation of CFP. Emissions were detected with filters at 435-515 nm [cyan fluorescent protein (CFP)] and 500-550 nm [yellow fluorescent protein (YFP)]. The Perkin Elmer's Harmony software was used to setup experiment acquisition parameters. 11 or 12 fields were imaged per well for time-course experiments, with fields evenly distributed across the well. Initial baseline images were acquired before drug stimulation. Subsequently, the assay microplate was ejected from the system and the vehicle or drug solution was added directly to each well. Care was taken to not move the microplate during drug addition. The drugs were added with staggered timing to ensure that the images of each well were taken after the specified time, in order to cope with the imaging delay between the sequential imaged wells of the plate. Images were then acquired at the indicated time intervals for the pilot experiment images were acquired every 2.5 minutes up to 40 minutes after addition of drug. For the final concentration-response curves images were acquired every 2 mins for up to 30 mins after addition of drug. Approximately 12 fields were imaged per well for time-course experiments, with fields evenly distributed across the well.

*Image analysis:* Data was processed in R based on a previously published in-house single-cell analytical approach formerly applied to neuronal cultures, neonatal rat cardiomyocytes and hiPSC-CMs with minor modifications (155, 168, 174), as well as an analysis pipeline adapted by Dr. Karima Alim from previous published work by the Goedhart Lab (175). Perkin Elmer's Columbus image analysis software was used for image analysis. The "Find Nuclei" or the "Find Cells" tool was used to

identify transfected nuclei or cells using the YFP emission at 500-550 nm. The identified cells were filtered based on morphological parameters such as roundness and size so as to exclude apoptotic cells and cell debris. Fluorescence was then quantified from all remaining the cells and values exported to Microsoft Excel for bulk-analysis or R for single-cell data analysis. The FRET ratio was calculated as YFP/CFP and expressed as the percent change in FRET ratio relative to the baseline for each well (bulk analysis) or cell (for single-cell analysis). This measurement was termed %dF/F or %ΔF/F. The F in the denominator is the average basal FRET ratio for all cells in the same well for both bulk and single-cell analysis. Given that cells can drift slightly over the time-course some cells may drift out of view, therefore the image data was preprocessed using an analysis script written in R to track individual cells which appeared in all 16 timepoints (i.e., timepoint zero to the final time point post-stimulation). Objects were matched from timepoint to timepoint by using Cartesian coordinates of each object in the image. To make certain that the objects were matched correctly at each time point, we set a threshold for the distance an object can move from each time point and ensured that an object did not show a deviation in fluorescence intensity that was greater than 15%.

Single-cells from independent experiments were combined from independent experiments and combined into heat maps and response clusters visualized in this thesis. A time-series clustering algorithm provided by the TSclust package, and R's 'pam' function were used to cluster by magnitude of response (i.e. %ΔF/F) and time/kinetic, respectively (176). All data from all treatments was clustered together to allow for comparability between clustering patterns identified. The individual treatments were split and plotted as heat maps or bar plots indicating the percentage of cells in each cluster for each time point.

## 2.8 STATISTICAL ANALYSIS

To estimate $EC_{50}$ values we used a three-parameter logistic curve using GraphPad Prism. The average value per biological replicate was used for each concentration. A biological replicate was defined as the hiPSC-CFs obtained from a separate experiment carried out from hiPSCs to hiPSC-CFs. As log 0 is undefined, the response from the negative control has been entered as the lowest concentration on the dose-response graphs.

Statistical analysis for comparison in gene expression between hiPSCs and the cardiac fibroblast derived from them was done using a paired t-test in GraphPad Prism.

Immunofluorescent imaging analysis was done from a script in R, and statistics were calculated in GraphPad Prism.

Error bars on the graph represent the standard error of the mean (SEM) calculated using the following formula: $SD/\sqrt{n}$ where SD is the standard deviation of the dataset from the mean and n is the sample size. For the purposes of this study, sample size was counted as the number of replicates of the experiment (each experiment was performed either in duplicate or in triplicate).

# 3 RESULTS

## 3.1 VALIDATION OF PROTOCOL TO DIFFERENTIATE HIPCS TO CARDIAC FIBROBLASTS

The heart is the first functional organ to form *in utero*. It forms from the cardiogenic region of the mesoderm layer in an embryo and it starts beating around 21 days after fertilization(177). Pathways modulating heart development include BMP-4, Wnt, activin, nodal and, FGF signaling. To differentiate hiPSC into quiescent hiPSC-CFs, we used a protocol that uses small molecules to modulate Wnt signaling in a temporal fashion (171).

To comprehend the utilized protocol, it's important to grasp the fundamentals of Wnt signaling, which is briefly explained here. Essentially, Wnt ligands, belonging to a family of cysteine-rich glycoproteins that interact with their respective receptors to regulate essential cellular processes such as proliferation, differentiation, and migration (178, 179). To understand Wnt signaling, it's useful to consider its ON and OFF states. In the OFF state, cytoplasmic β-catenin is constitutively targeted for degradation by a complex that consists of the axis inhibition protein (AXIN) and Adenomatus polyposis coli (APC). This complex facilitates phosphorylation of β-catenin by glycogen synthase kinase 3β (GSK3β) and casein kinase 1α (CKIα). Phosphorylated β-catenin is subsequently targeted for degradation by E3 ubiquitin ligase β-trcp (180). Conversely, in the ON state, Wnt binds its receptors (Frizzled and LRP5/6), leading to the recruitment of the destruction complex (AXIN, GSK3β, CK1, APC) to the receptor (181). This prevents the phosphorylation of β-catenin, allowing its accumulation in the cell and subsequent translocation to the nucleus. Following this translocation, β-catenin partners with transcription factors, like T-cell-specific factor (TCF) and lymphoid enhancer-binding factor, to activate a Wnt-induced gene-

expression profile. For a more comprehensive review, the reader is referred to references (180, 182).

The differentiation protocol used in this thesis uses small molecules that regulate Wnt signaling, FGF signaling and ALK signaling. The development of the protocol was guided by the understanding of signaling pathways that undergo temporal modulation during the course of heart development (183). In the initial 6 days of the protocol, the approach follows the established GSK3 inhibitor and Wnt inhibitor (GiWi) protocol, steering cells towards the mesoderm lineage and further down the cardiac cell path. In the initial step, the Wnt signaling pathway is activated through the use of the small molecule CHIR99021, which inhibits GSKβ3. This inhibition prevents the phosphorylation and degradation of β-catenin, effectively activating β-catenin signaling. Subsequently, Wnt signaling is sequentially inhibited using a porcupine inhibitor, IWP2. This inhibitor targets porcupine, an enzyme responsible for the palmitoylation of WNT proteins. This modification is vital for the secretion of WNT proteins and their subsequent signaling via their receptors (184). Consequently, inhibiting porcupine leads to the suppression of Wnt signaling. At this stage, the cells assume the identity of cardiac progenitor cells, and if left undisturbed for a few days, they naturally differentiate into beating cardiomyocytes. However, our goal was to direct these cells towards an epicardial lineage- as this is the source of the majority of resident cardiac fibroblasts. To achieve this, we once again activated Wnt signaling by employing CHIR99021 to inhibit GSKβ3. Additionally, we initiate retinoic acid signaling using retinoic acid to further enhance the expression of epicardial genes. By Day 11, the cells have transitioned into epicardial progenitor cells, and at this point, we treated them with the ALK inhibitor, SB431542. This inhibitor serves a dual purpose: firstly, it supports the extended renewal of hiPSC-epicardial cells *in vitro*, and secondly, it hinders the transition of epicardial cells into the mesenchymal state,

thereby inhibiting epicardial-to-mesenchymal transition (Epi-MT) (185). In the final phase of the protocol, spanning the last 6 days, proepicardial cells are intentionally directed towards the cardiac fibroblast differentiation pathway. This is achieved by treating them with fibroblast growth factor 2 (FGF2) to drive a cardiac fibroblast gene expression signature. In parallel, SB431542 is added to the media to inhibit epicardial cells from differentiating into cardiac smooth muscle cells and pericytes which are also derived from the epicardial lineage (171). A visual representation of cells at Day 0, Day 11 (epicardial cells) and Day 20 (cardiac fibroblasts) is shown in Figure 4.

At day 20 onwards, different techniques were employed to characterize the cells: qPCR was used to look at gene expression, light microscopy allowed us to examine cell morphology, and immunofluorescent microscopy enabled assessment of both purity and protein expression. We used qPCR to validate whether hiPSC-CFs had a gene expression signatures typical of cardiac fibroblasts (refer to Table 3 for the specific gene panel examined). A comparison was established between our hiPSC-CFs and their hiPSC counterparts before differentiation, with all genes normalized to the reference housekeeping gene, *GAPDH*. As expected, the gene *NANOG* which is typically expressed by hiPSCs was turned off upon the differentiation of cells into cardiac fibroblasts, this change in expression was significant by paired t-test. Genes such as *VIM* and *ACTA2* displayed a significant increase in expression, as confirmed by paired t-tests. In the case of *DDR2*, *COL1A1* and *POSTN*, there was a discernible trend towards upregulation in hiPSC-CFs in comparison to their corresponding hiPSC samples at Day 0, although this trend wasn't statistically significant (Figure 5A).

When examined using light microscopy, the cells displayed the characteristic flat and spindle-shaped morphology typical of cardiac fibroblasts (Figure 5B). Additionally, cells were fixed and stained for vimentin and α-SMA. Vimentin is a type-IV filament protein that is a marker

of cardiac fibroblasts, and this allowed us to assess the percentage of cells that were cardiac fibroblasts. Nuclei were stained with Hoechst, and the percent of nuclei in cells expressing vimentin were assessed. Our results indicated that the protocol yielded >89% cardiac fibroblasts. In the case of the AIW cell line, the mean percent of hiPSCs on a dish over 3 separate differentiations was ≥92% cells being vimentin-expressing cells indicative of a cardiac fibroblast phenotype (Figure 5C). To quantify the percent of fibroblasts expressing vimentin, the criterion was that that was at least the proportion of the cell expressing vimentin was at the least the same size as the nucleus. However, this approach might have led to an underestimation of the number of vimentin-positive cells. While all cells did express vimentin, the orientation of cells in relation to the imaging plane could result in some cells not meeting the criteria of vimentin-expressed area being at least the same size as the nucleus. Additionally, we also measured α-SMA to access the percent of myofibroblasts in our culture. The percent of cells that were myofibroblasts at passage 1 on the dish (vimentin-positive cells expressing α-SMA stress fibres) expressed by myo-fibroblasts were <2% over 3 different differentiation of the AIW cell line. The developers of the protocol, Zhang et al. (171), report that the percent of cells remains under 5% up to passage 5. Hence, all experiments were done using fibroblast at passage 4 at the most to minimize the number of myofibroblasts. Furthermore, they were able to get a population of cells that was ≥90% which was consistent with our findings where the AIW cell line yielded ≥ 89% VIM+ cardiac fibroblast.

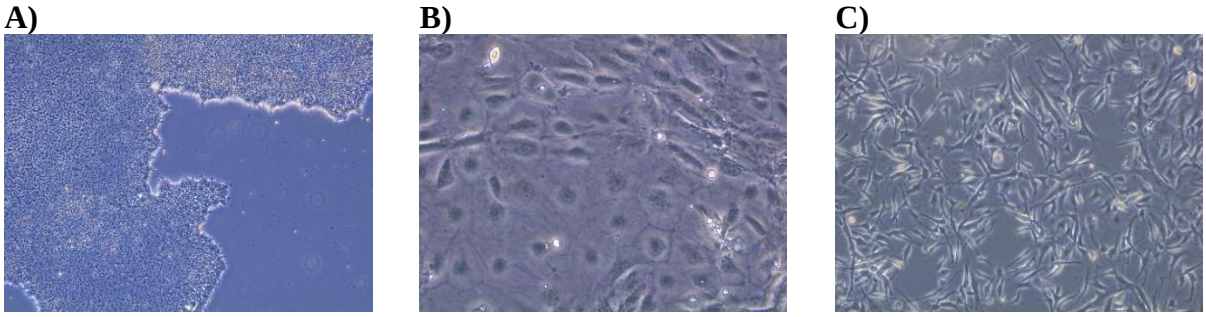


***Figure 4: Representative images of hiPSCs at Day 0, hiPSC-epicardial cells at Day 14 and hiPSC-cardiac fibroblasts at day 20 of our protocol. – AIW cell line***

(A) Day 0 cells show typical clusters and 'halo' border typical of hiPSCs. (B) Day 14 cells show cobblestone morphology that is in line with epicardial cell morphology. (C) At Day 20 we were able to see cardiac fibroblasts with the flat spindle shape that is typical of CFs. Images taken at magnification of 20X. Panels A-C represent images typical of three or more independent differentiations.

| Gene | Function |
|---|---|
| DDR2 (Discoidin Domain Receptor Tyrosine Kinase 2) | Tyrosine receptor kinase for several ECM proteins |
| AGTR1 (Angiotensin type II receptor) | Receptor we are interested in studying. |
| TCF21 (Transcription factor 21) | Epicardial marker, transcription factor; necessary for differentiation of CFs from proepicardial cells |
| VIM (vimentin) | Intermediate filament |
| ACTA2 (Actin Alpha 2, Smooth Muscle) | Contractile Intermediate filament-associated protein |
| COL1A1 (collagen 1) | Fibrous ECM protein that is part of structure. |
| POSTN (periostin) | Periostin functions as a ligand for integrins to support adhesion and migration. It is expressed in CFs in development and activated CFs. |
| NANOG (Nanog Homeobox) | Pluripotent stem cell marker. It is a transcription factor involved in stem cell pluripotency, cell proliferation and renewal. |

***Table 3: Function of genes expressed by cardiac fibroblasts.***

A)

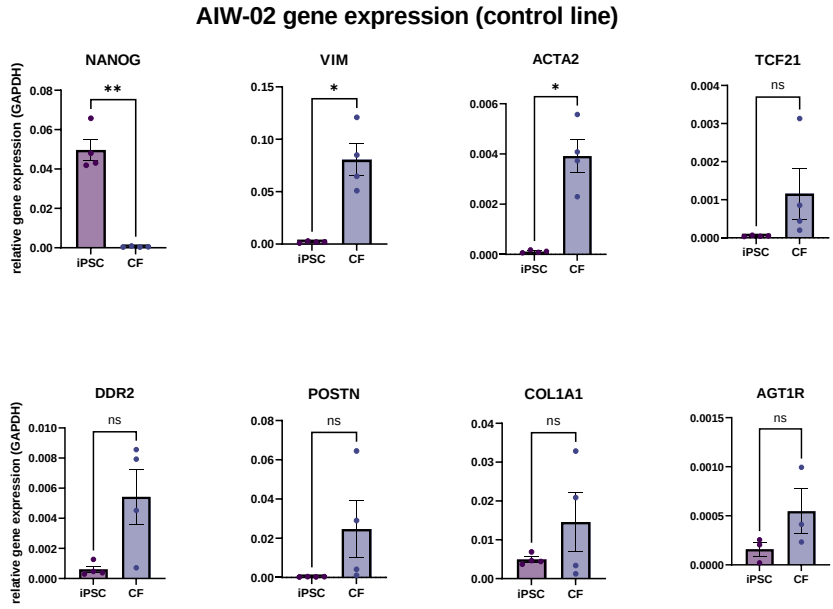


B)

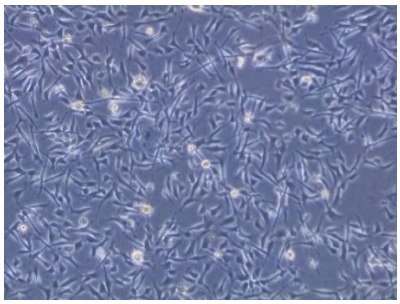

C)

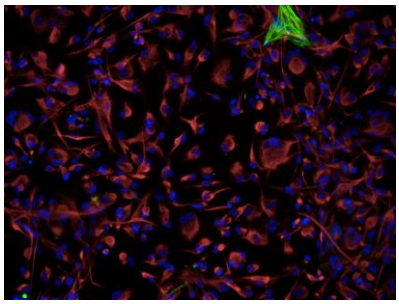


***Figure 5: hiPSC derived cardiac fibroblasts express morphological and gene expression patterns of fibroblasts.***

A) Differentiations of hiPSCs into hiPSC-CFs changes the mRNA signature of cells and turns off pluripotency genes and turns on genes that are typical of cardiac fibroblasts. Data represent means of three or more independent differentiations; error bars represent mean ± SEM. Two-sided paired t-tests were performed on hiPSCs at Day 0 and their CF derivative at Day 21-24. Asterisks represent significance levels: * $p \leq 0.05$, ** $p \leq 0.01$, *** $p \leq 0.001$. B) Light microscopy of hiPSC-CFs reveals that hiPSC-CFs have spindle shaped morphology typical of cardiac fibroblasts. Images serve as representatives from three or more separate and independent differentiations. C) Immunofluorescent imaging of hiPSC-CFs with nuclei stained with blue DAPI, vimentin in red and α-SMA (marker of myofibroblasts) in green. Immunofluorescent images are representative images from three or more independent differentiations.

## 3.2 THE PROTOCOL TO DIFFERENTIATE HIPSCS TO CARDIAC FIBROBLASTS WORKS IN CELL LINES FROM PATIENTS AND CONTROL SUBJECTS

Overall, our protocol consistently generated over 89% cardiac fibroblasts across various cell lines, with a notably low proportion of activated fibroblasts. To ensure the applicability of our protocol across different cell lines we used this protocol on 3 other cell lines (HID-04C and HID-19D and HID041100). HID041100 later on was shown to have an abnormal karyotype and it was excluded from further study. We evaluated the protocol by examining key genes, revealing a consistent pattern observed previously. In HID-19D and HID-04C, Nanog expression was downregulated, while critical genes typical of cardiac fibroblasts were upregulated as anticipated (Figure 6A and 6B). Morphologically, the cells exhibited the characteristic features of cardiac fibroblasts under light microscopy (Figure 6C). In HID04-C the percent of fibroblasts obtained using the protocol ranged from 89% to 98%, with a mean of 94% cardiac fibroblasts in a dish over 4 separate differentiations. Through immunofluorescent staining utilizing vimentin and α-SMA antibodies, we observed a lack of α-SMA stress fibers in HID-04C, indicating cellular quiescence (Figure 6D). In the case of HID041100 (cells not shown), the efficiency ranged from 90% to 96%, with an average of 93% across three distinct differentiations. Similar to HID-04C, the absence of αSMA stress fibers affirmed the state of cellular quiescence. Overall, our protocol consistently yielded more than 89% cardiac fibroblasts while maintaining a small proportion of activated cardiac fibroblasts.

A)

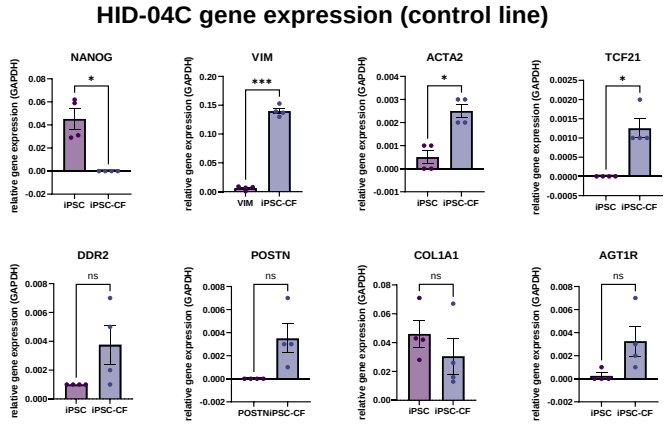


B)

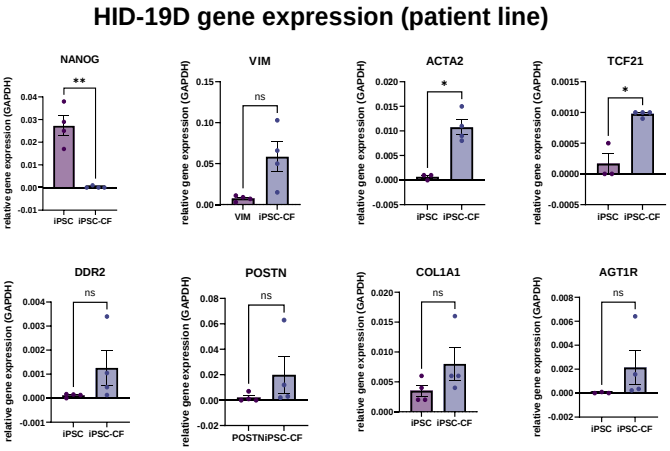


C)

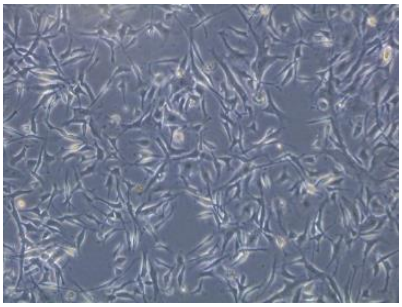

D)

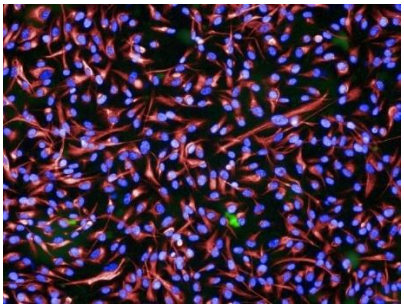


***Figure 6: Our differentiation protocol worked for different hiPSC cell lines.***

A and B) mRNA expression levels of key genes that change in expression as hiPSCs are differentiated into hiPSC-CFs. Data represent means of four independent differentiations; error bars represent mean ± SEM. One-way Paired t-tests were performed on hiPSCs at Day 0 and their CF derivative at Day 21-24. Asterisks represent significance levels: * $p \leq 0.05$, ** $p \leq 0.01$, *** $p \leq 0.001$. C) Images show the typical morphological features of cardiac fibroblasts as observed

under a light microscope for the HID-04C hiPSC-CFs. These images serve as representatives from four independent differentiations. D) Immunofluorescent staining of HID-04C cell line showing vimentin in red and α-SMA in green. It's worth noting that no cells exhibited α-SMA stress fibers characteristic of myofibroblasts in this specific cell line and in HID-19D. Immunofluorescent images are representative images from four independent differentiations.

## 3.3 PRELIMINARY RESULTS SHOW DIFFERENCES IN MRNA EXPRESSION OF *ACTA2* IN HID-04C (HEALTHY) VERSUS HID-19D (DCM PATIENT) DERIVED CFS

As a proof-of-concept experiment to show that differences were seen in hiPSC-CFs of control and DCM-hiPSC-CFs, we compared the expression of two genes whose expression is increased in activated fibroblasts (POSTN and α-SMA). In a rat model of DCM using a mutation in troponin IQ13, it was shown that matricellular proteins such as POSTN are increased in CFs well before fibrosis sets in (25), which is why we chose to look at POSTN. Furthermore, as cardiac fibroblasts become more activated, they produce α-SMA, which eventually becomes incorporated into stress fibres as fibroblasts become "terminally differentiated" into myofibroblasts. To see if there were differences in control line and patient cell line, we examined HID-04C and HID-19D, these were age-matched female control and patient lines. These were cells obtained from 4 separate differentiations for each cell line. There was a significant increase in α-SMA expression in the HID-19D patient cell line using a paired t-test (Figure 7B). There was no significant difference in periostin expression between the control and patient line, but the trend was similar (Figure 7A).

This finding was obtained by comparing only 2 cell lines and was simply an exploratory study to see if differences could be seen between a control and disease cell line.

A) B)

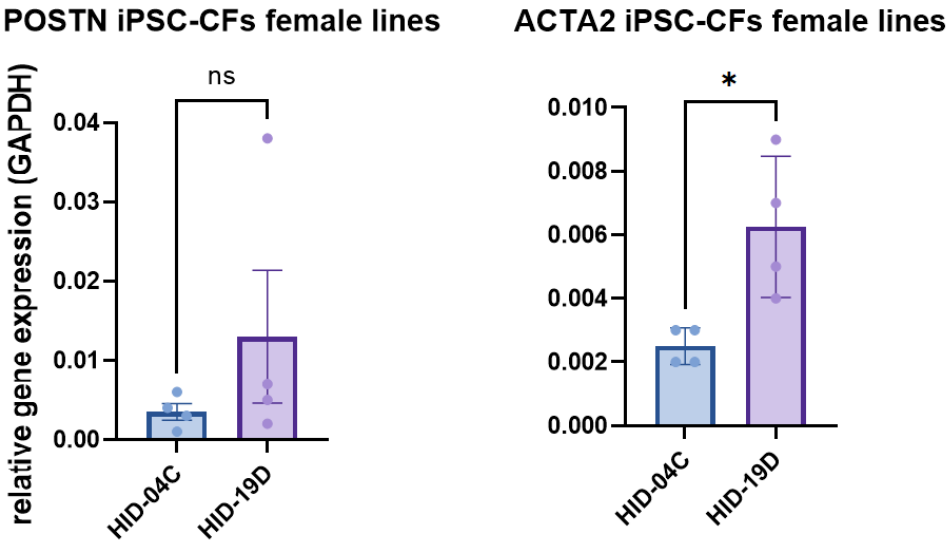


***Figure 7: Gene expression differences can be seen between in hiPSC-CFs from the HID-04C control line and the HID-19D DCM-patient hiPSC-CF.***

The cell lines compared are sex- and age-matched. A) Illustrates the mRNA expression of POSTN in hiPSC-CFs from both the HID-04C (control) and HID-19D (DCM patient) cell lines. B) Depicts the mRNA expression of ACTA2 in both the control and disease lines. Data represent means of four independent differentiations; error bars represent mean ± SEM. Two-tailed paired t-tests were performed on hiPSC-CFs at Day 21-24 for the respective lines. Asterisks denote significance levels: * $p \leq 0.05$.

## 3.4 IPSC-CFS EXPRESS ETR, ADBR1 AND ADBR2 AND AGT1R

In this thesis, we were interested in looking at signalling of GPCRs responding to Ang II, ET-1, and adrenergic agonists. It was important to verify that our cell did express the receptors of interest. To establish receptor expression, we employed immunofluorescence to validate ETR expression and utilized qPCR to quantify the presence of ATRs and β-adrenergic receptors. In the AIW cell line we confirmed ETR expression using immunofluorescent microscopy (Figure 8A). However, it is worth noting that caution is necessary when utilizing GPCR antibodies, as they often lack specificity, particularly when sourced from commercial suppliers. Unfortunately, our antibody has not been assessed in-house for specificity. However, in the next portion of the thesis we show that hiPSC-CFs do respond to Endothelin-1, thus confirming their expression of the ligand receptor. We also investigated the expression of different β-ARs in hiPSC-CFs in the male control AIW line (Figure 8B). As expected *ADRB3* was undetectable and there was a trend for *ADRB2* to have a higher expression than *ADRB1*, although this wasn't significant by ANOVA ($p=0.207$). However the trend is consistent with previous research that demonstrated the expression of both $\beta_2$ARs and $\beta_1$ARs in heart explants, with $\beta_2$AR being the predominant subtype in cardiac fibroblasts (138, 186). We also examined expression of both AT1R and AT2R in HID-05C and HID-19D (Figure 8C). The AT1R was expressed in both cell types, with AT2R was either not detected with RT-qPCR or expressed at very small quantities in comparison to AT1R. This is in line with findings where cultured rat cardiac fibroblasts exhibited lower mRNA levels of AT2R in comparison to AT1R (187).

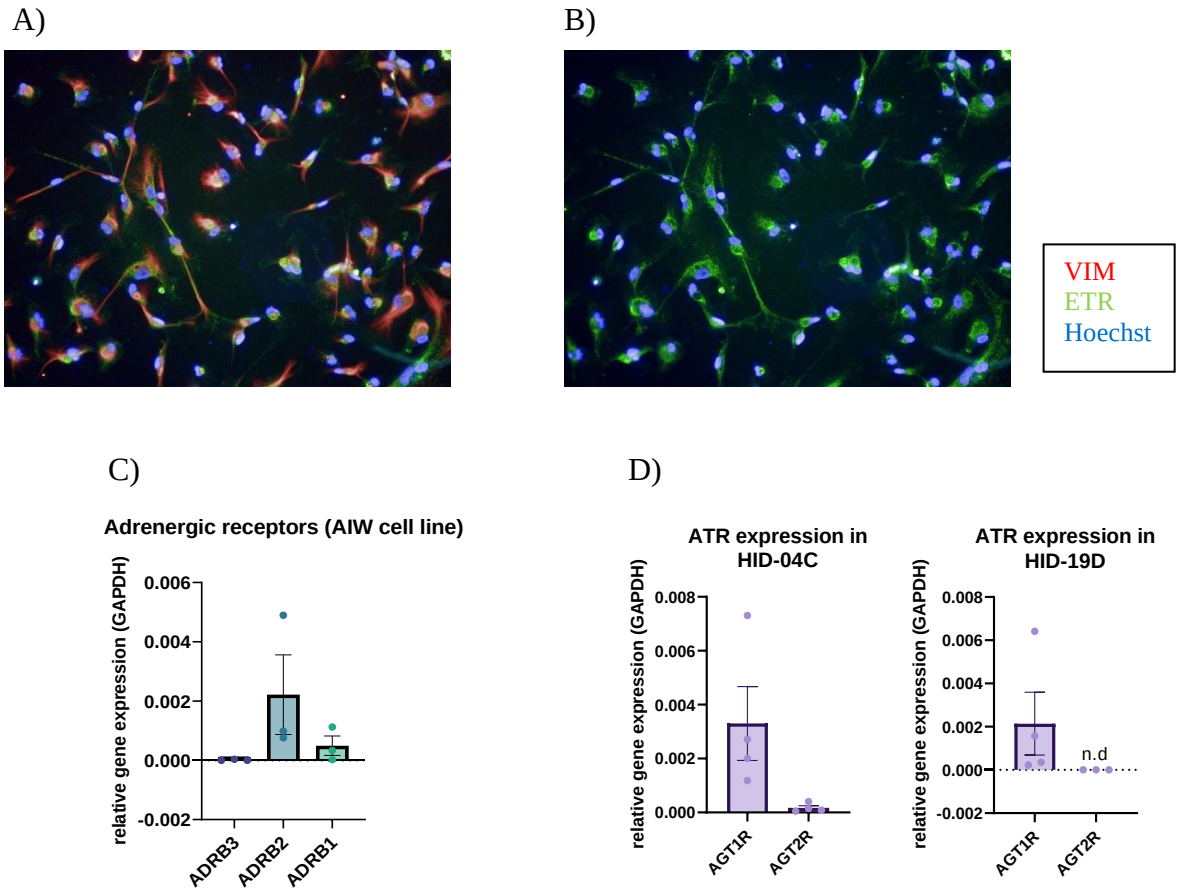


***Figure 8: hiPSC-CFs express angiotensin II, endothelin-1, and β-adrenergic receptors.***

A and B) Immunofluorescent staining of hiPSCs reveals that hiPSCs express endothelin receptors. Image A shows vimentin (red) co-stained with an antibody for the endothelin receptor (green). In B only staining for ETR is shown. In both images nuclei are stained in blue. B) hiPSCs express β2- an β1 adrenergic receptors. D) hiPSCs express mRNA encoding the AT1R and negligible amounts of AT2R (if any). Data represent means of three or more independent differentiations; error bars represent mean ± SEM. ANOVA was used to compare the means of adrenergic receptors. For ATR expression, two-tailed paired t-tests were performed on hiPSC-CFs at Day 21-24 for the respective lines. Both tests showed non-significance. ATR: angiotensin receptors; ETR endothelin receptors.

## 3.5 FRET SIGNALING TO PROFILE SIGNALING IN HIPSC-CFS

### 3.5.1 AAV/DJ is the best serotype for transducing hiPSC-derived cardiac fibroblasts

In order to express our FRET biosensors of interest, we cloned our biosensors in a plasmid under the ubiquitously expressed CAG promotor. We opted to use recombinant adeno-associated virus (AAV) to package our biosensor-containing vector. The recombinant AAVs used here are compact non-enveloped viruses classified within the *Parvoviridae* family. These viruses possess a genome size of approximately 4.7 kilobases and persist as episomal entities, avoiding integration into the host genome (188). Currently, eleven natural serotypes of AAVs have been identified, each showing different ability to infect specific tissues and cell-types (tropism)(189). As a first step, we focused on determining the most appropriate AAV serotype and conditions for delivering our biosensor into hiPSC-CFs. This was accomplished by optimizing the transduction procedure by considering factors such as serotype selection, optimizing the multiplicity of infection (MOI: represents the number of infectious particles per target cell), and determining the ideal transduction duration. Our experimentation involved transducing hiPSC-CF cells using seven different AAV serotypes (AAV 1, 2, 5, 6, 8, DJ, DJ8). Specifically, these cells were exposed to vectors encoding enhanced green fluorescent protein (eGFP) under the control of the constitutive CAG promoter. Varied MOIs (5,000, 10,000, and 50,000) and transduction durations (ranging from 24 hours to 7 days) were implemented. Following transduction under serum-free conditions, cell imaging was performed at 12-hour intervals for up to 7 days. Optimal eGFP expression levels were consistently observed starting at the 48-hour mark, maintaining stability throughout the 7-day period. Furthermore, we conducted microscopic assessments of cell viability, revealing morphological alterations associated with higher MOIs. A representative image of the expression of GFP in hiPSC-CFs at different MOIs is shown in Figure 9. A visual representation of GFP expression in

hiPSC-CFs across different MOIs is presented in Figure 9. The MOI was systematically adjusted to enhance biosensor expression while ensuring cellular health. Our iterative process led to the determination that the optimal MOI for our objectives was 20,000 (data not shown).

Despite testing AAV1, which had previously shown efficacy in transducing rat neonatal cardiac fibroblasts within our lab, it failed to achieve high transduction efficiency in our hiPSC-CFs, thus suggesting species differences. Conversely, AAVDJ and AAV2 exhibited the best transduction efficiency. Consequently, we continued to focus on these two AAV variants, evaluating their transduction efficiency in both a control and DCM-hiPSC-CF line to ensure that they worked in lines from different subjects. AAVDJ worked best for our hiPSC-CFs (data not shown). Therefore, we packaged our vector in AAVDJ. AAVDJ is a hybrid serotype created by combining different serotypes, it has been shown in the literature to have a higher transduction efficiency *in vitro* than any wild type (190).

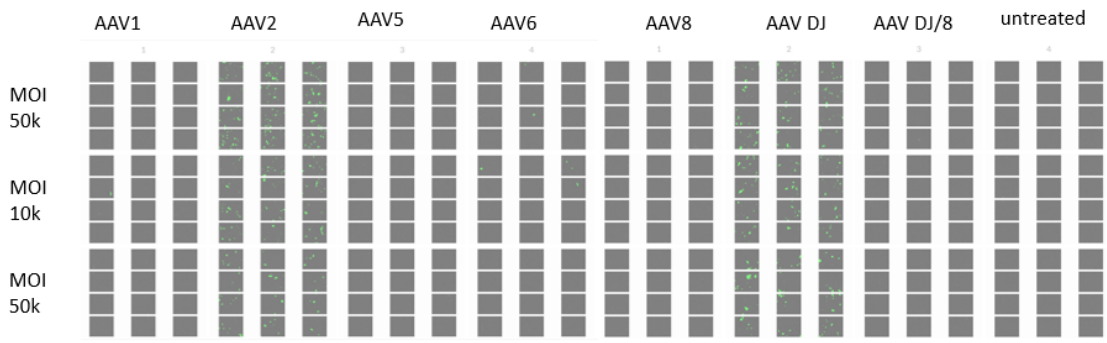


***Figure 9: Determining virus serotype for transduction of hiPSC-CFs.***

Fluorescent microscopy images depicting the delivery of eGFP into hiPSC-CFs using different AAV serotypes. hiPSC-CFs transduced at various MOIs revealed that AAVDJ and AAV2 were the best serotype foy hiPSC-CFs derived from HID0401100. These cells were imaged 96hrs post-transduction, and biosensor expression was stable up to 7 days post-transduction. Follow-up studies (not shown) was done using hiPSC-CFs from AIW and HID04041100 and AAVDJ was shown to outperform AAV2. Correspondingly, all biosensors in this study were packaged in serotype DJ.

### 3.5.2 Proof of concept experiment in (male control line) shows that hiPSC-CFs respond to Ang II, ET-1, norepinephrine and isoproterenol

Mitogen-associated protein kinases (MAPKs) are activated by GPCRs, or growth factor receptors and they integrate signaling pathways from different ligands and receptors and effect among other things, changes in cellular proliferation, apoptosis, and differentiation. We sought to examine ERK1/2 signaling in hiPSC-CFs. To visualize these events over time we used a FRET-based biosensor EKAREV, tagged with a domain that localizes the biosensor to either the nucleus or the cytoplasm. The biosensor consists of a donor CFP molecule fused to a YFP domain. In between the 2 linkers is an ERK binding domain and a substrate ERK domain, which can be phosphorylated by ERK. Phosphorylation of the substrate domain by ERK leads to the WW domain binding to the phosphorylated region, causing a conformational change in the biosensor whereby the fluorophores become closer in distance, thus increasing transfer of resonance energy from CFP to YFP (173, 191). The ratio of YFP to CFP (termed FRET/CFP) is used as a surrogate measure for ERK activity. A schematic of cells transduced with the EKAR-NLS and EKAR-NES biosensor, as well as the biosensor is shown in (Figure 10 A-C)

In our initial pilot experiment to show that our system worked, we used hiPSC-CFs derived from a male control line and used stimulated them with a high, low and/or medium dose of different ligands. We looked at Ang II, ET-1 and the adrenergic receptor agonists, NE, and Iso. In brief, we transduced our cells with AAV2/DJ-EKAREV-NLS to measure nuclear ERK signaling. Cells were imaged at least 48 hours after transduction using a high content microscope. Cells were imaged at baseline and then every 2.5 minutes post-treatment. The difference in FRET/CFP compared to baseline was calculated (ΔFRET), and this difference was normalized to the basal FRET/CFP per

well and converted to a percentage by multiplying by 100 (%F/F) We then looked at %ΔF/F to look at the change in ERK from baseline.

We started by looking at the average responses (%ΔF/F) over time for all cells subjected to each treatment (Figure 10D). We used PMA which is a DAG mimetic that activates PKC as a positive control. We noticed that ET-1 and PMA gave a robust response, and there was a moderate response with Ang II in comparison to vehicle. However, NE and Iso did not appear to respond compared to the vehicle. To further dissect these results, we looked at single-cell signaling ERK dynamics for each treatment. We depicted our observations using heat maps to visualize the temporal behavior of individual cells (Figure 10E). The heat maps illustrating single-cell signaling patterns unveiled that ET-1 induced both robust and transient ERK responses among different cells. For instance, when exposed to 10 nM ET-1, some cells exhibited a delayed response that began around the 20-minute mark, while others initiated their response at around 2 minutes and maintained it over time. These nuances in dynamics are typically not discernible through conventional bulk analyses. Notably, no significant distinction was observed between Iso and NE treatments when compared to the control group.

To further dissect these signaling pathways we used k-mediod clustering using time series data from the TSclust package in R. In particular we used the ‘pam’ algorithm- short for ‘partition around mediods’. This algorithm offers the advantage of robustness against outliers, in comparison to k-means clustering (192). We fed our data set for all ligands and the number of clusters required into the algorithm, and the algorithm assigned the data into the specified number of clusters based on the variable it is given. In this case the magnitude of the response (%dF/F) was the variable used to cluster time series data. We used all the data regardless of treatment for determining the clusters, this was to allow us to make comparisons between treatments later on.

We clustered the signaling data into 3 clusters using the algorithm and thereafter we plotted the average response of all cells assigned to the cluster. The black line shows the average of all cells in each specific cluster with SEM shown in grey (Figure 11A). One of the reasons the SEM bars may be large is because ERK signaling fluctuates and such fluctuations are not necessarily synchronised, Nonetheless, our data was in 3 clusters which we arbitrarily called cluster 1 "non-responders", cluster 2 as "positive responders" and cluster 3 as "negative responders". We could see an increase in the positive responders in response to ET-1 and Ang II compared to their respective controls, acetic acid (AcOH) and water respectively (Figures 11 B and C). Iso and NE appeared to have more positive responders in comparison to the water vehicle control at a single cell level, yet interesting in the bulk data, neither NE nor Iso were different from the vehicle (Figure 11D).

Given that we can tell the algorithm how many clusters to form, we used our algorithm to obtain 6 clusters instead of 3 (Figure 11E). Using a higher number of clusters allows us to see more subtle differences in the responses. However, one caveat is that you can get clusters which may appear to be quite similar when cells in the cluster are averaged. For example, when we opted for 6 clusters, we see that there are 2 groups of negatively responding cells (cluster 4 and cluster 5) emerged, whereby the percentage change in fluorescence intensity in cluster 4 goes down to approximately -30% while cluster 5 only goes down to approximately -10%. Whereas previously these cells were clustered as on group and these differences could not be seen. Cluster 3 reveals that some cells may drop initially then go back to baseline. Clusters 1 and 6 seem fairly similar, thus showing how clusters can appear similar when the number of clusters chosen is similar. Interestingly this new clustering system revealed that although NE and Iso had a larger group of cells in cluster 2 cells ("positive responders") in comparison to the water control (~20% versus 1-

3%). Treatment with NE and Iso produced a group of "highly negative responders (cluster 4) which was not seen in the vehicle control. This would explain why NE and Iso appeared to have no effect in the bulk data, as there were both positive responders and highly negative responders which may have masked the response.

Given that we obtained the most favorable responses in ERK1/2 observed with Ang II and ET-1 stimulations, we chose to focus our efforts on Ang II and ET-1 for further investigation. Furthermore, ERK1/2 signaling dynamics in response to these ligands present an unexplored avenue in the characterization of hiPSC-CFs, as their effects have not been thoroughly examined in this context before using single-cell technology. This strategic shift allowed us to delve deeper into the characterization of Ang II and ET-1 responses within hiPSC-CFs.

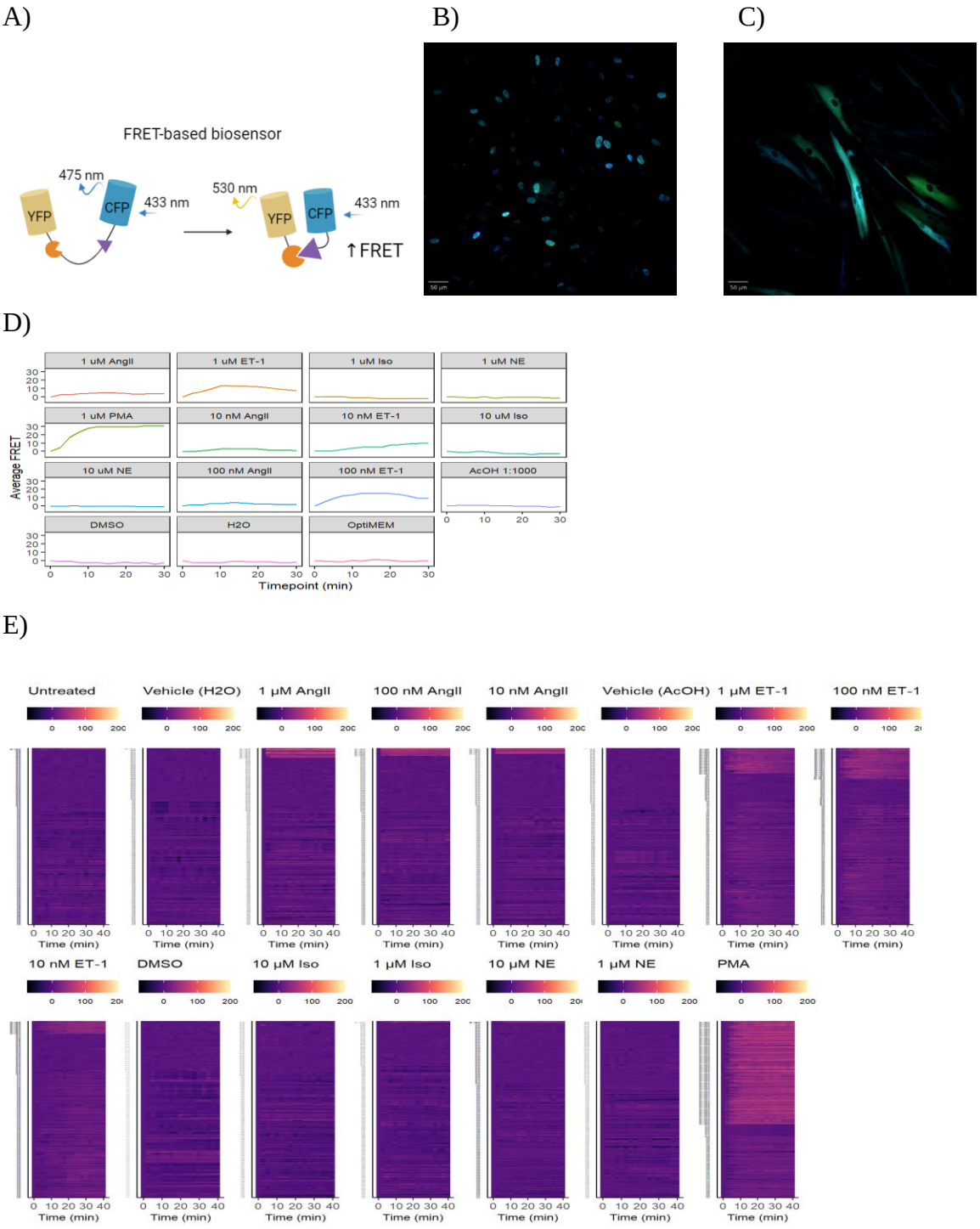


***Figure 10: Measuring nuclear ERK signaling for hiPSC-CFs derived from male control line AIW.***

A) The FRET-based biosensor, EKAREV, undergoes a conformational change following phosphorylation by ERK. This alteration facilitates the transfer of resonance energy from CFP to YFP [Image made using BioRender.com]. B and C) Representative fluorescent microscopy image

of hiPSC-CFs transduced with AAVDJ/EKAREV with either a nuclear localisation signal (B) or a cytoplasmic localisation signal (C). Image represents images typical of hiPSC-CFs. D) Averaged responses of all cells for each treatment showing ET-1 and PMA as robust responders. Weak responses were seen in response to treatment with Ang II; NE and Iso appear to show no response. Data represent means of two independent differentiations. Imaging was done every 2.5 minutes for up to 40 minutes after stimulation with Ang II, ET-1, NE, Iso, PMA, and their respective controls. E) Heat maps depicting single-cell signaling patterns reveal that ET-1 triggers robust responses in certain cells and fluctuations in ERK signaling in others. In the case of 10 nM ET-1 treatment, some cells exhibit delayed responses, with an increase observed around the 20-minute mark. Conversely, other cells respond at around 2 minutes and maintain their response. These results are derived from two distinct independent differentiations. This serves as a preliminary proof-of-concept experiment.

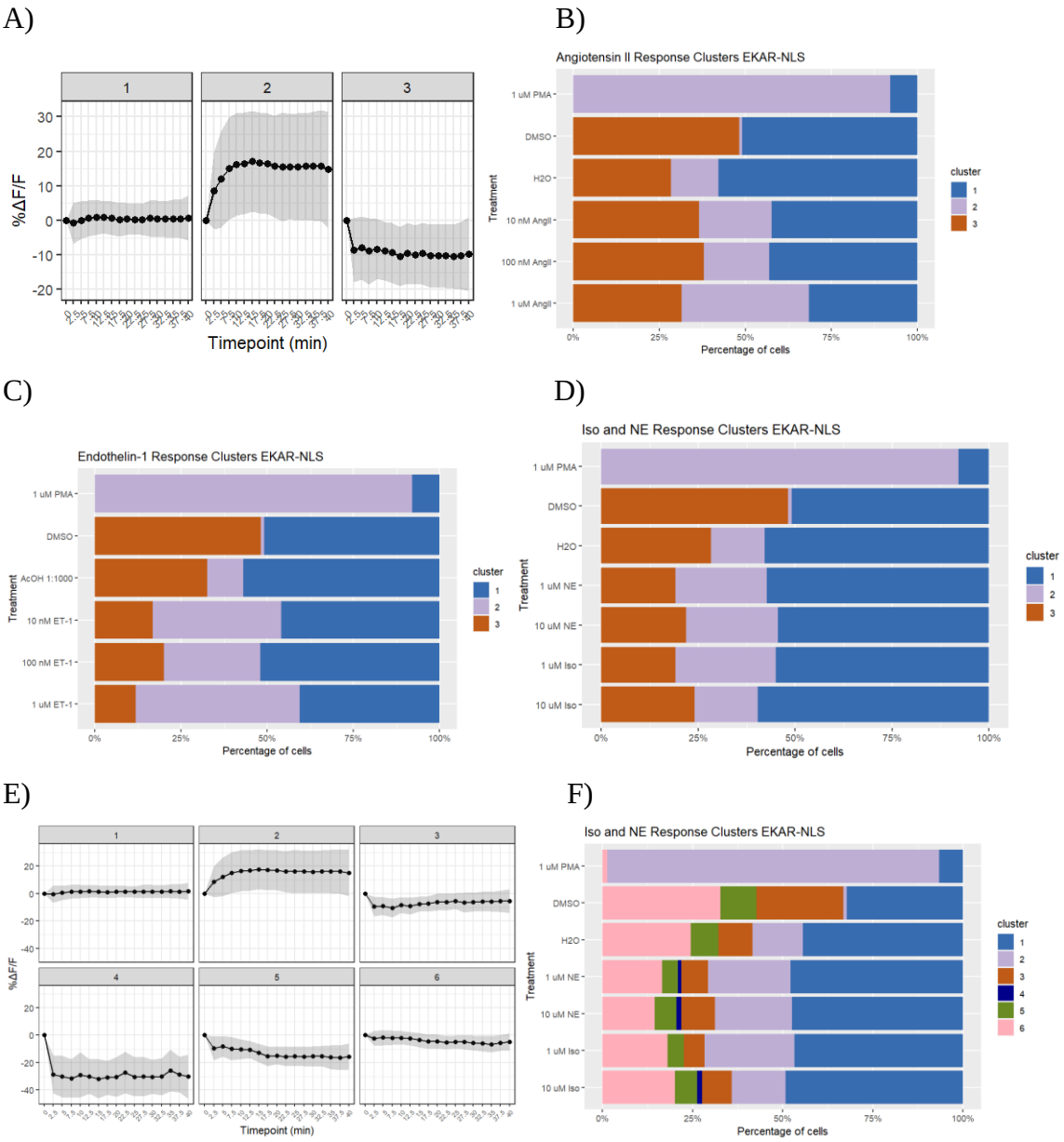


***Figure 11: The number of clusters chosen can reveal differences what bulk analysis will not.***

Clustering data into 5 clusters: (A) Averaging all nuclei within each cluster generates the mean response for each group. Error bars indicate the standard error of the mean for nuclei in each cluster. The kinetics of each cluster is shown with %ΔF/F on the y-axis, and time on the x-axis. (B-D) The distribution of cells within each cluster after treatment with aforementioned ligands. Clustering data into 6 clusters reveals nuances not seen with 5 clusters, particularly for β-adrenergic agonists. Averaging all nuclei within each cluster generates the mean response for each group. Error bars indicate the standard error of the mean for nuclei in each cluster. The kinetics of each cluster is shown with %ΔF/F on the y-axis, and time on the x-axis. (F) The distribution of cells within each cluster after treatment with aforementioned ligands. Data in A-F represents two independent differentiations.

## 3.6 ET-1 INDUCED BOTH NUCLEAR AND CYTOPLASMIC ERK1/2 SIGNALING IN HIPSC-CFS IN A DOSE-DEPENDENT MANNER

Next, we sought examine ERK1/2 activity in hiPSC-CFs from a healthy control to assess how hiPSC-CFs respond to different concentrations of the ligand, as well as examine kinetics. Such characterization of hiPSC-CFs has not been done before to the best of our knowledge. With this in mind, we transduced our cells with EKAREV which was tagged with either nuclear localization signal or a nuclear export signal. Following this we stimulated our cells with different doses of ET-1 for every 2 minutes after stimulation, for up to 30 mins and recorded the changes in FRET. We opted for imaging every 2 minutes to allow us to capture early-phase ERK signaling dynamics.

### 3.6.1 Bulk-analysis

ERK1/2 signaling can lead to phosphorylation of different target proteins and can translocate to the nucleus where it can affect gene expression in the nucleus. Using the EKAREV-NLS biosensor to track ERK activation in the nucleus and EKAR-NES to track cytoplasmic ERK signaling where ERK can phosphorylate effectors in the cytoplasm as well. Using the biosensor localized to the nucleus, our findings revealed that ET-1 signaling peaks between 6-8 minutes, followed by a decline toward baseline within 30 minutes (Figure 12A). In contrast, cytoplasmic ET-1-induced ERK signaling showed a peak at approximately 10 minutes and the peak response was sustained throughout the 30 min of recorded observations. Protein kinase C (PKC)-induced signaling, as represented by treatment with PMA, exhibited a peak around 8 minutes with a sustained plateau.

Quantitatively, the half-maximal effective concentrations ($EC_{50}$s) for cytoplasmic ERK activation taken 10 minutes after stimulation was found to be in the nanomolar range, as depicted

in Figure 13B. Interestingly, the $EC_{50}$ for nuclear ERK activation at 10 minutes appeared slightly lower than that of cytoplasmic ERK (17.5 +/-3.87 nM compared 0.414 +/- 8.6 nM, respectively). Notably, nuclear ERK signaling exhibited a heightened maximal response compared to cytoplasmic ERK, with PMA causing a FRET change of around 20% in the nucleus compared to 10% in the cytoplasm (Figures 12A and 13A). Visualizing average responses over time at each dose through heat maps revealed that higher doses (100 nM and 500 nM) yielded the most significant changes in $\%\Delta F/F$ for nuclear ERK activation (Figure 12C). In contrast, cytoplasmic ERK signaling exhibited pronounced responses even at lower doses (Figure 13C). Finally, we noted a shift in the shape for nuclear ERK dose-response curves at different timepoints, with the DR curves with the maximal range increasing from 2 minutes and reaching a peak at 8 minutes and declining thereafter (Figures 12B).

A)

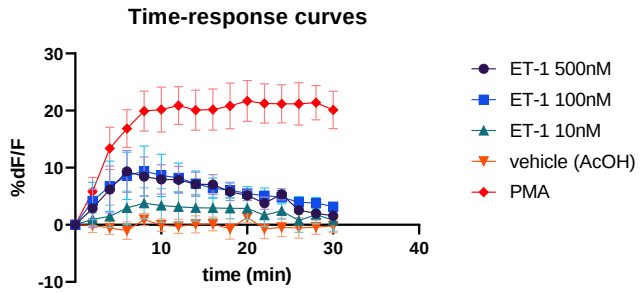


B)

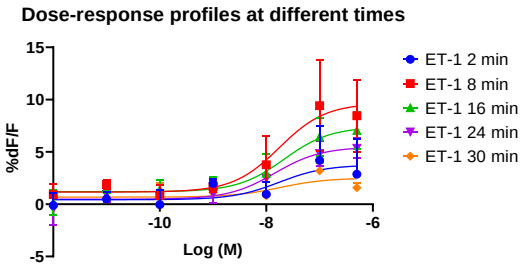


C)

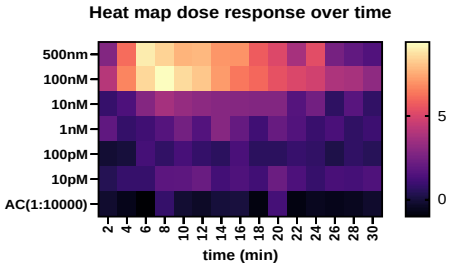


***Figure 12: ERK1/2 Activation Patterns in Nuclei of hiPSC-CFs following ET-1 Treatment – HID04C Female Control Line.***

This figure explores the ERK1/2 activation patterns within nuclei of hiPSC-CFs transduced with EKAREV biosensor, subsequent to ET-1 treatment. Bulk analysis was conducted to measure the response dynamics.(A) The average kinetics of each nuclear ERK1/2 response is quantified as %ΔF/F (y-axis) across time (x-axis) for respective treatment conditions.(B) Dose-response curves are presented at different time intervals, elucidating the variation in ERK1/2 activation with increasing ET-1 doses(The $EC_{50}$ value in nM for the time points were as follows: **2 min**: 17.3+/-15.3 nM; **8 min**: 17.6+/-3.8 nM; **16 min**: 21.5+/-3.0 nM; **24 min**: 14.5+/-3.0 nM; **30 min**: 17.7+/-26.7 nM).(C) A heat map showing the mean nuclear ERK1/2 responses for each treatment condition.For these experiments, data from hiPSC-CFs originating from four separate fibroblast differentiations was utilized. In panels A and B, the bars represent the mean of four replicates, with error bars indicating the standard error of the mean (SEM).

A)

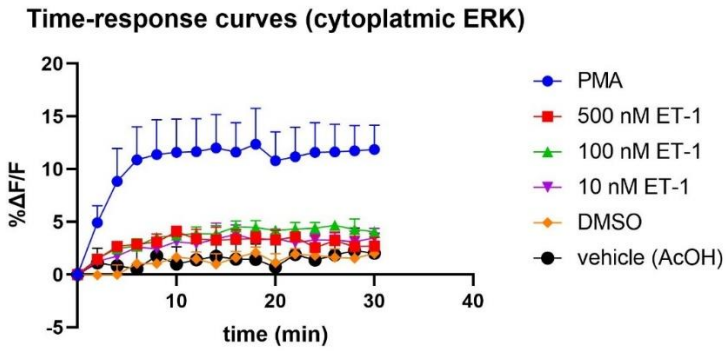


B)

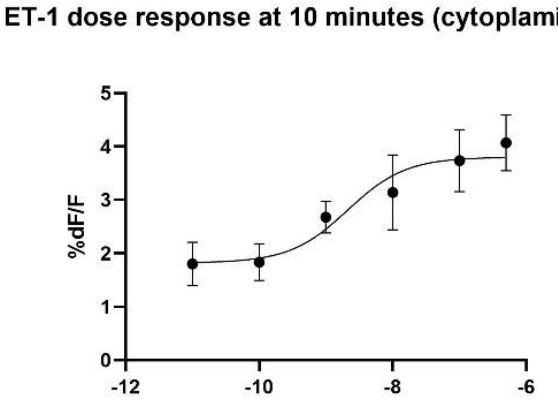


C)

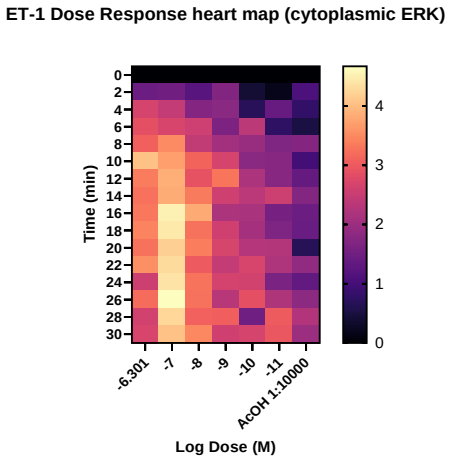


***Figure 13: ERK1/2 Activation Patterns in Cytoplasm of hiPSC-CFs following ET-1 Treatment – HID04C Female Control Line.***

This figure explores the ERK1/2 activation patterns within nuclei of hiPSC-CFs transduced with EKAREV biosensor, subsequent to ET-1 treatment, employing the HID04C female control line for investigation. Bulk analysis was conducted to measure the response dynamics.(A) The average kinetics of each cellular ERK1/2 response is quantified as %ΔF/F (y-axis) across time (x-axis) for respective treatment conditions.(B) Dose-response curves at 10 minutes.($EC_{50}$ is 0.414 +/- 8.6 nM) (C) A heat map showing the mean nuclear ERK1/2 responses for each treatment condition. For these experiments, data from hiPSC-CFs originating from 3 separate fibroblast differentiations was utilized. In panels A and B, the bars represent the mean of three replicates, with error bars indicating the standard error of the mean (SEM).

### 3.6.2 Single-cell nuclear signaling

We then proceeded to analyze our cells at a single cell level. Here we wanted to visualize signaling nuances that might be masked by bulk analysis and better understand subtle distinctions between hiPSC-CF signaling responses to different ligands. To achieve this, we used a single-cell analytical approach that has previously been used in the lab for neurons and hiPSC-CMs (155, 168). Following this, we employed the TSclust algorithm to cluster our cells (176). However, due to constraints in available computer memory (RAM), it was not feasible to include all hiPSC-CFs, as doing so would have exceeded the memory capacity. As a result, our attention was directed towards CFs that demonstrated cells expressing the biosensor within the 400 to 1100 relative fluorescence units (RFU) range.

Before delving into the examination of individual cell profiles, we initially conducted tests on our single cells to ascertain that the expression of biosensors (RFU) did not exert substantial influence on our output measurement (%ΔF/F). Our analysis revealed a slight and practically insignificant correlation of R=-0.021, accompanied by a noteworthy p-value of 2.2e-16. Nonetheless, considering the exceedingly low magnitude of our correlation (below 0.3), we deemed it to be of negligible consequence. The R-squared value of 0.000441, indicated that a mere 0.004% of the variance in %ΔF/F could be explained by the least-square regression lie relating %ΔF/F to biosensor expression.

As mentioned earlier, selecting the optimal number of clusters is necessary to get the best out of the data. When it comes to clustering there is no way to determine the validity of clusters, however, we can use metrics such as the Silhouette coefficient and Dunn index to compare the performance of different models(193, 194). As an illustration, we can contrast a model employing 3 clusters with an alternative one that partitions the data into 5 clusters. During our analysis, we

employed these coefficients to guide us in determining the optimal number of clusters for our dataset. We further conducted visual assessments of cluster distinctiveness, highlighting the clusters that exhibited the most pronounced separation. Guided by these coefficients, we generated graphical representations and selected plots showcasing the most evident clusters, specifically focusing on the average response time profile for all cells within each cluster. As previously mentioned, we used all the data regardless of treatment for determining the clusters, this was to allow us to make comparisons between treatments later on.

Subsequently, we generated heatmaps to depict single-cell ERK responses induced by ET-1, as shown in Figure 14A. Upon closer examination at the single-cell level, a diverse range of responses became evident. Some cells displayed transient patterns, peaking around 1 minute before diminishing, while others maintained sustained responses or exhibited fluctuations in %ΔF/F. We proceeded to categorize these cells into positive responders, non-responders, and negative responders (Figure 14B). Notably, the proportion of positive responders increased with increasing doses of ET-1, rising from 34% at 10pM to 68% at the highest dose of 500 nM. Conversely, non-responder numbers decreased with higher ET-1 doses. Across all treatments and vehicles, the percentage of non-responders remained relatively constant, ranging from 8% to 11%, with PMA showing a striking absence of non-responders. Notably, the vehicle control displayed a 48% responder rate.

We generated plots depicting the average response of all cells grouped within each cluster. The black line represents the mean of all cells within the given cluster regardless of treatment, while the grey shading depicts the standard error of the mean (SEM), as illustrated in Figure 14C. We identified distinct clusters of positive responders, arbitrarily refer to as ‘mild-positive responders’ (cluster 1), ‘robust-positive responders’ (cluster 3), and ‘transient-positive responders’

(cluster 5). Further exploration of cluster dynamics revealed that although the vehicle control (AcOH 1:10000) exhibited a higher count of positive responders compared to lower ET-1 doses, these responders primarily fell within the ‘mild-responders’ category. In contrast, cells treated with ET-1 displayed a distinct cluster of highly responsive cells (cluster 3), a feature absent in the vehicle (Figure 14C and D).

In line with the bulk analysis, response clusters (clusters 1, 3, and 5) peaked around 6 minutes before either declining or maintaining a sustained level. Positive responders (comprising clusters 1, 3, and 5) increased with dose, with an increase in transient and robust positive responders from 10 nM to 100 nM. Interestingly, from a dose of 100 nM to 500 nM, the percentage and distribution of positive responders remained consistent between the two doses. However, the negative responder cluster (cluster 2) increases at the higher 500 nM dose. This phenomenon might be attributed to potential off-target effects at high doses or receptor desensitization at elevated concentrations (195).

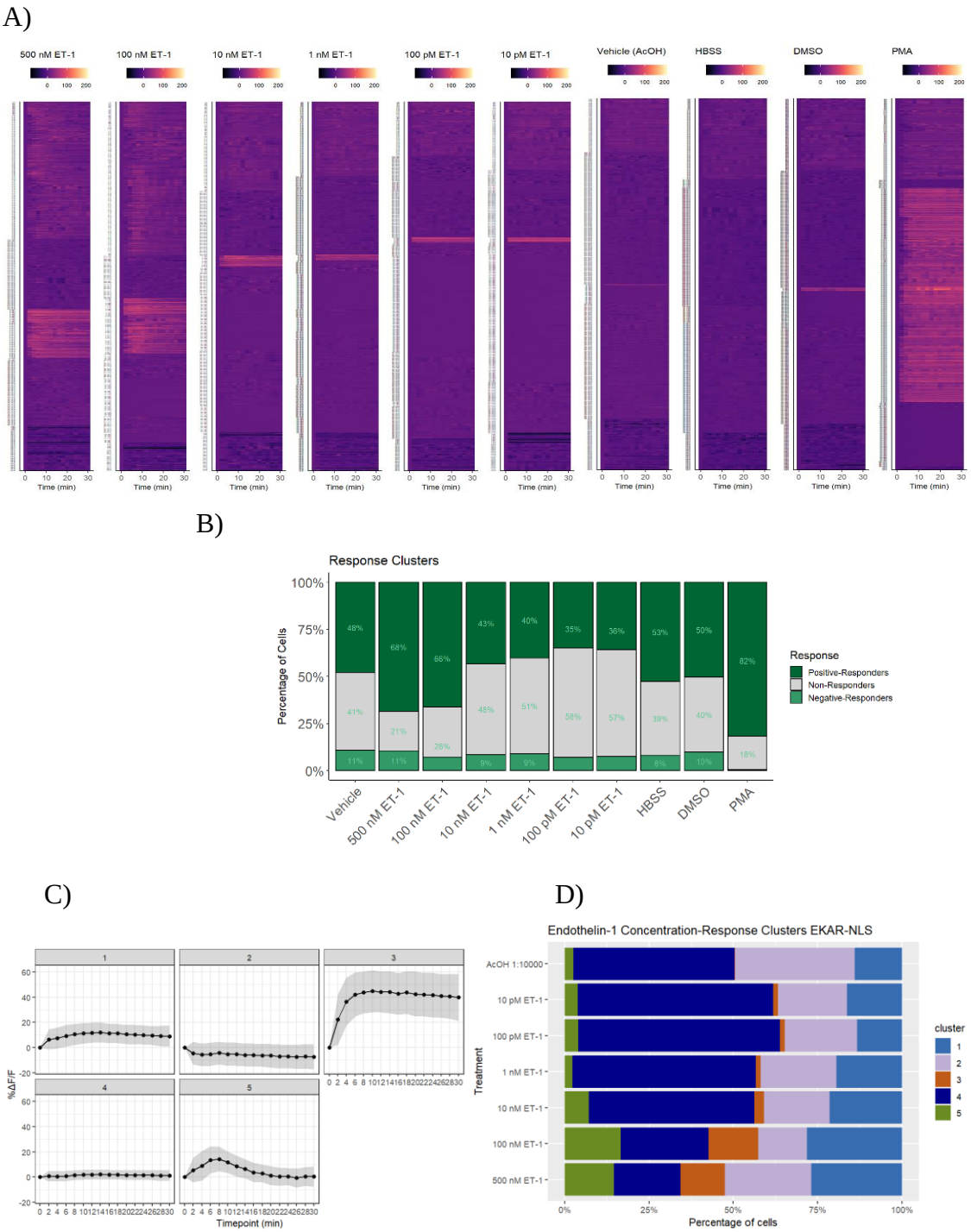


***Figure 14: ERK1/2 Activation Patterns in Single Nuclei of hiPSC-CFs after ET-1 Treatment - HID04C Female Control Line.***

(A) Heatmaps visually represent nuclear ERK1/2 activity in hiPSC-CFs subjected to various doses of vasoactive ET-1 peptide. The kinetics of each nuclear ERK1/2 response are quantified as %ΔF/F (y-axis) over time (x-axis). (B) single-nuclei data was partitioned into five clusters to capture diverse nuclear behaviors, based on the magnitude of response. While certain CF nuclei displayed responses, leading to increased or diminished ERK1/2 activation, others exhibited minimal

deviation from baseline and were grouped as 'non-responders'. The nuclei were categorized as 'positive-responders', 'non-responders', and 'negative-responders', depicted as stacked bar charts showcasing the percentage of nuclei in each cluster. (C) Averaging all nuclei within each cluster generates the mean response for each group. Error bars indicate the standard error of the mean for nuclei in each cluster. The kinetics of each cluster is shown with %ΔF/F on the y-axis, and time on the x-axis.(D) The distribution of cells within each cluster is depicted across various ET-1 doses. (E and F) The data was re-clustered into 6 clusters and the response with respect to time for all nuclei in each cluster are shown, with SEM indicated by the highlighted region. The distribution of clusters is depicted across various doses of ET-1. Data from hiPSC-CFs derived from 4 distinct fibroblast differentiations was employed for these experiments.

### 3.6.3 Single-cell cytoplasmic signaling

We examined the effect of ET-1 on hiPSC-CFs transduced with EKAR-NES. As a first step, we assessed the correlation between biosensor expression and measurement %ΔF/F for all cells, regardless of treatment. The Pearson correlation coefficient was negligible at -0.0019, and the associated p-value was insignificant ($p = 0.00012$), as shown in Figure S2A. This indicates that the variation in data cannot be significantly explained by the relationship between biosensor expression (RFU) and %ΔF/F. Upon examining overall responses prior to delving into single-cell clustering, we observed that PMA displayed the most robust response compared to ET-1 or Ang II treatment (Figure S2A). Cytoplasmic ERK signaling induced by ET-1 and Ang II appeared more variable than nuclear ERK signaling (see Figure S2B and Figure S1C).

Next, we employed our algorithm to cluster the data into four distinct clusters. By plotting the data on a heatmap and in comparison, to it to nuclear ERK signaling, we observed that PMA had a lower proportion of highly responding cells in the cytoplasm (Figure 15A). Unlike nuclear signaling, the majority of cells displayed fluctuating ERK signaling without distinct sustained or

transient responders. Analyzing the distribution of 'positive responders,' 'negative responders,' and 'non-responders,' we found that the trend was a consistent range of approximately 30% to 40% for positive responders bet, without a clear increase (Figure 15B).

To delve deeper, we examined the dynamics of each cluster by plotting the average %ΔF/F over time for cells within each cluster (Figure 15C). Additionally, we calculated the average of all cells within each cluster from all treatments, providing insights into kinetics (Figure 15C). We labeled the clusters as follows: cluster 1 as 'high responders,' cluster 2 as 'negative responders,' cluster 3 as 'non-responders,' and cluster 4 as 'mild responders.' Analyzing the percentage of cells assigned to each cluster, we noticed a trend of increasing percent in cluster 1 (high responders) upon ET-1 treatment (Figure 15D). Previously classified broadly as 'positive responders,' we distinguished that positive responder encompassed both mild and high responders. This suggests that the high responders contribute to the heightened response observed with increasing ET-1 treatment.

To leverage the potential of clustering, we organized the data into five distinct clusters. Remarkably, a previously unseen transient cluster emerged during this process (referred to as cluster 4 in Figure 15E). Interestingly, this cluster was observed exclusively in response to treatment with ET-1, as it was absent in the vehicle condition (AcOH 1:10000) (as illustrated in Figure 15E and 15F).

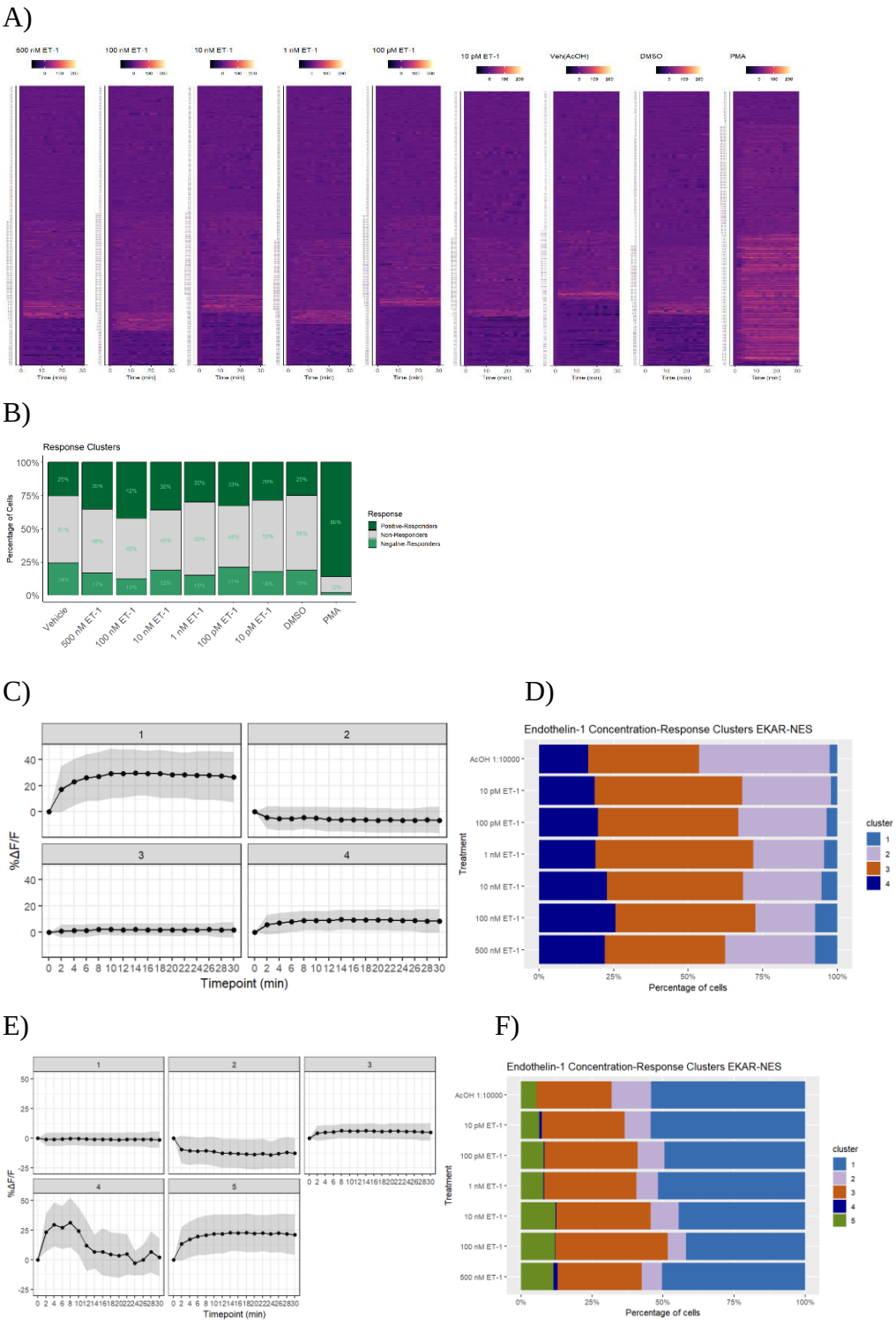


***Figure 15: Single-cell analysis of ET-1-induced cytoplasmic ERK1/2 signaling - HID04C Female Control Line.***

A) Heatmaps visually represent nuclear ERK1/2 activity in hiPSC-CFs subjected to various doses of vasoactive ET-1 peptide. The kinetics of each nuclear ERK1/2 response are quantified as %ΔF/F (y-axis) over time (x-axis). (B) single-nuclei data was partitioned into five clusters to capture

diverse nuclear behaviors, based on the magnitude of response. While certain CF nuclei displayed responses, leading to increased or diminished ERK1/2 activation, others exhibited minimal deviation from baseline and were grouped as 'non-responders'. The nuclei were categorized as 'positive-responders', 'non-responders', and 'negative-responders', depicted as stacked bar charts showcasing the percentage of nuclei in each cluster. (C) Averaging all nuclei within each cluster generates the mean response for each group. Error bars indicate the standard error of the mean for nuclei in each cluster. The kinetics of each cluster is shown with %ΔF/F on the y-axis, and time on the x-axis. (D) The distribution of cells within each cluster is depicted across various ET-1 doses. Data from hiPSC-CFs derived from 3 distinct fibroblast differentiations was employed for these experiments.

## 3.7 ANG II INDUCES NUCLEAR ERK1/2 SIGNALING IN HIPSC-CFS IN A DOSE-DEPENDENT MANNER, BUT DOES NOT ACTIVATE CYTOSOLIC ERK1/2 SIGNALING

Our experiments were conducted following the methods previously outlined for ET-1 in hiPSC-CFs transduced with EKAR-NES or EKARNLS, images were taken every 2 minutes for up to 30 minutes after treatment with different doses of Ang II.

### 3.7.1 Bulk Analysis

Our analysis of bulk data revealed that Ang II mediated ERK activity specifically within the cell nucleus, but not in the cytoplasm. When compared to the effects of Endothelin-1 (ET-1), the percentage change in fluorescence intensity (%ΔF/F) for Ang II was consistently below 5% (Figure 16A). In contrast, the response to endothelin resulted in a mean %ΔF/F reading of 10%, suggesting that ET-1 increased nuclear ERK activity approximately twice that of Ang II.

Upon generating a heatmap of nuclear ERK activity over time, we observed that the 100 nM concentration of Ang II triggered a response that peaked at 10 minutes and maintained a relatively stable level, unlike other doses which peaked around 8 to 10 minutes before declining (Figure 16B). We constructed a dose-response curve at the 10-minute mark, determining the $EC_{50}$ to be 4.6 nM using a three-parameter dose-response curve analysis with GraphPad. Our measurements fell within the nanomolar range, consistent with observations in neonatal rat cardiac fibroblasts. These prior findings indicated that Ang II induced ERK activity in a dose-dependent manner, with an $EC_{50}$ of 2.5 nM after 5 minutes of stimulation, as assessed through immunoblot analysis (196).

With regard to cytoplasmic ERK activity stimulated by Ang II, we observed no significant response across any dosage when compared to the vehicle control treated with water (Figure 17A and 17B). Our analysis at the single-cell level corroborated these results, revealing no notable distinction between the effects of vehicle and treatment with Ang II (Refer to Figure S3).

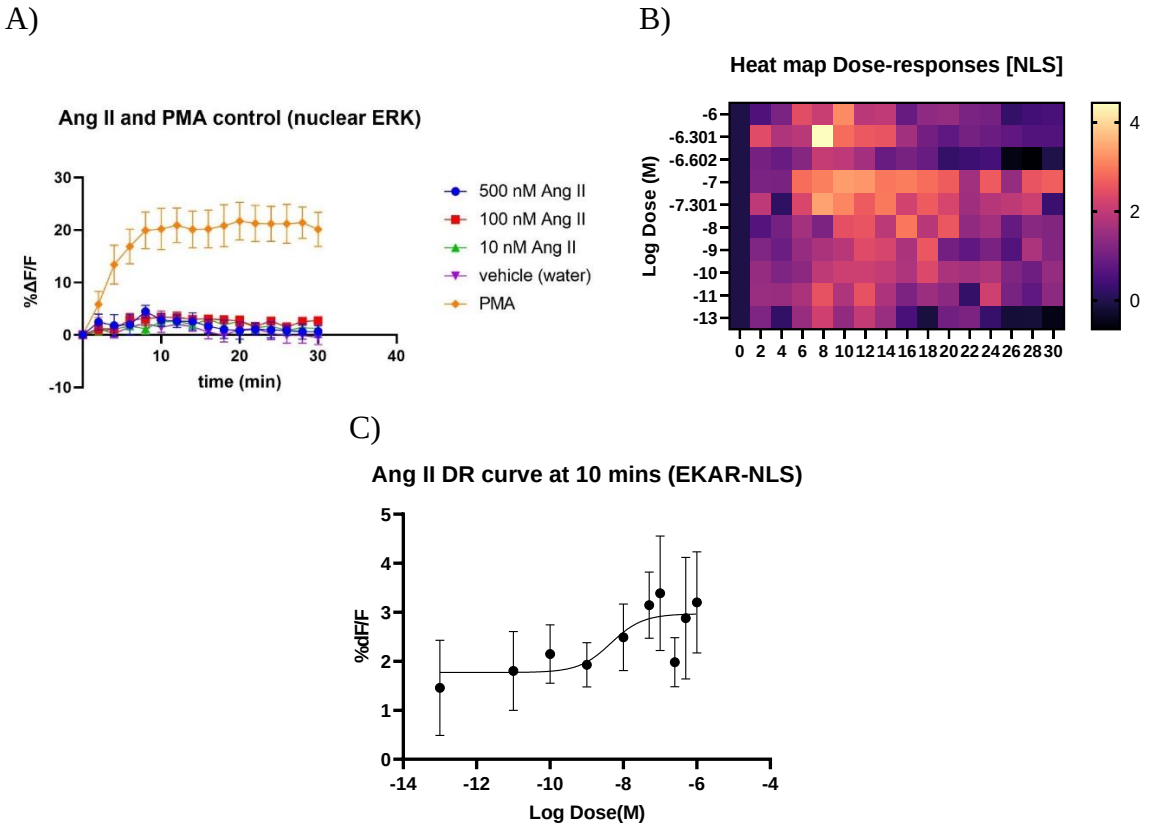


***Figure 16: ERK1/2 Activation Patterns in Nuclei of hiPSC-CFs following Ang II Treatment - HID04C Female Control Line.***

This figure explores the ERK1/2 activation patterns within nuclei of hiPSC-CFs transduced with EKAREV-NLS biosensor, subsequent to ET-1 treatment. Bulk analysis was conducted to measure the response dynamics.(A) The average kinetics of each cellular ERK1/2 response is quantified as %ΔF/F (y-axis) across time (x-axis) for respective treatment conditions. (B) A heat map showing the mean nuclear ERK1/2 responses for each treatment condition. (C) Dose-response curves at 10 minutes post-treament. For these experiments, data from hiPSC-CFs originating from 3 separate fibroblast differentiations was utilized. In panels A and C, the bars represent the mean of four replicates, with error bars indicating the standard error of the mean (SEM).

A) B)

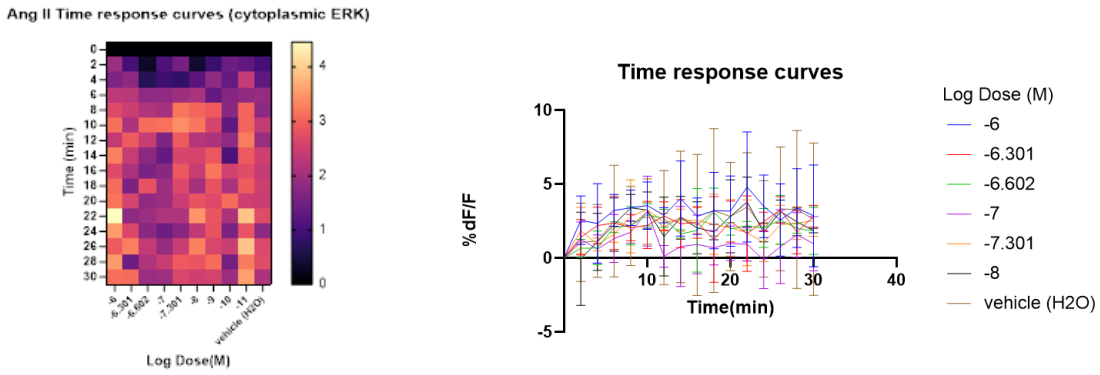


***Figure 17: ERK1/2 Activation Patterns in Cytoplasm of hiPSC-CFs following Ang II Treatment -HID04C Female Control Line***

This figure explores the ERK1/2 activation patterns within cytoplasm of hiPSC-CFs transduced with EKAREV-NES biosensor, subsequent to AngII treatment. Bulk analysis was conducted to measure the response dynamics. No significant difference was seen in response to treatment with Ang II, as compared to the vehicle control. (A) A heat map showing the mean nuclear ERK1/2 responses for each treatment condition. (B) The average kinetics of each cellular ERK1/2 response is quantified as %ΔF/F (y-axis) across time (x-axis) for respective treatment conditions For these experiments, data from hiPSC-CFs originating from 3 separate fibroblast differentiations was utilized. In B, the bars represent the mean of three replicates, with error bars indicating the standard error of the mean (SEM).

### 3.7.2 Single cell analysis of nuclear ERK in response to Ang II

In terms of Ang II-induced nuclear ERK activation, a discernible pattern emerged, characterized by a dose-dependent escalation in responsive cells when contrasted with the vehicle control (Figure 18A and 18B). We clustered our data into 5 clusters as described before, and visualization of the average of all the cells in each cluster regardless of treatment was plotted (Figure 18C). Notably, cluster 5, harboring the transient responders, exhibited a trend to increase

with increasing doses of Ang II. Cluster 3, which we had previously classed as ‘high positive responders’, also displayed an increase upon treatment with Ang II compared however, intriguingly the percent of cells in that cluster plateau at a dose of 50 nM and remains the same beyond that even with increasing dose. Remarkably, among the clusters, cluster 5, which contains transiently responding cells, appears to be the population of cells exhibiting heightened responsiveness as the dose of Ang II increases, in contrast to the findings with ET-1 treatment, where it was cluster 1 (highly responsive cells), that primarily contributed to the overall increase in %ΔF/F (see Figures 18D and 14D for comparison).

In summary, this delineates a divergence in the impact of ET-1 and Ang II on specific clusters. ET-1 targeted and elevated cluster 1, the high responders, while Ang II's effects revolved around increasing the percent of transient responders, thus molding their cumulative effect.

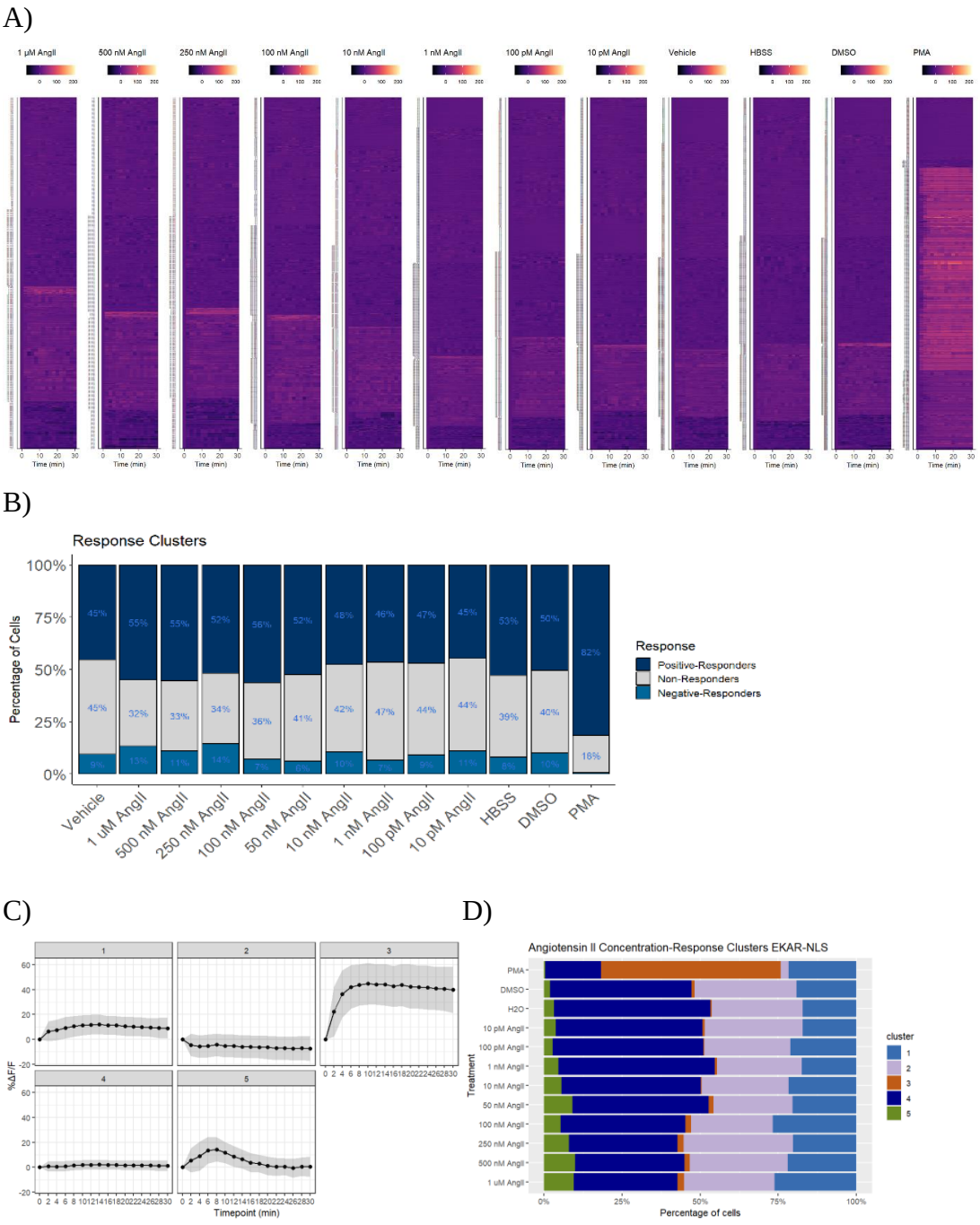


***Figure 18: Single-Nucle ERK1/2 Activation Patterns in hiPSC-CFs following Ang II Treatment. - HID04C Female Control Line***

Cytoplasmic ERK1/2 Activation Patterns in Single Cells of hiPSC-CFs after Ang II Treatment. HID04C female control line used. (A) Heatmaps visually represent nuclear ERK1/2 activity in hiPSC-CFs subjected to various doses of vasoactive ET-1 peptide. The kinetics of each nuclear ERK1/2 response are quantified as %ΔF/F (y-axis) over time (x-axis) (B). single-nuclei data was

partitioned into five clusters to capture diverse nuclear behaviors, based on the magnitude of response. While certain CF nuclei displayed responses, leading to increased or diminished ERK1/2 activation, others exhibited minimal deviation from baseline and were grouped as 'non-responders'. The nuclei were categorized as 'positive-responders', 'non-responders', and 'negative-responders', depicted as stacked bar charts showcasing the percentage of nuclei in each cluster(C). Averaging all nuclei within each cluster generates the mean response for each group. Error bars indicate the standard error of the mean for nuclei in each cluster. The kinetics of each cluster is shown with %ΔF/F on the y-axis, and time on the x-axis. (D) The distribution of cells within each cluster is depicted across various ET-1 doses. Data from hiPSC-CFs derived from four distinct fibroblast differentiations was employed for these experiments.

# 4 DISCUSSION AND FUTURE DIRECTIONS

Here, we showed that we could successfully differentiate hiPSCs into hiPSCs that resembled cardiac fibroblasts as assessed by RT-qPCR and immunofluorescent staining. Differentiation of hiPSCs led to a gene signature typical of cardiac fibroblasts. Furthermore, the protocol produced a high yield of hiPSC-CFs (>89%) and worked for differentiation of different cell lines into hiPSC-CFs. We also investigated the response of hiPSC-CFs to Angiotensin II (Ang II) and Endothelin-1 (ET-1) induced signaling pathways. While Ang II triggered nuclear ERK signaling, ET-1 led to both cytoplasmic and nuclear ERK signaling in hiPSC-CFs.

*Validation of protocol to convert hiPSCs to hiPSC cardiac fibroblasts.*

To validate our protocol, we examined the expression level of key genes that are characteristic of cardiac fibroblast phenotype. Notably, certain genes such as *TCF21* exhibited considerable variation in expression. One plausible explanation is that certain genes are known to follow a circadian rhythm of expression. For instance, previous research has highlighted the

circadian clock influence on *TCF21* gene expression in podocytes (197). Additionally, the rhythmic nature of collagen secretion, even though not extensively explored for mRNA expression, suggests the possibility of fluctuating *COL1A1* mRNA expression over time (198). It stands to reason that the expression of *COL1A1* mRNA may fluctuate with time as well. Furthermore, variations in gene expression may also arise from differences in fibroblast activation levels among batches. While genes like TCF21 tend to decrease with activation, others such as *COL1A1*, *POSTN*, and *DDR2* (a tyrosine kinase receptor activated by fibrillar collagen) tend to increase with fibroblast activation (199-202). Hence, differing levels of activated cells in each batch could contribute to the observed variations in the expression of these genes. Lastly, one has to consider batch-to-batch variability. We demonstrated that the percentage of hiPSC-CFs obtained from our protocol ranged from 89% to 98%. Consequently, this variability could influence effects observed at the level of gene expression. To address this, one approach would involve using FACS to enrich hiPSC-Fs prior to examining gene expression patterns.

We conducted a comparative analysis between a control cell line (HID-04C) and a patient cell line matched for age and sex (HID-19). The disparities observed in *ACTA2* expression suggest that HID-19 exhibits higher mRNA expression of *ACTA2* in its quiescent state. This initial investigation involved only two cell lines and was primarily exploratory in nature, aimed at detecting potential differences between a control and a disease-associated cell line. To establish significance, this experiment would need to be replicated across multiple control and patient cell lines, achieving a sufficiently robust sample size to draw meaningful conclusions. Moreover, the observed gene expression patterns could be influenced by the specific mutations present in each cell line. Different mutations might lead to varied effects on gene expression—some mutations

could enhance or diminish the expression of specific genes. Consequently, the trends identified in this preliminary study might not be consistent across all cell lines within the broader HID project. Nonetheless, it would be intriguing to extend the analysis by employing qPCR to assess whether hiPSC-derived cardiac fibroblasts from DCM patient lines demonstrate elevated activation levels in their basal or quiescent states. Key genes like *POSTN, ACTA2*, and cell cycle-related genes could be investigated in this context, as they have been seen to be elevated in DCM induced by cTnT mutation (25). Furthermore, given our intention to conduct comprehensive RNA-seq analysis on all cell lines derived from patients enrolled in the study, integrating gene mutations with the level of cellular activation and signaling profiles could facilitate data clustering. This approach has the potential to shed light on appropriate targets based on specific gene perturbations and disease characteristics.

*Ang II signaling in cardiac fibroblasts*

Despite our efforts to generate a dose-response curve for Ang II, we observed that the effect size was not large enough to allow us to determine the $EC_{50}$ for nuclear ERK1/2 signaling. This moderate effect size can be understood when we consider our single-cell data analysis. As previously mentioned, the increase in nuclear ERK activity induced by ET-1, as shown in Figure 14, was primarily driven by an increase in both high responders and transient responders. In contrast, when hiPSC-CFs were exposed to Ang II, the observed increase was predominantly due to an increase in transient responders (Figure 16). Consequently, it is not surprising that the increase in ERK activity in response to Ang II stimulation was only moderate. Future experiments could focus on better segregated populations of cells.

We note that Ang II plays a pivotal role in the hierarchy of events leading to the activation of cardiac fibroblasts. We might speculate that the relatively smaller effect size associated with Ang II serves a purpose. It's plausible that Ang II doesn't elicit a large response every time, as Ang II is in constant flux in the body to regulate blood pressure homeostasis. Thus, a check-point mechanism may be necessary to ensure that Ang II signaling does not mediate activation of cardiac fibroblasts every time there is a surge in circulating Ang II. Previous research has shown that Ang II can lead to an increase in ET-1 mRNA levels (62). Consequently, ET-1 may act to further enhance and upregulate the ERK signaling pathway leading to activation of cardiac fibroblasts. An intriguing concept is that ERK1/2 may function as a coincidence detector, which triggers cardiac fibroblast activation only when certain conditions are met.

As for our choice of experimental set-up, localized biosensors provide an elevated degree of precision by concentrating their measurement on specific regions, thereby reducing the potential for interference or noise from surrounding cellular areas. For example, in a comparative investigation utilizing the calcium biosensor RGECO, the impact of diffusing the biosensor throughout the entire cell versus directing it to troponin was examined. The results revealed that when RGECO was specifically targeted to cardiac troponin, the effect size observed upon treating cardiomyocytes with levosimendan (a calcium sensitizer used in the treatment of heart failure) was notably amplified (203). It is possible that the widespread distribution of EKAREV throughout the cytoplasm may have concealed/obscured differences existing within subcellular regions where the expression of AT1Rs has previously been demonstrated, such as the mitochondria or endoplasmic reticulum. In future studies employing localised to subdomains such as the plasma membrane, endoplasmic reticulum and mitochondria could help us rule out receptor signaling in the

cytoplasm. Notably, biosensors situated at the plasma membrane and ER are discussed in a separate study (84).

A logical next step to complement our results would entail conducting western blot or immunofluorescent staining analyses. This examination would focus on assessing ERK activation within both the cytoplasmic and nuclear compartments of hiPSC-CFs following Ang II treatment. This follow-up investigation holds the potential to substantiate our initial discovery, specifically confirming that Ang II indeed triggers ERK activation in the nuclear region while not affecting the cytoplasmic compartment.

Building on the intriguing contrast between our findings that Ang II stimulates nuclear ERK but not cytoplasmic ERK, an avenue worth exploring involves employing caged ligands to delve deeper into the ramifications of intracellular AT1R signaling. This innovative approach could provide invaluable insights into the intricate mechanisms underlying the signaling pathways mediated by intracellular AT1Rs. Dallagnol et al. recently developed tools for studying intracellular GPCR signaling using caged ligands, whereby ligands such as Ang II can be ‘caged’ with a 4,5-dimethoxy-2-nitrobenzyl (DMNB) moiety (204). These DMNB-functionalized peptides are cell-permeable and undergo rapid photolysis upon UV exposure, generating functionally active peptides within cells—a process termed 'uncaging.' This facilitates controlled intracellular peptide release, enabling the study of intracellular receptors.

In our FRET assays, ligands were added to the assay medium before and imaging our cells. With regards to how Ang II may be taken up by hiPSC-CFs to drive intracellular signaling, several studies have demonstrated that extracellular Ang II can indeed be transported into cells and accumulate within them. Several studies suggest that this may be in part through a receptor-mediated pathway. For instance, in mouse proximal tubule cells treated with fluorescein (FITC)-

labeled Ang II, the uptake of FITC-Ang II was detected within the cytoplasm 30 minutes post-treatment, and even within the nuclei at 1 hour after exposure (205). Importantly, the uptake of FITC-ANG II in these cells was entirely prevented by blocking the AT1R receptor using losartan. Similarly, in another study it was demonstrated that antagonizing the AT1R receptor with candesartan led to the inhibition of Ang II uptake by rat cardiac fibroblasts, as visualized using immunofluorescence with an Alexa Fluor 488-labeled Ang II (206). Therefore, one could speculate that Ang II might enter our cells via pathways mediated by the AT1R receptor.

Various mechanisms have been proposed to explain the uptake and intracellular signaling of other ligands that activate intracellular GPCR signaling, but this remains to be elucidated. In rat neonatal cardiac fibroblasts treated with ET-1, there was a transient increase in steady-state pre-pro endothelin-1 mRNA levels at 30 mins post-stimulation, as detected by northern blot analysis (207). Extracellular ET-1 potentially exerts its intracellular signaling effects by stimulating the synthesis of ET-1 within the cells, where it remains in the cytoplasm before potentially being trafficked to the nucleus. In the case of ligands like noradrenaline, treating rat neonatal cardiomyocytes with [$^3$H]-labeled noradrenaline results in rapid uptake by cells, with accumulation within the nucleus occurring within hours (208). However, the mechanism by which it enters the cells remains unknown. Unlike ET-1 and Ang II, which are synthesized within cardiac cells, adrenaline would need to be transported into the cell. It has been suggested that these ligands may cross the plasma membrane via an active transport mechanism, or perhaps through channels, or pores (41, 209).

Notably, Tadevosyan et al. (116) demonstrated the significance of intracellular AT1R signaling in pathological processes. By using a canine model of congestive heart failure, they observed augmented intracellular Ang II levels and an increase in nuclear AT1R expression, as

well as modified glycosylation patterns of nuclear AT2Rs. The utilization of this canine model of congestive heart failure and caged Ang II offered a valuable framework to elucidate the intricate dynamics of these signaling elements under pathological conditions. Moreover, these mechanisms could potentially be further investigated in the context of dilated cardiomyopathy (DCM) in future studies. The same group used a photo- releasable caged-Ang-II derivative to interrogate intracellular Ang-II signaling in CFs, and they showed that Ang II intracellular signalling plays a crucial role by increasing *de novo* RNA synthesis, cell proliferation, and collagen I secretion in cardiac fibroblasts. These results align with another study, which revealed that intracellular Ang II led to an increase in transforming growth factor-β (TGF-β) and collagen-1 secretion in rat cardiac fibroblasts (206). Additionally, their work showcased that the presence of isoproterenol and high glucose concentrations could further elevate Ang II levels in fibroblasts (206). This collective body of evidence strongly underscores the critical role played by intracellular angiotensin receptors, highlighting their profound importance in cellular processes.

The clinical implications are intriguing, particularly considering the distinct outcomes of two potent inhibitors, valsartan and losartan. Dallagnol and colleagues indicated that losartan abrogated intracellular AT1R effects on collagen release, while valsartan only led to a minor decrease in collagen release. They attributed this variation in effect to losartan being more cell permeable than valsartan (210). A significant observation from Dallagnol et al. was that intracellularly targeted Ang II, in conjunction with TRV055 (G protein-biased AT1R agonists), triggered increased collagen secretion, while TRV027, a β-arrestin-biased analog did not. Interestingly, both TRV055 (G protein-biased) and TRV027 (β-arrestin-biased) peptides successfully induced collagen secretion extracellularly (204). The same group also showed preliminary data whereby treating cells with Ang II for 15 minutes resulted in the activation of

phosphorylated ERK (pERK), which was not only detected within the nucleus but also appeared to be present within the endoplasmic reticulum (ER) of rat cardiac myofibroblasts, as revealed through immunofluorescent imaging. Relating this to our findings, it is important to note that our study involved quiescent human cardiac fibroblasts, distinct from the activated myofibroblasts in this context. Furthermore, our investigation focused on human cardiac fibroblasts (CFs) rather than rat CFs. In in a prior RNA-seq analysis by Bourque et al., it was highlighted that angiotensin receptors are expressed at lower levels in human induced pluripotent stem cell-derived cardiomyocytes (hiPSC-CMs) compared to rat cardiomyocytes. This underscores a species difference in angiotensin receptor expression between species (174). An additional explanation for the presence of phosphorylated ERK (pERK) in the rat myofibroblasts could be related to the fact that these cells were cultured on a relatively rigid plastic substrate. In contrast, our experiments involving induced pluripotent stem cell-derived cardiac fibroblasts (hiPSC-CFs) were conducted on a softer Matrigel substrate. This observation aligns with a previous study that highlighted how cells respond differently based on the mechanical environment they are in. Specifically, the study found that MCF10A human mammary epithelial cells cultured on softer substrates consistently exhibited lower levels of ERK signaling, while cells on stiffer substrates displayed higher and more rhythmic ERK activity (164).

To further our understanding of disease-relevant biological processes forward, an integrative approach combining caged ligands, biosensors, live-cell imaging, and single-cell analysis holds immense promise. This approach holds the potential to shed light on the complex signaling pathways linked to intracellular AT1R-mediated responses, especially within physiologically relevant cell models such as human-induced pluripotent stem cell-derived cardiac

fibroblasts and cardiomyocytes obtained from patients with dilated cardiomyopathy (DCM) as well as healthy controls.

*Endothelin-1 signaling in cardiac fibroblasts.*

We showed that ET-1 signaling increases ERK activation in both the nucleus and the cytoplasm. This aligns with previous findings that ET-1 induces ERK activation through the ETAR/Gq/ERK signaling pathway in cardiac fibroblasts (60). Our findings add another dimension that was previously not appreciated that both nuclear and cytoplasmic ERK are active in human hiPSC-derived cardiac fibroblasts by offering spatial and temporal resolution of ET-1 signalling. Notably, in comparison to Ang II, ET-1 elicited a higher increase in ERK activity as detected by our EKAREV biosensors. This could potentially be attributed to heightened receptor expression. Our prior investigations within our laboratory unveiled an elevated expression of endothelin receptors in hiPSC-cardiomyocytes, rat neonatal cardiomyocytes and HEK cells, when compared to angiotensin receptors which were expressed at lower levels in all three cell types (174). Whether this pattern is mirrored in hiPSC-cardiac fibroblasts (CFs) remains uncertain, necessitating an examination of quantifying mRNA or protein expression for the angiotensin and endothelin receptors.

Activation of endothelin receptors has been established to induce fibroblast proliferation, activation, and conversion to a myofibroblast phenotype. In human cardiac fibroblasts, this activation is mediated through the ETAR/Gq/ERK signaling pathway (60). Notably, Ang II has been hypothesized to be atop the hierarchy of events leading to cardiac fibrosis. In studies done axis in adult human cardiac fibroblasts, Ang II has been found to induce the synthesis of collagen

I and α-smooth muscle actinα-SMA through the AT1R/Gαq/ TGF-β1/ERK signaling pathway (106, 107). In human cardiac fibroblasts, activation of AT1R triggers the upregulation of both TGF-β1 and ET-1 via the Gαq signaling. The AT1R/Gαq cascade transmits signals to TGF-β1, which subsequently upregulates ET-1 through pathways mediated by Smad and ERK1/2. In consequence, ET-1 engages and activates the endothelin receptor type A (ETAR), ultimately leading to an augmented synthesis of collagen I and α-SMA, accompanied by the integration of α-SMA into stress fibers typical of the mF phenotype. Interestingly, simultaneous inhibition of TGF-β and ET-1 signaling effectively counteracts the Ang II-induced conversion of CFs of myofibroblasts (211). In a holistic perspective, these observations suggest a potential hierarchy of events where Ang II may hold a prominent position in initiating fibroblast activation. Conceivably, ET-1 acts to amplify ERK signaling downstream of Ang II, acting as a mechanism to potentiate ERK signaling. Alternatively, considering that Ang II is believed to mediate its enhancement of ERK via TGFβ1, it is plausible that our short-term treatment might not have allowed sufficient time for TGFβ1, and ET-1 release and produce a more pronounced ERK increase in Ang II. Longer-term experiments with tools established in this paper can aid in addressing this question. Employing our approach with genetically encoded biosensors, which allow prolonged imaging and repeated assessments, can facilitate the modeling of ERK activation in response to chronic Ang II stimulation in hiPSC-CFs, thus enabling an assessment of this hierarchy. For example, imaging over a 24-hour period with Ang II treatment together with a TGFβ inhibitor or an ET-1 inhibitor may help elucidate whether ET-1 amplifies ERK signaling downstream of Ang II. This may shed light on the order of events leading to fibrosis and offer spatio-temporal resolution of ERK activity downstream of these ligands.

*Gaining more from clustering*

In our study, we designated one cluster as "non-responders" for the sake of simplicity. However, it's important to recognize that these cells could exhibit fluctuations around zero. A limitation of our clustering approach lies in the fact that our algorithm relies solely on the magnitude of responses from individual cells. Yet, it's noteworthy that the dynamics of ERK signaling are inherently intricate and may involve patterns encoded within the frequency of these fluctuations/pulses (212-214). Our data (as depicted in Figure S4) highlights an interesting observation: the cells we arbitrarily referred to as 'non-responders' might not truly fit that description. Some of these cells exhibit fluctuations around a baseline of zero; however, this behavior becomes less apparent when the individual responses of all cells in the cluster are averaged, creating the impression of non-responsiveness. These cells are perceived as non-responders based on their proximity to zero in terms of magnitude. This is illustrated in supplementary figures, where re-clustering cells previously in the cluster labelled as non-responders reveals distinct fluctuating clusters (Figure S5). However, if our algorithm could also capture these fluctuation patterns, we could gain more insightful perspectives.

Furthermore, other aspects of ERK signaling, such as the frequency of fluctuations, hold the potential to furnish us with valuable supplementary insights. A potential avenue for capturing these fluctuation patterns involves exploring the variations between different time points. By

quantifying the changes in measurements between each time point and incorporating that information into our clustering, we might uncover fluctuation patterns that include frequency-related changes. These nuances, which our initial signal analysis might overlook, could enhance our understanding of ERK signaling dynamics. However, if we could enhance our algorithm to capture the underlying fluctuations, it could lead to insights. One potential avenue to achieve this is by investigating the variations between different time points. By quantifying the changes in measurements between each time point and incorporating this data into our machine-learning algorithm, we could gain valuable insights into fluctuation patterns. This approach has the potential to reveal frequency-related changes that might not be evident in our initial signal analysis. Furthermore, we used 'Euclidean distance' to cluster our cells; however, there are other distance measures that could also help us better capture these differences. Exploring these is another avenue to obtain more insight from our dataset, as it is essential to consider various distance metrics in clustering analysis (215). Given that the clustering methodology was formerly developed for ERK signaling data acquired at 10-minute intervals (155, 216), our present investigation involves a richer dataset, with imaging conducted every 2 minutes to capture the intricate dynamics of early-phase ERK signaling. In light of this, it is reasonable to consider reexamining the distance measure used within our algorithm to capture other modalities such as frequency of fluctuations in ERK signaling seen in our data. Doing so could potentially unveil previously obscured nuances, particularly those that manifest as fluctuations when images are acquired at more widely spaced intervals. This reevaluation promises to provide a fresh perspective and a deeper understanding of the data.

This complementary strategy has the potential to bridge the gap between fluctuation patterns and the magnitude of responses. This, in turn, could enable a more comprehensive

exploration of the dynamics of ERK signaling. Taking a broader perspective, integrating these findings with RNA-seq data could offer a deeper understanding of how specific signaling modalities impact genes and their resulting effects. Essentially, by integrating diverse clustering techniques that shed light on different aspects of ERK signaling dynamics, we open the door to uncovering a more complete and intricate view of these signaling processes. This comprehensive approach, in conjunction with RNA-seq analyses, holds the promise of unraveling the subtle interplay between signaling patterns, gene expression, and cellular responses. In doing so, we can move closer to a holistic understanding of the complex mechanisms at play.

*Future Directions*

Previous work by Verdonschot and colleagues involved performing RNA-seq analysis on biopsies taken from a cohort of 795 patients with DCM. Their investigations unveiled distinct phenotypic clusters within DCM, each characterized by a unique cardiac transcriptomic signature. These differences in molecular pathology delineate variations among phenogroups, while still sharing a common pathophysiology when compared to patients in other phenogroups (17). Their study underscores the heterogeneous nature of DCM and potentially provides insights into the varying degrees of efficacy in clinical trials and overall treatment outcomes (17, 217).

The present approach to treating heart failure patients involves administering drugs in the sequence of their discovery. Furthermore, doctors are advised to incrementally fine-tune drug dosages within each category before advancing to the subsequent treatment stage. Nonetheless, this method can result in notable time delays, surpassing six months, when integrating new medications. As time elapses without incorporating the complete range of necessary therapies,

patients face avoidable hospitalizations and, tragically, even fatalities due to the absence of crucial treatments. The urgency of initiating timely treatment cannot be overstated (3). Furthermore, taking into account the variability of the disease, enhanced strategies are expected to produce more favorable outcomes, as different disease pathologies might necessitate distinct treatment strategies.

The overarching objective of the 'Heart-In-a-Dish' project is to categorize patients in a way that offers enhanced guidance for treatment strategies and drug development. In collaborating with clinicians and researchers, we aim to provide a more personalized approach and establish a seamless pathway from bedside-to-bench-to-bedside. Such an approach could prioritize patients for drug classes most beneficial to them and streamline drug development for specific phenogroups. This specificity could lead to improved drug targeting and effectiveness.

The central aim of this thesis was to establish a protocol for studying hiPSC-CFs with the goal of characterizing these cells within our patient population. Through the creation of dose-response curves, a framework has been established for selecting suitable doses for characterizing patient and control cell lines. Subsequent experiments will delve into disparities among patients and assess their response to stress induced by neurohormonal stimulation, along with using caged ligands to probe nuclear and extracellular signaling. Additionally, understanding the biological implications of the identified clusters is a forthcoming step.

While the central focus of this project revolves around hiPSC-CFs, it is a component of a more comprehensive initiative that includes participation from lab members who delve into other aspects of DCM. Currently we are in the process of developing cell-painting assays to study morphological features to characterize the various morphological features that can be seen in DCM patients with or without neurohormonal stimulation. For instance, hiPSC-CMs derived from DCM

patients with an RBM20 mutation have shown disrupted sarcomere arrangements. This specific mutation also causes CMs to be sensitive to β-adrenergic stress, resulting in enhanced sarcomeric disorganization (218). Furthermore, this mutation leads to compromised calcium signaling and contractility. As such, our lab's previous efforts work has laid foundational work to study calcium signaling assays and contractility assays to study hiPSC-CMs. Additionally, in alignment with the work undertaken in this thesis, we are also investigating ERK1/2 and PKA signaling downstream of GPCRs associated with heart failure in hiPSC-CMs (155).

Concurrently with the signaling assays, our strategy includes employing RNA-seq on both hiPSC-CMs and cardiac resident cells. This will be conducted baseline RNA-seq to identify patient-specific gene expression changes, as well as investigating the effects of neurohormonal modulation through drug stimulation. We expect to gain insights into the possibility of reversing vulnerabilities through pre-treatment with ARBs and β-blockers. Simultaneously, efforts are underway to enhance the basic 2D model by transitioning to more intricate 3D organoid cultures and co-cultures involving diverse cardiac cell types, aiming to replicate intercellular interactions more faithfully. By integrating morphological features, cellular signaling profiles, RNA-seq data, and clinical information, patients can be clustered into groups with shared characteristics. Moreover, our pipeline enables us to continue monitoring patients post-treatment, allowing us to use patient outcome data as a means to harness the potential of both retrospective and retroactive studies.

Utilizing the wealth of data gathered, our aim is to integrate it with machine learning and clustering techniques. These methods have been previously employed to discern patterns within

both clinical and molecular data (17). This endeavor holds the potential to significantly enhance the process of making therapeutic decisions for individuals afflicted DCM. By extracting valuable insights from these intricate datasets, we can make more informed choices regarding the most suitable treatments for patients with DCM.

# *5* CONCLUSION

Dilated cardiomyopathy (DCM) is a condition affecting the heart muscle, leading to reduced pumping efficiency, and often requiring heart transplantation due to its high mortality rate. Existing therapies are insufficient, mainly targeting the cardiomyocytes without addressing fibrosis, a significant factor in chamber remodeling that impairs heart function in DCM. This thesis is part of a larger effort to enhance therapy strategies for DCM patients and provide a platform for drug development based on different pheno-groups due to the diverse nature of DCM. Collaborating with clinicians and other laboratories, we've assembled a pool of 228 individuals who consented to participate in the "Heart-in-a-Dish" project. This resource includes patient samples from those diagnosed with DCM as well as age-matched healthy controls. Here, I have established a pipeline to use hiPSCs to generate hiPSC-CFs for further study.

Through detailed analysis of Ang II and ET-1 dose-response curves, I established a foundational framework for investigating hiPSC-CFs within the broader scope of our project. These findings aid in determining appropriate doses for our research. Our work serves as a proof of concept, demonstrating that coupling hiPSC-CFs with biosensors enables the exploration of signaling pathways potentially disrupted in disease progression. Our research revealed that Ang II

triggers ERK signaling in the nucleus but not the cytoplasm, while ET-1 elicits signaling in both compartments. This spatial and temporal resolution of ERK signaling downstream of these agents is novel. Moreover, we employed single-cell analysis and clustering techniques to reveal nuances often overlooked in bulk analysis. By creating these investigative tools and laying the groundwork for our 'bed to bench' approach, we aspire to contribute meaningfully to the well-being of individuals with DCM. These tools represent a significant stride towards unraveling the intricate complexities of cardiac fibrosis and heart disease as a whole.

# 6 REFERENCES


1. Cuenca S, Ruiz-Cano MJ, Gimeno-Blanes JR, Jurado A, Salas C, Gomez-Diaz I, et al. Genetic basis of familial dilated cardiomyopathy patients undergoing heart transplantation. J Heart Lung Transplant. 2016;35(5):625-35.
2. Hershberger R, Hedges D, Morales A. Dilated cardiomyopathy: The complexity of a diverse genetic architecture. Nature reviews Cardiology. 2013;10.
3. Teshnisi MA, Vakilian F, Zirak N, Sedaghat A, Hoseini Khah SHR, Mohammadpoor AH, et al. Prognosis of heart transplant patients in Mashhad University of Medical Sciences. Kardiochir Torakochirurgia Pol. 2020;17(1):33-8.
4. Khayata M, Al-Kindi SG, Oliveira GH. Contemporary characteristics and outcomes of adults with familial dilated cardiomyopathy listed for heart transplantation. World J Cardiol. 2019;11(1):38-46.
5. Gustav M, Peter M. Familial Dilated Cardiomyopathy: Risk Stratification for Sudden Cardiac Death. In: Peter M, Jo Ann L, editors. Sudden Cardiac Death. Rijeka: IntechOpen; 2020. p. Ch. 9.
6. Elliott P, Andersson B, Arbustini E, Bilinska Z, Cecchi F, Charron P, et al. Classification of the cardiomyopathies: a position statement from the European Society Of Cardiology Working Group on Myocardial and Pericardial Diseases. Eur Heart J. 2008;29(2):270-6.
7. Buckberg G, Athanasuleas C, Conte J. Surgical ventricular restoration for the treatment of heart failure. Nature Reviews Cardiology. 2012;9(12):703-16.
8. Lymperopoulos A, Rengo G, Koch WJ. Adrenergic nervous system in heart failure: pathophysiology and therapy. Circ Res. 2013;113(6):739-53.
9. Hori M, Kagiya T, Sato H, Sato H, Kitabatake A, Fukunami M, et al. Neurohumoral Mechanisms in Chronic Heart Failure. In: Sasayama S, Suga H, editors. Recent Progress in Failing Heart Syndrome. Tokyo: Springer Japan; 1991. p. 221-40.
10. Hartupee J, Mann DL. Neurohormonal activation in heart failure with reduced ejection fraction. Nat Rev Cardiol. 2017;14(1):30-8.
11. Travers JG, Kamal FA, Robbins J, Yutzey KE, Blaxall BC. Cardiac Fibrosis. Circulation Research. 2016;118(6):1021-40.
12. Perestrelo AR, Silva AC, Cruz JO-DL, Martino F, Horváth V, Caluori G, et al. Multiscale Analysis of Extracellular Matrix Remodeling in the Failing Heart. Circulation Research. 2021;128(1):24-38.
13. Mahmaljy H YV, Singhal M. Dilated Cardiomyopathy. [Updated 2023 Apr 7]. In: StatPearls [Internet]. Treasure Island (FL): StatPearls Publishing; 2023 Jan-.
14. Jefferies JL, Towbin JA. Dilated cardiomyopathy. Lancet. 2010;375(9716):752-62.
15. Sweet M, Taylor MR, Mestroni L. Diagnosis, prevalence, and screening of familial dilated cardiomyopathy. Expert Opin Orphan Drugs. 2015;3(8):869-76.
16. Day SM, Tardiff JC, Ostap EM. Myosin modulators: emerging approaches for the treatment of cardiomyopathies and heart failure. J Clin Invest. 2022;132(5).
17. Verdonschot JAJ, Merlo M, Dominguez F, Wang P, Henkens MTHM, Adriaens ME, et al. Phenotypic clustering of dilated cardiomyopathy patients highlights important pathophysiological differences. European Heart Journal. 2020;42(2):162-74.

18. McNally EM, Mestroni L. Dilated Cardiomyopathy: Genetic Determinants and Mechanisms. Circ Res. 2017;121(7):731-48.
19. Widyastuti HP, Norden-Krichmar TM, Grosberg A, Zaragoza MV. Gene expression profiling of fibroblasts in a family with LMNA-related cardiomyopathy reveals molecular pathways implicated in disease pathogenesis. BMC Med Genet. 2020;21(1):152.
20. Yang J, Argenziano MA, Burgos Angulo M, Bertalovitz A, Beidokhti MN, McDonald TV. Phenotypic Variability in iPSC-Induced Cardiomyocytes and Cardiac Fibroblasts Carrying Diverse LMNA Mutations. Front Physiol. 2021;12:778982.
21. Rouhi L, Auguste G, Zhou Q, Lombardi R, Olcum M, Pourebrahim K, et al. Deletion of the Lmna gene in fibroblasts causes senescence-associated dilated cardiomyopathy by activating the double-stranded DNA damage response and induction of senescence-associated secretory phenotype. J Cardiovasc Aging. 2022;2(3).
22. Fu X, Mishra R, Chen L, Arfat MY, Sharma S, Kingsbury T, et al. Exosomes mediated fibrogenesis in dilated cardiomyopathy through a MicroRNA pathway. iScience. 2023;26(2):105963.
23. Kane C, Dias P, Helen N, Trantidou T, Camelliti P, Gorelik J, et al. 267Direct contact between human cardiac fibroblasts and human induced pluripotent stem cell-derived cardiomyocytes counteracts changes in calcium cycling induced by soluble mediators. Cardiovascular Research. 2014;103(suppl_1):S48-S.
24. Maurer W, Koehne S, Maus A, Tiburcy M, Schlick S, Zibat A, et al. Dysfunctional crosstalk of cardiomyocytes and cardiac fibroblasts in a pluripotent stem cell model of dilated cardiomyopathy. European Heart Journal. 2020;41(Supplement_2):ehaa946.3706.
25. Bretherton RC, Reichardt IM, Zabrecky KA, Goldstein AJ, Bailey LRJ, Bugg D, et al. Correcting dilated cardiomyopathy with fibroblast-targeted p38 deficiency. bioRxiv. 2023.
26. Koenig AL, Shchukina I, Amrute J, Andhey PS, Zaitsev K, Lai L, et al. Single-cell transcriptomics reveals cell-type-specific diversification in human heart failure. Nature Cardiovascular Research. 2022;1(3):263-80.
27. Litviňuková M, Talavera-López C, Maatz H, Reichart D, Worth CL, Lindberg EL, et al. Cells of the adult human heart. Nature. 2020;588(7838):466-72.
28. Frangogiannis NG. Matricellular Proteins in Cardiac Adaptation and Disease. Physiological Reviews. 2012;92(2):635-88.
29. Theocharis AD, Skandalis SS, Gialeli C, Karamanos NK. Extracellular matrix structure. Adv Drug Deliv Rev. 2016;97:4-27.
30. Yue B. Biology of the extracellular matrix: an overview. J Glaucoma. 2014;23(8 Suppl 1):S20-3.
31. Tao H, Chen Z-W, Yang J-J, Shi K-H. MicroRNA-29a suppresses cardiac fibroblasts proliferation via targeting VEGF-A/MAPK signal pathway. International Journal of Biological Macromolecules. 2016;88:414-23.
32. Asli N, Xaymardan M, Patrick R, Farbehi N, Cornwell J, Forte E, et al. PDGFRα signaling in cardiac fibroblasts modulates quiescence, metabolism and self-renewal, and promotes anatomical and functional repair. bioRxiv; 2017.
33. Fix C, Bingham K, Carver W. Effects of interleukin-18 on cardiac fibroblast function and gene expression. Cytokine. 2011;53(1):19-28.
34. Palmer JN, Hartogensis WE, Patten M, Fortuin FD, Long CS. Interleukin-1 beta induces cardiac myocyte growth but inhibits cardiac fibroblast proliferation in culture. The Journal of Clinical Investigation. 1995;95(6):2555-64.

35. Bang C, Batkai S, Dangwal S, Gupta SK, Foinquinos A, Holzmann A, et al. Cardiac fibroblast–derived microRNA passenger strand-enriched exosomes mediate cardiomyocyte hypertrophy. The Journal of Clinical Investigation. 2014;124(5):2136-46.
36. Walters NJ, Gentleman E. Evolving insights in cell-matrix interactions: elucidating how non-soluble properties of the extracellular niche direct stem cell fate. Acta Biomater. 2015;11:3-16.
37. Pellman J, Zhang J, Sheikh F. Myocyte-fibroblast communication in cardiac fibrosis and arrhythmias: Mechanisms and model systems. J Mol Cell Cardiol. 2016;94:22-31.
38. Picchio V, Bordin A, Floris E, Cozzolino C, Dhori X, Peruzzi M, et al. The dynamic facets of the cardiac stroma: from classical markers to omics and translational perspectives. Am J Transl Res. 2022;14(2):1172-87.
39. Looi JL, Edwards C, Armstrong GP, Scott A, Patel H, Hart H, et al. Characteristics and prognostic importance of myocardial fibrosis in patients with dilated cardiomyopathy assessed by contrast-enhanced cardiac magnetic resonance imaging. Clin Med Insights Cardiol. 2010;4:129-34.
40. Daseke MJ, 2nd, Tenkorang MAA, Chalise U, Konfrst SR, Lindsey ML. Cardiac fibroblast activation during myocardial infarction wound healing: Fibroblast polarization after MI. Matrix Biol. 2020;91-92:109-16.
41. Mazarura GR, Dallagnol JCC, Chatenet D, Allen BG, Hébert TE. The complicated lives of GPCRs in cardiac fibroblasts. American Journal of Physiology-Cell Physiology. 2022;323(3):C813-C22.
42. Souders CA, Bowers SL, Baudino TA. Cardiac fibroblast: the renaissance cell. Circ Res. 2009;105(12):1164-76.
43. Zhang W, Lavine KJ, Epelman S, Evans SA, Weinheimer CJ, Barger PM, et al. Necrotic myocardial cells release damage-associated molecular patterns that provoke fibroblast activation in vitro and trigger myocardial inflammation and fibrosis in vivo. J Am Heart Assoc. 2015;4(6):e001993.
44. Daseke MJ, 2nd, Valerio FM, Kalusche WJ, Ma Y, DeLeon-Pennell KY, Lindsey ML. Neutrophil proteome shifts over the myocardial infarction time continuum. Basic Res Cardiol. 2019;114(5):37.
45. Jacobs M, Staufenberger S, Gergs U, Meuter K, Brandstätter K, Hafner M, et al. Tumor necrosis factor-alpha at acute myocardial infarction in rats and effects on cardiac fibroblasts. J Mol Cell Cardiol. 1999;31(11):1949-59.
46. Wang J-H, Zhao L, Pan X, Chen N-N, Chen J, Gong Q-L, et al. Hypoxia-stimulated cardiac fibroblast production of IL-6 promotes myocardial fibrosis via the TGF-β1 signaling pathway. Laboratory Investigation. 2016;96(8):839-52.
47. Mouton AJ, Ma Y, Rivera Gonzalez OJ, Daseke MJ, 2nd, Flynn ER, Freeman TC, et al. Fibroblast polarization over the myocardial infarction time continuum shifts roles from inflammation to angiogenesis. Basic Res Cardiol. 2019;114(2):6.
48. Tille JC, Pepper MS. Mesenchymal cells potentiate vascular endothelial growth factor-induced angiogenesis in vitro. Exp Cell Res. 2002;280(2):179-91.
49. Squires CE, Escobar GP, Payne JF, Leonardi RA, Goshorn DK, Sheats NJ, et al. Altered fibroblast function following myocardial infarction. Journal of Molecular and Cellular Cardiology. 2005;39(4):699-707.
50. Ma Y, Iyer RP, Jung M, Czubryt MP, Lindsey ML. Cardiac Fibroblast Activation Post-Myocardial Infarction: Current Knowledge Gaps. Trends Pharmacol Sci. 2017;38(5):448-58.

51. Ahuja P, Sdek P, MacLellan WR. Cardiac myocyte cell cycle control in development, disease, and regeneration. Physiol Rev. 2007;87(2):521-44.
52. Blaxall BC, Baudino TA, Kirshenbaum LA. Cardiac Fibroblasts and Cellular Cross Talk in Heart Failure. Journal of Cardiovascular Translational Research. 2012;5(6):737-8.
53. Tian G, Ren T. Mechanical stress regulates the mechanotransduction and metabolism of cardiac fibroblasts in fibrotic cardiac diseases. European Journal of Cell Biology. 2023;102(2):151288.
54. Niu L, Jia Y, Wu M, Liu H, Feng Y, Hu Y, et al. Matrix stiffness controls cardiac fibroblast activation through regulating YAP via AT1R. Journal of Cellular Physiology. 2020;235(11):8345-57.
55. van Amerongen MJ, Bou-Gharios G, Popa E, van Ark J, Petersen AH, van Dam GM, et al. Bone marrow-derived myofibroblasts contribute functionally to scar formation after myocardial infarction. J Pathol. 2008;214(3):377-86.
56. Bucala R, Spiegel LA, Chesney J, Hogan M, Cerami A. Circulating fibrocytes define a new leukocyte subpopulation that mediates tissue repair. Mol Med. 1994;1(1):71-81.
57. Han M, Liu Z, Liu L, Huang X, Wang H, Pu W, et al. Dual genetic tracing reveals a unique fibroblast subpopulation modulating cardiac fibrosis. Nature Genetics. 2023;55(4):665-78.
58. Rupert CE, Kim TY, Choi B-R, Coulombe KLK. Human Cardiac Fibroblast Number and Activation State Modulate Electromechanical Function of hiPSC-Cardiomyocytes in Engineered Myocardium. Stem Cells International. 2020;2020:9363809.
59. Chaffin M, Papangeli I, Simonson B, Akkad A-D, Hill MC, Arduini A, et al. Single-nucleus profiling of human dilated and hypertrophic cardiomyopathy. Nature. 2022.
60. Duangrat R, Parichatikanond W, Likitnukul S, Mangmool S. Endothelin-1 Induces Cell Proliferation and Myofibroblast Differentiation through the ET(A)R/G(αq)/ERK Signaling Pathway in Human Cardiac Fibroblasts. Int J Mol Sci. 2023;24(5).
61. Gray MO, Long CS, Kalinyak JE, Li H-T, Karliner JS. Angiotensin II stimulates cardiac myocyte hypertrophy via paracrine release of TGF-β1 and endothelin-1 from fibroblasts. Cardiovascular Research. 1998;40(2):352-63.
62. Cheng TH, Cheng PY, Shih NL, Chen IB, Wang DL, Chen JJ. Involvement of reactive oxygen species in angiotensin II-induced endothelin-1 gene expression in rat cardiac fibroblasts. J Am Coll Cardiol. 2003;42(10):1845-54.
63. Rask-Andersen M, Almén MS, Schiöth HB. Trends in the exploitation of novel drug targets. Nat Rev Drug Discov. 2011;10(8):579-90.
64. Robert F, Malin CL, Lars-Gustav L, Helgi BS. The G-Protein-Coupled Receptors in the Human Genome Form Five Main Families. Phylogenetic Analysis, Paralogon Groups, and Fingerprints. Molecular Pharmacology. 2003;63(6):1256.
65. Zeghal M, Laroche G, Freitas JD, Wang R, Giguère PM. Profiling of basal and ligand-dependent GPCR activities by means of a polyvalent cell-based high-throughput platform. Nature Communications. 2023;14(1):3684.
66. Oldham WM, Hamm HE. Heterotrimeric G protein activation by G-protein-coupled receptors. Nature Reviews Molecular Cell Biology. 2008;9(1):60-71.
67. Duc NM, Kim HR, Chung KY. Structural mechanism of G protein activation by G protein-coupled receptor. European Journal of Pharmacology. 2015;763:214-22.
68. Wettschureck N, Offermanns S. Mammalian G proteins and their cell type specific functions. Physiol Rev. 2005;85(4):1159-204.

69. Mizuno N, Itoh H. Functions and regulatory mechanisms of Gq-signaling pathways. Neurosignals. 2009;17(1):42-54.
70. Opazo F, Schulz JB, Falkenburger BH. PKC links Gq-coupled receptors to DAT-mediated dopamine release. J Neurochem. 2010;114(2):587-96.
71. Pierce KL, Premont RT, Lefkowitz RJ. Seven-transmembrane receptors. Nature reviews Molecular cell biology. 2002;3(9):639-50.
72. Gilman AG. G proteins and dual control of adenylate cyclase. Cell. 1984;36(3):577-9.
73. Siderovski DP, Willard FS. The GAPs, GEFs, and GDIs of heterotrimeric G-protein alpha subunits. Int J Biol Sci. 2005;1(2):51-66.
74. Higashijima T, Ferguson KM, Sternweis PC, Smigel MD, Gilman AG. Effects of Mg2+ and the beta gamma-subunit complex on the interactions of guanine nucleotides with G proteins. J Biol Chem. 1987;262(2):762-6.
75. Khan SM, Sleno R, Gora S, Zylbergold P, Laverdure JP, Labbé JC, et al. The expanding roles of Gβγ subunits in G protein-coupled receptor signaling and drug action. Pharmacol Rev. 2013;65(2):545-77.
76. Khan SM, Sung JY, Hébert TE. Gβγ subunits-Different spaces, different faces. Pharmacol Res. 2016;111:434-41.
77. Reiter E, Lefkowitz RJ. GRKs and beta-arrestins: roles in receptor silencing, trafficking and signaling. Trends Endocrinol Metab. 2006;17(4):159-65.
78. Pierce KL, Lefkowitz RJ. Classical and new roles of beta-arrestins in the regulation of G-protein-coupled receptors. Nat Rev Neurosci. 2001;2(10):727-33.
79. Wisler JW, DeWire SM, Whalen EJ, Violin JD, Drake MT, Ahn S, et al. A unique mechanism of β-blocker action: Carvedilol stimulates β-arrestin signaling. Proceedings of the National Academy of Sciences. 2007;104(42):16657-62.
80. Jain R, Watson U, Vasudevan L, Saini DK. ERK Activation Pathways Downstream of GPCRs. Int Rev Cell Mol Biol. 2018;338:79-109.
81. Tsvetanova NG, Trester-Zedlitz M, Newton BW, Peng GE, Johnson JR, Jimenez-Morales D, et al. Endosomal cAMP production broadly impacts the cellular phosphoproteome. J Biol Chem. 2021;297(1):100907.
82. Nikolaev VO, Moshkov A, Lyon AR, Miragoli M, Novak P, Paur H, et al. β2-Adrenergic Receptor Redistribution in Heart Failure Changes cAMP Compartmentation. Science. 2010;327(5973):1653-7.
83. Ahn S, Shenoy SK, Wei H, Lefkowitz RJ. Differential Kinetic and Spatial Patterns of β-Arrestin and G Protein-mediated ERK Activation by the Angiotensin II Receptor*. Journal of Biological Chemistry. 2004;279(34):35518-25.
84. Kwon Y, Mehta S, Clark M, Walters G, Zhong Y, Lee HN, et al. Non-canonical β-adrenergic activation of ERK at endosomes. Nature. 2022;611(7934):173-9.
85. Kim J, Eckhart AD, Eguchi S, Koch WJ. β2-Adrenergic Receptor-mediated DNA Synthesis in Cardiac Fibroblasts Is Dependent on Transactivation of the Epidermal Growth Factor Receptor and Subsequent Activation of Extracellular Signal-regulated Kinases *. Journal of Biological Chemistry. 2002;277(35):32116-23.
86. Murasawa S, Mori Y, Nozawa Y, Gotoh N, Shibuya M, Masaki H, et al. Angiotensin II Type 1 Receptor-Induced Extracellular Signal-Regulated Protein Kinase Activation Is Mediated by Ca2+/Calmodulin-Dependent Transactivation of Epidermal Growth Factor Receptor. Circulation Research. 1998;82(12):1338-48.

87. Zou Y, Komuro I, Yamazaki T, Kudoh S, Aikawa R, Zhu W, et al. Cell Type–Specific Angiotensin II–Evoked Signal Transduction Pathways. Circulation Research. 1998;82(3):337-45.
88. Morgan K, Wharton J, Webb JC, Keogh BE, Smith PLC, Taylor KM, et al. Co-expression of renin—angiotensin system component genes in human atrial tissue. Journal of Hypertension. 1994;12:S11-S20.
89. Serneri GGN, Boddi M, Coppo M, Chechi T, Zarone N, Moira M, et al. Evidence for the Existence of a Functional Cardiac Renin-Angiotensin System in Humans. Circulation. 1996;94(8):1886-93.
90. Asazuma-Nakamura Y, Dai P, Harada Y, Jiang Y, Hamaoka K, Takamatsu T. Cx43 contributes to TGF-β signaling to regulate differentiation of cardiac fibroblasts into myofibroblasts. Experimental Cell Research. 2009;315(7):1190-9.
91. Lee AA, Dillmann WH, McCulloch AD, Villarreal FJ. Angiotensin II stimulates the autocrine production of transforming growth factor-beta 1 in adult rat cardiac fibroblasts. J Mol Cell Cardiol. 1995;27(10):2347-57.
92. Lijnen PJ, Petrov VV, Fagard RH. Angiotensin II-induced stimulation of collagen secretion and production in cardiac fibroblasts is mediated via angiotensin II subtype 1 receptors. J Renin Angiotensin Aldosterone Syst. 2001;2(2):117-22.
93. Chen K, Chen J, Li D, Zhang X, Mehta JL. Angiotensin II Regulation of Collagen Type I Expression in Cardiac Fibroblasts. Hypertension. 2004;44(5):655-61.
94. Campbell SE, Janicki JS, Weber KT. Temporal differences in fibroblast proliferation and phenotype expression in response to chronic administration of angiotensin II or aldosterone. Journal of Molecular and Cellular Cardiology. 1995;27(8):1545-60.
95. Hafizi S, Wharton J, Morgan K, Allen SP, Chester AH, Catravas JD, et al. Expression of Functional Angiotensin-Converting Enzyme and AT1 Receptors in Cultured Human Cardiac Fibroblasts. Circulation. 1998;98(23):2553-9.
96. Burrell LM, Johnston CI, Tikellis C, Cooper ME. ACE2, a new regulator of the renin-angiotensin system. Trends Endocrinol Metab. 2004;15(4):166-9.
97. Iwata M, Cowling RT, Gurantz D, Moore C, Zhang S, Yuan JX-J, et al. Angiotensin-(1–7) binds to specific receptors on cardiac fibroblasts to initiate antifibrotic and antitrophic effects. American Journal of Physiology-Heart and Circulatory Physiology. 2005;289(6):H2356-H63.
98. Bottari SP, Taylor V, King IN, Bogdal Y, Whitebread S, de Gasparo M. Angiotensin II AT2 receptors do not interact with guanine nucleotide binding proteins. European Journal of Pharmacology: Molecular Pharmacology. 1991;207(2):157-63.
99. Zhang H, Han GW, Batyuk A, Ishchenko A, White KL, Patel N, et al. Structural basis for selectivity and diversity in angiotensin II receptors. Nature. 2017;544(7650):327-32.
100. Matavelli LC, Siragy HM. AT2 receptor activities and pathophysiological implications. J Cardiovasc Pharmacol. 2015;65(3):226-32.
101. Arina R, Sana K, Ali A-H. Update on Angiotensin II Subtype 2 Receptor: Focus on Peptide and Nonpeptide Agonists. Molecular Pharmacology. 2021;99(6):469.
102. Tsutsumi Y, Matsubara H, Ohkubo N, Mori Y, Nozawa Y, Murasawa S, et al. Angiotensin II Type 2 Receptor Is Upregulated in Human Heart With Interstitial Fibrosis, and Cardiac Fibroblasts Are the Major Cell Type for Its Expression. Circulation Research. 1998;83(10):1035-46.
103. Oro C, Qian H, Thomas WG. Type 1 angiotensin receptor pharmacology: signaling beyond G proteins. Pharmacol Ther. 2007;113(1):210-26.

104. Yong KW, Li Y, Liu F, Bin G, Lu TJ, Wan Abas WA, et al. Paracrine Effects of Adipose-Derived Stem Cells on Matrix Stiffness-Induced Cardiac Myofibroblast Differentiation via Angiotensin II Type 1 Receptor and Smad7. Sci Rep. 2016;6:33067.
105. Paradis P, Dali-Youcef N, Paradis FW, Thibault G, Nemer M. Overexpression of angiotensin II type I receptor in cardiomyocytes induces cardiac hypertrophy and remodeling. Proc Natl Acad Sci U S A. 2000;97(2):931-6.
106. Parichatikanond W, Duangrat R, Mangmool S. G(αq) protein-biased ligand of angiotensin II type 1 receptor mediates myofibroblast differentiation through TGF-β1/ERK axis in human cardiac fibroblasts. Eur J Pharmacol. 2023;951:175780.
107. Duangrat R, Parichatikanond W, Morales NP, Pinthong D, Mangmool S. Sustained AT1R stimulation induces upregulation of growth factors in human cardiac fibroblasts via Gαq/TGF-β/ERK signaling that influences myocyte hypertrophy. European Journal of Pharmacology. 2022;937:175384.
108. Kim KS, Abraham D, Williams B, Violin JD, Mao L, Rockman HA. β-Arrestin-biased AT1R stimulation promotes cell survival during acute cardiac injury. Am J Physiol Heart Circ Physiol. 2012;303(8):H1001-10.
109. Pang PS, Butler J, Collins SP, Cotter G, Davison BA, Ezekowitz JA, et al. Biased ligand of the angiotensin II type 1 receptor in patients with acute heart failure: a randomized, double-blind, placebo-controlled, phase IIB, dose ranging trial (BLAST-AHF). Eur Heart J. 2017;38(30):2364-73.
110. Felker GM, Butler J, Collins SP, Cotter G, Davison BA, Ezekowitz JA, et al. Heart failure therapeutics on the basis of a biased ligand of the angiotensin-2 type 1 receptor. Rationale and design of the BLAST-AHF study (Biased Ligand of the Angiotensin Receptor Study in Acute Heart Failure). JACC Heart Fail. 2015;3(3):193-201.
111. Ryba DM, Li J, Cowan CL, Russell B, Wolska BM, Solaro RJ. Long-Term Biased β-Arrestin Signaling Improves Cardiac Structure and Function in Dilated Cardiomyopathy. Circulation. 2017;135(11):1056-70.
112. Khan SM, Martin RD, Bayne A, Pétrin D, Bourque K, Jones-Tabah J, et al. Gβγ subunits colocalize with RNA polymerase II and regulate transcription in cardiac fibroblasts. J Biol Chem. 2023;299(4):103064.
113. Wang J, Hanada K, Gareri C, Rockman HA. Mechanoactivation of the angiotensin II type 1 receptor induces β-arrestin-biased signaling through Gα(i) coupling. J Cell Biochem. 2018;119(4):3586-97.
114. Rakesh K, Yoo B, Kim IM, Salazar N, Kim KS, Rockman HA. beta-Arrestin-biased agonism of the angiotensin receptor induced by mechanical stress. Sci Signal. 2010;3(125):ra46.
115. De Paolis P, Porcellini A, Savoia C, Lombardi A, Gigante B, Frati G, et al. Functional cross-talk between angiotensin II and epidermal growth factor receptors in NIH3T3 fibroblasts. J Hypertens. 2002;20(4):693-9.
116. Tadevosyan A, Xiao J, Surinkaew S, Naud P, Merlen C, Harada M, et al. Intracellular Angiotensin-II Interacts With Nuclear Angiotensin Receptors in Cardiac Fibroblasts and Regulates RNA Synthesis, Cell Proliferation, and Collagen Secretion. Journal of the American Heart Association. 2017;6(4):e004965.
117. Merlen C, Farhat N, Luo X, Chatenet D, Tadevosyan A, Villeneuve LR, et al. Intracrine endothelin signaling evokes IP3-dependent increases in nucleoplasmic $Ca^{2+}$ in adult cardiac myocytes. J Mol Cell Cardiol. 2013;62:189-202.

118. Boivin B, Lavoie C, Vaniotis G, Baragli A, Villeneuve LR, Ethier N, et al. Functional beta-adrenergic receptor signalling on nuclear membranes in adult rat and mouse ventricular cardiomyocytes. Cardiovasc Res. 2006;71(1):69-78.
119. Vaniotis G, Glazkova I, Merlen C, Smith C, Villeneuve LR, Chatenet D, et al. Regulation of cardiac nitric oxide signaling by nuclear β-adrenergic and endothelin receptors. J Mol Cell Cardiol. 2013;62:58-68.
120. Kawanabe Y, Nauli SM. Endothelin. Cell Mol Life Sci. 2011;68(2):195-203.
121. King KL, Lai J, Winer J, Luis E, Yen R, Hooley J, et al. Cardiac fibroblasts produce leukemia inhibitory factor and endothelin, which combine to induce cardiac myocyte hypertrophy in vitro. Endocrine. 1996;5(1):85-93.
122. Cheng CM, Hong HJ, Liu JC, Shih NL, Juan SH, Loh SH, et al. Crucial role of extracellular signal-regulated kinase pathway in reactive oxygen species-mediated endothelin-1 gene expression induced by endothelin-1 in rat cardiac fibroblasts. Mol Pharmacol. 2003;63(5):1002-11.
123. Boivin B, Chevalier D, Villeneuve LR, Rousseau E, Allen BG. Functional endothelin receptors are present on nuclei in cardiac ventricular myocytes. J Biol Chem. 2003;278(31):29153-63.
124. Katwa L, Guarda E, Weber K. Endothelin receptors in cultured adult rat cardiac fibroblasts. Cardiovascular research. 1994;27:2125-9.
125. Modesti PA, Vanni S, Paniccia R, Bandinelli B, Bertolozzi I, Polidori G, et al. Characterization of endothelin-1 receptor subtypes in isolated human cardiomyocytes. J Cardiovasc Pharmacol. 1999;34(3):333-9.
126. Kennedy RA, Kemp TJ, Sugden PH, Clerk A. Using U0126 to dissect the role of the extracellular signal-regulated kinase 1/2 (ERK1/2) cascade in the regulation of gene expression by endothelin-1 in cardiac myocytes. Journal of molecular and cellular cardiology. 2006;41(2):236-47.
127. Zhang CL, Xie S, Qiao X, An YM, Zhang Y, Li L, et al. Plasma endothelin-1-related peptides as the prognostic biomarkers for heart failure: A PRISMA-compliant meta-analysis. Medicine (Baltimore). 2017;96(50):e9342.
128. Jankowich M, Choudhary G. Endothelin-1 levels and cardiovascular events. Trends in Cardiovascular Medicine. 2020;30(1):1-8.
129. Pieske B, Beyermann B, Breu V, Löffler BM, Schlotthauer K, Maier LS, et al. Functional Effects of Endothelin and Regulation of Endothelin Receptors in Isolated Human Nonfailing and Failing Myocardium. Circulation. 1999;99(14):1802-9.
130. Leenen FH, Skarda V, Yuan B, White R. Changes in cardiac ANG II postmyocardial infarction in rats: effects of nephrectomy and ACE inhibitors. American Journal of Physiology-Heart and Circulatory Physiology. 1999;276(1):H317-H25.
131. Bujak M, Frangogiannis NG. The role of TGF-β signaling in myocardial infarction and cardiac remodeling. Cardiovascular Research. 2007;74(2):184-95.
132. Adiarto S, Heiden S, Vignon-Zellweger N, Nakayama K, Yagi K, Yanagisawa M, et al. ET-1 from endothelial cells is required for complete angiotensin II-induced cardiac fibrosis and hypertrophy. Life Sci. 2012;91(13-14):651-7.
133. Ammarguellat FZ, Gannon PO, Amiri F, Schiffrin EL. Fibrosis, Matrix Metalloproteinases, and Inflammation in the Heart of DOCA-Salt Hypertensive Rats: Role of ET(A) receptors. Hypertension. 2002;39(2):679-84.

134. Kohan DE, Cleland JG, Rubin LJ, Theodorescu D, Barton M. Clinical trials with endothelin receptor antagonists: what went wrong and where can we improve? Life Sci. 2012;91(13-14):528-39.
135. Turner NA, O'Regan D J, Ball SG, Porter KE. Endothelin-1 is an essential co-factor for beta2-adrenergic receptor-induced proliferation of human cardiac fibroblasts. FEBS Lett. 2004;576(1-2):156-60.
136. Turner NA, Porter KE, Smith WHT, White HL, Ball SG, Balmforth AJ. Chronic β2-adrenergic receptor stimulation increases proliferation of human cardiac fibroblasts via an autocrine mechanism. Cardiovascular Research. 2003;57(3):784-92.
137. Tanner MA, Thomas TP, Maitz CA, Grisanti LA. β2-Adrenergic Receptors Increase Cardiac Fibroblast Proliferation Through the Gαs/ERK1/2-Dependent Secretion of Interleukin-6. Int J Mol Sci. 2020;21(22).
138. Aránguiz-Urroz P, Canales J, Copaja M, Troncoso R, Vicencio JM, Carrillo C, et al. Beta2-adrenergic receptor regulates cardiac fibroblast autophagy and collagen degradation. Biochimica et Biophysica Acta (BBA) - Molecular Basis of Disease. 2011;1812(1):23-31.
139. Travers JG, Kamal FA, Valiente-Alandi I, Nieman ML, Sargent MA, Lorenz JN, et al. Pharmacological and Activated Fibroblast Targeting of Gβγ-GRK2 After Myocardial Ischemia Attenuates Heart Failure Progression. Journal of the American College of Cardiology. 2017;70(8):958-71.
140. Swaney JS, Roth DM, Olson ER, Naugle JE, Meszaros JG, Insel PA. Inhibition of cardiac myofibroblast formation and collagen synthesis by activation and overexpression of adenylyl cyclase. Proceedings of the National Academy of Sciences. 2005;102(2):437-42.
141. Liu X, Sun SQ, Hassid A, Ostrom RS. cAMP inhibits transforming growth factor-β-stimulated collagen synthesis via inhibition of extracellular signal-regulated kinase 1/2 and Smad signaling in cardiac fibroblasts. Molecular pharmacology. 2006;70(6):1992-2003.
142. Ostrom RS, Naugle JE, Hase M, Gregorian C, Swaney JS, Insel PA, et al. Angiotensin II enhances adenylyl cyclase signaling via Ca2+/calmodulin. Gq-Gs cross-talk regulates collagen production in cardiac fibroblasts. J Biol Chem. 2003;278(27):24461-8.
143. Stork PJ, Schmitt JM. Crosstalk between cAMP and MAP kinase signaling in the regulation of cell proliferation. Trends Cell Biol. 2002;12(6):258-66.
144. Zhang Y, Hou MC, Li JJ, Qi Y, Zhang Y, She G, et al. Cardiac β-adrenergic receptor activation mediates distinct and cell type-dependent changes in the expression and distribution of connexin 43. J Cell Mol Med. 2020;24(15):8505-17.
145. Peter A, Walker C, Ceccato T, Trexler C, Ozeroff C, Lugo K, et al. Cardiac Fibroblasts Mediate a Sexually Dimorphic Fibrotic Response to β-Adrenergic Stimulation. Journal of the American Heart Association. 2021;10.
146. de la Roche J, Angsutararux P, Kempf H, Janan M, Bolesani E, Thiemann S, et al. Comparing human iPSC-cardiomyocytes versus HEK293T cells unveils disease-causing effects of Brugada mutation A735V of Na(V)1.5 sodium channels. Sci Rep. 2019;9(1):11173.
147. Gao Z-G, Auchampach JA, Jacobson KA. Species dependence of A3 adenosine receptor pharmacology and function. Purinergic Signalling. 2022.
148. Strasser A, Wittmann HJ, Buschauer A, Schneider EH, Seifert R. Species-dependent activities of G-protein-coupled receptor ligands: lessons from histamine receptor orthologs. Trends Pharmacol Sci. 2013;34(1):13-32.
149. Takahashi K, Yamanaka S. Induction of pluripotent stem cells from mouse embryonic and adult fibroblast cultures by defined factors. Cell. 2006;126(4):663-76.

150. Funakoshi S, Yoshida Y. Recent progress of iPSC technology in cardiac diseases. Arch Toxicol. 2021;95(12):3633-50.
151. Nazor KL, Altun G, Lynch C, Tran H, Harness JV, Slavin I, et al. Recurrent variations in DNA methylation in human pluripotent stem cells and their differentiated derivatives. Cell Stem Cell. 2012;10(5):620-34.
152. Briganti F, Sun H, Wei W, Wu J, Zhu C, Liss M, et al. iPSC Modeling of RBM20-Deficient DCM Identifies Upregulation of RBM20 as a Therapeutic Strategy. Cell Reports. 2020;32(10):108117.
153. Wyles SP, Hrstka SC, Reyes S, Terzic A, Olson TM, Nelson TJ. Pharmacological Modulation of Calcium Homeostasis in Familial Dilated Cardiomyopathy: An In Vitro Analysis From an RBM20 Patient-Derived iPSC Model. Clin Transl Sci. 2016;9(3):158-67.
154. Dai Y, Amenov A, Ignatyeva N, Koschinski A, Xu H, Soong PL, et al. Troponin destabilization impairs sarcomere-cytoskeleton interactions in iPSC-derived cardiomyocytes from dilated cardiomyopathy patients. Sci Rep. 2020;10(1):209.
155. Bourque K, Derish I, Hawey C, Jones-Tabah J, Khan K, Alim K, et al. Effective use of genetically-encoded optical biosensors for profiling signalling signatures in iPSC-CMs derived from idiopathic dilated cardiomyopathy patients. bioRxiv. 2022:2022.09.06.506800.
156. Brodehl A, Ebbinghaus H, Deutsch MA, Gummert J, Gärtner A, Ratnavadivel S, et al. Human Induced Pluripotent Stem-Cell-Derived Cardiomyocytes as Models for Genetic Cardiomyopathies. Int J Mol Sci. 2019;20(18).
157. Guo YJ, Pan WW, Liu SB, Shen ZF, Xu Y, Hu LL. ERK/MAPK signalling pathway and tumorigenesis. Exp Ther Med. 2020;19(3):1997-2007.
158. Mutlak M, Schlesinger-Laufer M, Haas T, Shofti R, Ballan N, Lewis YE, et al. Extracellular signal-regulated kinase (ERK) activation preserves cardiac function in pressure overload induced hypertrophy. Int J Cardiol. 2018;270:204-13.
159. Umbarkar P, Tousif S, Singh AP, Anderson JC, Zhang Q, Tallquist MD, et al. Fibroblast GSK-3α Promotes Fibrosis via RAF-MEK-ERK Pathway in the Injured Heart. Circulation Research. 2022;131(7):620-36.
160. Rubino M, Travers JG, Headrick AL, Enyart BT, Lemieux ME, Cavasin MA, et al. Inhibition of Eicosanoid Degradation Mitigates Fibrosis of the Heart. Circulation Research. 2023;132(1):10-29.
161. Karhu ST, Ruskoaho H, Talman V. Distinct Regulation of Cardiac Fibroblast Proliferation and Transdifferentiation by Classical and Novel Protein Kinase C Isoforms: Possible Implications for New Antifibrotic Therapies. Molecular Pharmacology. 2021;99(2):104-13.
162. Sipieter F, Cappe B, Leray A, De Schutter E, Bridelance J, Hulpiau P, et al. Characteristic ERK1/2 signaling dynamics distinguishes necroptosis from apoptosis. iScience. 2021;24(9):103074.
163. Albeck JG, Mills GB, Brugge JS. Frequency-modulated pulses of ERK activity transmit quantitative proliferation signals. Mol Cell. 2013;49(2):249-61.
164. Farahani PE, Lemke SB, Dine E, Uribe G, Toettcher JE, Nelson CM. Substratum stiffness regulates Erk signaling dynamics through receptor-level control. Cell Reports. 2021;37(13):110181.
165. Fortier SM, Penke LR, King D, Pham TX, Ligresti G, Peters-Golden M. Myofibroblast dedifferentiation proceeds via distinct transcriptomic and phenotypic transitions. JCI Insight. 2021;6(6).

166. Zhou X, Mehta S, Zhang J. Genetically Encodable Fluorescent and Bioluminescent Biosensors Light Up Signaling Networks. Trends Biochem Sci. 2020;45(10):889-905.
167. Greenwald EC, Mehta S, Zhang J. Genetically Encoded Fluorescent Biosensors Illuminate the Spatiotemporal Regulation of Signaling Networks. Chem Rev. 2018;118(24):11707-94.
168. Jones-Tabah J, Martin RD, Tanny JC, Clarke PBS, Hébert TE. High-Content Single-Cell Förster Resonance Energy Transfer Imaging of Cultured Striatal Neurons Reveals Novel Cross-Talk in the Regulation of Nuclear Signaling by Protein Kinase A and Extracellular Signal-Regulated Kinase 1/2. Mol Pharmacol. 2021;100(6):526-39.
169. Lee SH, Oh J, Lee ST, Won D, Kim S, Choi HK, et al. Generation of a human induced pluripotent stem cell line YCMi004-A from a patient with dilated cardiomyopathy carrying a protein-truncating mutation of the Titin gene and its differentiation towards cardiomyocytes. Stem Cell Res. 2021;59:102629.
170. Carol XQC, Narges A, Gilles M, Rhalena AT, Iveta D, Eddie C, et al. Standardized quality control workflow to evaluate the reproducibility and differentiation potential of human iPSCs into neurons. bioRxiv. 2021:2021.01.13.426620.
171. Zhang H, Tian L, Shen M, Tu C, Wu H, Gu M, et al. Generation of Quiescent Cardiac Fibroblasts From Human Induced Pluripotent Stem Cells for In Vitro Modeling of Cardiac Fibrosis. Circ Res. 2019;125(5):552-66.
172. Zhang H, Shen M, Wu JC. Generation of Quiescent Cardiac Fibroblasts Derived from Human Induced Pluripotent Stem Cells. In: Nagy A, Turksen K, editors. Induced Pluripotent Stem (iPS) Cells: Methods and Protocols. New York, NY: Springer US; 2022. p. 109-15.
173. Komatsu N, Aoki K, Yamada M, Yukinaga H, Fujita Y, Kamioka Y, et al. Development of an optimized backbone of FRET biosensors for kinases and GTPases. Mol Biol Cell. 2011;22(23):4647-56.
174. Bourque K, Jones-Tabah J, Pétrin D, Martin RD, Tanny JC, Hébert TE. Comparing the signaling and transcriptome profiling landscapes of human iPSC-derived and primary rat neonatal cardiomyocytes. Scientific Reports. 2023;13(1):12248.
175. Chavez-Abiega S, Grönloh MLB, Gadella TWJ, Bruggeman FJ, Goedhart J. Single-cell imaging of ERK and Akt activation dynamics and heterogeneity induced by G-protein-coupled receptors. J Cell Sci. 2022;135(6).
176. Montero P, Vilar JA. TSclust: An R Package for Time Series Clustering. Journal of Statistical Software. 2014;62(1):1 - 43.
177. J. Gordon Betts KAY, James A. Wise, Eddie Johnson, Brandon Poe, Dean H. Kruse, Oksana Korol, Jody E. Johnson, Mark Womble, Peter DeSaix. Anatomy and Physiology. Apr 25, 2013 ed. Houston, Texas: OpenStax; 2013.
178. He X, Semenov M, Tamai K, Zeng X. LDL receptor-related proteins 5 and 6 in Wnt/beta-catenin signaling: arrows point the way. Development. 2004;131(8):1663-77.
179. Komiya Y, Habas R. Wnt signal transduction pathways. Organogenesis. 2008;4(2):68-75.
180. Nusse R, Clevers H. Wnt/β-Catenin Signaling, Disease, and Emerging Therapeutic Modalities. Cell. 2017;169(6):985-99.
181. Bilic J, Huang YL, Davidson G, Zimmermann T, Cruciat CM, Bienz M, et al. Wnt induces LRP6 signalosomes and promotes dishevelled-dependent LRP6 phosphorylation. Science. 2007;316(5831):1619-22.
182. Zhang Y, Wang X. Targeting the Wnt/β-catenin signaling pathway in cancer. Journal of Hematology & Oncology. 2020;13(1):165.

183. Lian X, Zhang J, Azarin SM, Zhu K, Hazeltine LB, Bao X, et al. Directed cardiomyocyte differentiation from human pluripotent stem cells by modulating Wnt/β-catenin signaling under fully defined conditions. Nat Protoc. 2013;8(1):162-75.
184. Chen B, Dodge ME, Tang W, Lu J, Ma Z, Fan CW, et al. Small molecule-mediated disruption of Wnt-dependent signaling in tissue regeneration and cancer. Nat Chem Biol. 2009;5(2):100-7.
185. Bao X, Lian X, Hacker TA, Schmuck EG, Qian T, Bhute VJ, et al. Long-term self-renewing human epicardial cells generated from pluripotent stem cells under defined xeno-free conditions. Nat Biomed Eng. 2016;1.
186. Bristow MR, Ginsburg R, Umans V, Fowler M, Minobe W, Rasmussen R, et al. Beta 1- and beta 2-adrenergic-receptor subpopulations in nonfailing and failing human ventricular myocardium: coupling of both receptor subtypes to muscle contraction and selective beta 1-receptor down-regulation in heart failure. Circ Res. 1986;59(3):297-309.
187. Jeppesen PL, Christensen GL, Schneider M, Nossent AY, Jensen HB, Andersen DC, et al. Angiotensin II type 1 receptor signalling regulates microRNA differentially in cardiac fibroblasts and myocytes. British Journal of Pharmacology. 2011;164(2):394-404.
188. Penaud-Budloo M, Le Guiner C, Nowrouzi A, Toromanoff A, Chérel Y, Chenuaud P, et al. Adeno-associated virus vector genomes persist as episomal chromatin in primate muscle. J Virol. 2008;82(16):7875-85.
189. Haggerty DL, Grecco GG, Reeves KC, Atwood B. Adeno-Associated Viral Vectors in Neuroscience Research. Mol Ther Methods Clin Dev. 2020;17:69-82.
190. Grimm D, Lee Joyce S, Wang L, Desai T, Akache B, Storm Theresa A, et al. In Vitro and In Vivo Gene Therapy Vector Evolution via Multispecies Interbreeding and Retargeting of Adeno-Associated Viruses. Journal of Virology. 2008;82(12):5887-911.
191. Carlson HJ, Campbell RE. Genetically encoded FRET-based biosensors for multiparameter fluorescence imaging. Curr Opin Biotechnol. 2009;20(1):19-27.
192. Yu D, Liu G, Guo M, Liu X. An improved K-medoids algorithm based on step increasing and optimizing medoids. Expert Systems with Applications. 2018;92:464-73.
193. Dunn† JC. Well-Separated Clusters and Optimal Fuzzy Partitions. Journal of Cybernetics. 1974;4(1):95-104.
194. Luna-Romera JM, del Mar Martínez-Ballesteros M, García-Gutiérrez J, Riquelme-Santos JC, editors. An Approach to Silhouette and Dunn Clustering Indices Applied to Big Data in Spark. Advances in Artificial Intelligence; 2016 2016//; Cham: Springer International Publishing.
195. Freedman NJ, Ament AS, Oppermann M, Stoffel RH, Exum ST, Lefkowitz RJ. Phosphorylation and desensitization of human endothelin A and B receptors. Evidence for G protein-coupled receptor kinase specificity. J Biol Chem. 1997;272(28):17734-43.
196. Schorb W, Conrad KM, Singer HA, Dostal DE, Baker KM. Angiotensin II is a potent stimulator of MAP-kinase activity in neonatal rat cardiac fibroblasts. J Mol Cell Cardiol. 1995;27(5):1151-60.
197. Ansermet C, Centeno G, Nikolaeva S, Maillard MP, Pradervand S, Firsov D. The intrinsic circadian clock in podocytes controls glomerular filtration rate. Sci Rep. 2019;9(1):16089.
198. Strzyz P. Collagen around the clock. Nature Reviews Molecular Cell Biology. 2020;21(3):120-1.
199. Jia S, Agarwal M, Yang J, Horowitz JC, White ES, Kim KK. Discoidin Domain Receptor 2 Signaling Regulates Fibroblast Apoptosis through PDK1/Akt. Am J Respir Cell Mol Biol. 2018;59(3):295-305.

200. George M, Vijayakumar A, Dhanesh SB, James J, Shivakumar K. Molecular basis and functional significance of Angiotensin II-induced increase in Discoidin Domain Receptor 2 gene expression in cardiac fibroblasts. Journal of Molecular and Cellular Cardiology. 2016;90:59-69.
201. Titus AS, Venugopal H, Ushakumary MG, Wang M, Cowling RT, Lakatta EG, et al. Discoidin Domain Receptor 2 Regulates AT1R Expression in Angiotensin II-Stimulated Cardiac Fibroblasts via Fibronectin-Dependent Integrin-β1 Signaling. Int J Mol Sci. 2021;22(17).
202. V H, Titus AS, Cowling RT, Kailasam S. Collagen receptor cross-talk determines α-smooth muscle actin-dependent collagen gene expression in angiotensin II–stimulated cardiac fibroblasts. Journal of Biological Chemistry. 2019;294(51):19723-39.
203. Sparrow AJ, Sievert K, Patel S, Chang YF, Broyles CN, Brook FA, et al. Measurement of Myofilament-Localized Calcium Dynamics in Adult Cardiomyocytes and the Effect of Hypertrophic Cardiomyopathy Mutations. Circ Res. 2019;124(8):1228-39.
204. Dallagnol JCC, Volkovich M, Chatenet D, Allen BG, Hébert TE. G Protein-Biased Agonists for Intracellular Angiotensin Receptors Promote Collagen Secretion in Myofibroblasts. ACS Chemical Biology. 2023.
205. Li XC, Zhuo JL. Mechanisms of AT1a receptor-mediated uptake of angiotensin II by proximal tubule cells: a novel role of the multiligand endocytic receptor megalin. American Journal of Physiology-Renal Physiology. 2014;307(2):F222-F33.
206. Singh VP, Baker KM, Kumar R. Activation of the intracellular renin-angiotensin system in cardiac fibroblasts by high glucose: role in extracellular matrix production. Am J Physiol Heart Circ Physiol. 2008;294(4):H1675-84.
207. Fujisaki H, Ito H, Hirata Y, Tanaka M, Hata M, Lin M, et al. Natriuretic peptides inhibit angiotensin II-induced proliferation of rat cardiac fibroblasts by blocking endothelin-1 gene expression. The Journal of Clinical Investigation. 1995;96(2):1059-65.
208. Buu NT, Hui R-t, Falardeau P. Norepinephrine in Neonatal Rat Ventricular Myocytes: Association with the Cell Nucleus and Binding to Nuclear α1- and β-adrenergic Receptors. Journal of Molecular and Cellular Cardiology. 1993;25(9):1037-46.
209. Tadevosyan A, Vaniotis G, Allen BG, Hébert TE, Nattel S. G protein-coupled receptor signalling in the cardiac nuclear membrane: evidence and possible roles in physiological and pathophysiological function. J Physiol. 2012;590(6):1313-30.
210. Tosco P, Rolando B, Fruttero R, Henchoz Y, Martel S, Carrupt P-A, et al. Physicochemical Profiling of Sartans: A Detailed Study of Ionization Constants and Distribution Coefficients. Helvetica Chimica Acta. 2008;91(3):468-82.
211. Duangrat R, Parichatikanond W, Mangmool S. Dual Blockade of TGF-β Receptor and Endothelin Receptor Synergistically Inhibits Angiotensin II-Induced Myofibroblast Differentiation: Role of AT1R/Gαq-Mediated TGF-β1 and ET-1 Signaling. International Journal of Molecular Sciences. 2023;24(8):6972.
212. Guo L, Zhu K, Pargett M, Contreras A, Tsai P, Qing Q, et al. Electrically synchronizing and modulating the dynamics of ERK activation to regulate cell fate. iScience. 2021;24(11):103240.
213. Samson SC, Khan AM, Mendoza MC. ERK signaling for cell migration and invasion. Frontiers in Molecular Biosciences. 2022;9.
214. Sparta B, Pargett M, Minguet M, Distor K, Bell G, Albeck JG. Receptor Level Mechanisms Are Required for Epidermal Growth Factor (EGF)-stimulated Extracellular Signal-regulated Kinase (ERK) Activity Pulses. J Biol Chem. 2015;290(41):24784-92.

215. Sardá-Espinosa A. Comparing Time-Series Clustering Algorithms in R Using the dtwclust Package2018.
216. Jones-Tabah J, Mohammad H, Hadj-Youssef S, Kim LEH, Martin RD, Benaliouad F, et al. Dopamine D1 receptor signalling in dyskinetic Parkinsonian rats revealed by fiber photometry using FRET-based biosensors. Sci Rep. 2020;10(1):14426.
217. Verdonschot JAJ, Hazebroek MR, Ware JS, Prasad SK, Heymans SRB. Role of Targeted Therapy in Dilated Cardiomyopathy: The Challenging Road Toward a Personalized Approach. J Am Heart Assoc. 2019;8(11):e012514.
218. Wyles SP, Li X, Hrstka SC, Reyes S, Oommen S, Beraldi R, et al. Modeling structural and functional deficiencies of RBM20 familial dilated cardiomyopathy using human induced pluripotent stem cells. Hum Mol Genet. 2016;25(2):254-65.

# 7 SUPPLEMENTARY FIGURES

EKAR-NLS

A)

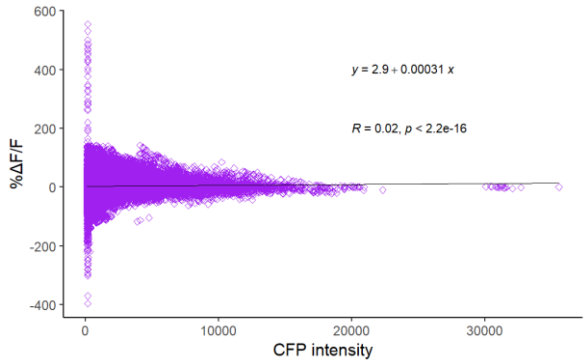


B)

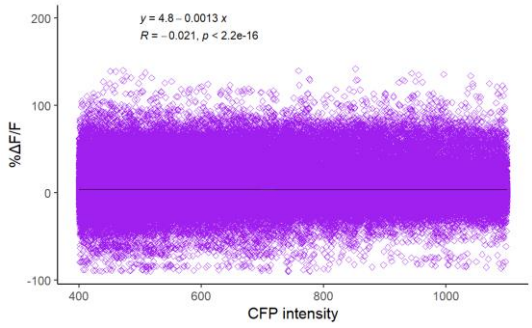


C)

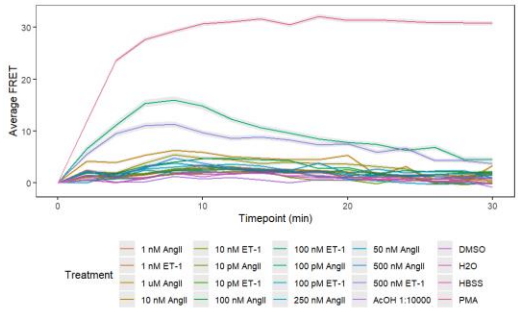


***Figure S 1: Data Preprocessing for Single-Nuclei Analysis in hiPSC-CFs - HID-04C cell line.***

This figure presents the essential data preprocessing steps conducted prior to single-nuclei analysis in hiPSC-CFs featuring EKAREV-NLS transduction. (A) FRET responses elicited by agonists are graphed against donor intensity within hiPSC-CFs. The correlation between these two variables is visually depicted. Notably, cells within the 400-1100 RFU range were selected due to memory constraints. (B) Agonist-induced FRET responses are plotted against donor intensity within hiPSC-CFs, for cells in the 400-1100 RFU range that were subsequently used in analysis. (C) The averaged time-response is showcased for all single nuclei across various treatments, each identified. The data is representative of four distinct differentiations of hiPSC-CFs.

EKAR-NES

A) B)

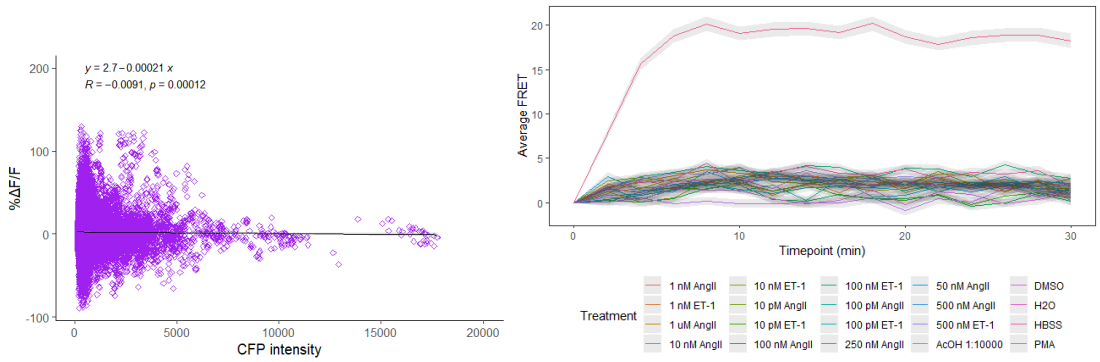


***Figure S 2: Data Preprocessing for Single-Cell Analysis in hiPSC-CFs - HID-04C cell line.***

This figure presents the essential data preprocessing steps conducted prior to single-nuclei analysis in hiPSC-CFs featuring EKAREV-NES transduction.(A) FRET responses elicited by agonists are graphed against donor intensity within hiPSC-CFs. The correlation between these two variables is visually depicted. (C) The averaged time-response is showcased for all single nuclei across various treatments, each identified. The data is representative of four distinct differentiations of hiPSC-CFs.

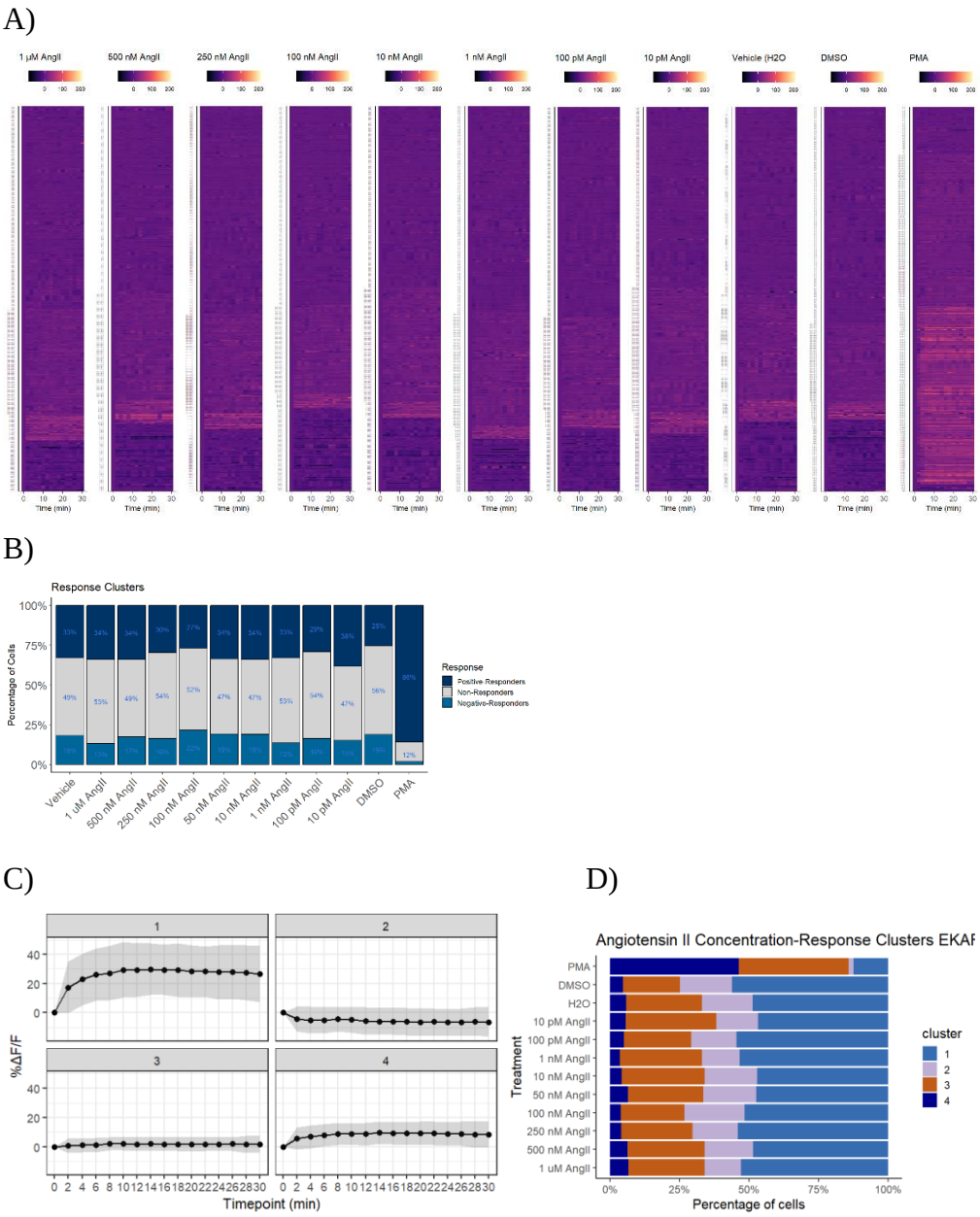


***Figure S 3: Cytoplasmic ERK1/2 Activation Patterns in Single Cells of hiPSC-CFs following Ang II Treatment - HID-04C cell line.***

This figure illustrates into the dynamic cytoplasmic ERK1/2 activation patterns observed in single cells of hiPSC-CFs post Ang II treatment. The study specifically employed the HID04C female control line for investigation. Cytoplasmic ERK1/2 Activation Patterns in Single Cells of hiPSC-CFs after Ang II Treatment. HID04C female control line used. (A) Heatmaps visually represent nuclear ERK1/2 activity in hiPSC-CFs subjected to various doses of vasoactive ET-1 peptide. The kinetics of each nuclear ERK1/2 response are quantified as %ΔF/F (y-axis) over time (x-axis). (B) single-nuclei data was partitioned into five clusters to capture diverse nuclear behaviors, based on the magnitude of response. While certain CF nuclei displayed responses, leading to increased or diminished ERK1/2 activation, others exhibited minimal deviation from baseline and were

grouped as 'non-responders'. The nuclei were categorized as 'positive-responders', 'non-responders', and 'negative-responders', depicted as stacked bar charts showcasing the percentage of nuclei in each cluster. (C) Averaging all nuclei within each cluster generates the mean response for each group. Error bars indicate the standard error of the mean for nuclei in each cluster. The kinetics of each cluster is shown with %ΔF/F on the y-axis, and time on the x-axis. (D) The distribution of cells within each cluster is depicted across various ET-1 doses. Data from hiPSC-CFs derived from four distinct fibroblast differentiations was employed for these experiments.

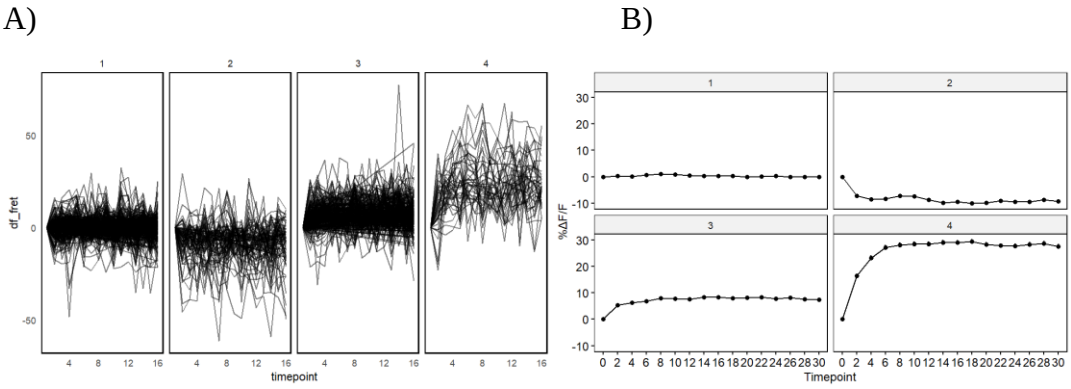


***Figure S 4: This figure captures the depiction of single-cell signaling within each cluster, showing FRET responses plotted across time intervals following the clustering of data into four distinct clusters.***

The dataset is derived from hiPSCs transduced with EKAR-NES . (A) Single cells are plotted individually within each cluster, illustrating their unique signaling trajectories. (B) Averaging the signals of all cells within each cluster brings forth an intriguing observation. Cluster 1, upon aggregation, seemingly portrays non-responding cells. However, upon closer examination, these cells exhibit dynamic fluctuations in their responses over time. The data is representative of four distinct differentiations of hiPSC-CFs.

CLUSTERING CELLS INTO 3 CLUSTERS USING EUCLIDEAN DISTANCE:

A)

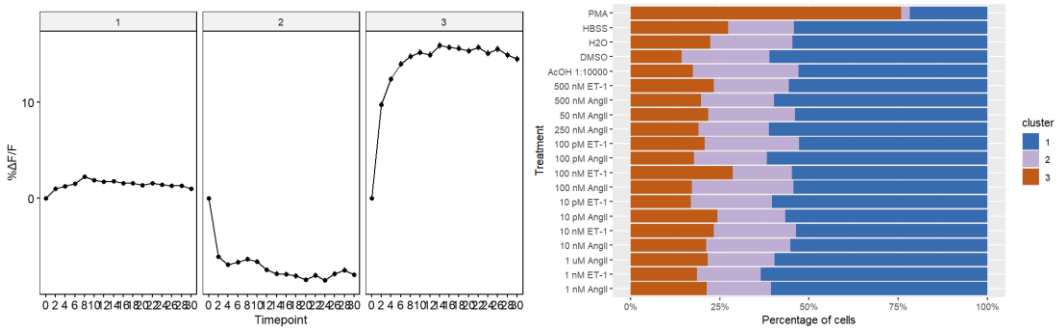


RECLUSTERING CELLS IN CLUSTER 1:

B)

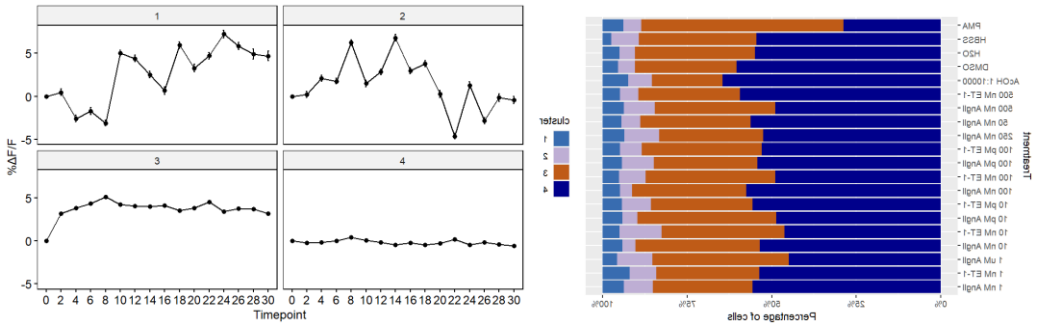


***Figure S 5: Revealing nuances within Cluster 1: Re-clustering of 'Non-Responders' in hiPSCs unveils the hidden intricacies within Cluster 1, initially perceived as 'non-responders'.***

The data is derived from hiPSCs subjected to EKAR-NES transduction. In the initial stage, the data is clustered into 3 primary clusters (A). Further examination shows that cluster 1, seemingly unresponsive upon initial aggregation, contains cells with subtler, hidden responses. To uncover these nuances, all cells within Cluster 1 are re-clustered into 4 additional sub-clusters(B). The data is representative of four distinct differentiations of hiPSC-CFs.